A STUDY OF POINT DEFECT PRODUCTION DURING JUMP DEFORMATION OF ZINC

Thesis

Submitted by

JAMES M. ANDERSON

for the degree of

Doctor of Philosophy

University of Edinburgh,

August, 1964.

PREFACE

This research was carried out in the Department of Natural Philosophy of the University of Edinburgh under the direction of Professor N. Feather, F.R.S. and Dr. A.F. Brown. A preliminary account of the work was presented at the Bristol Solid State Physics Conference, January 1964.

C O N T E N T S

Page

CHAPTER 3

CHAPTER 4

CHAPTER 1

1.1 General Introduction of Point Defects

In any solid at a temperature greater than $0^{o}K$ there must necessarily be a certain amount of disorder of the lattice. The simplest forms which this lattice disorder can take is that of vacant lattice sites (vacancies), and atoms occupying positions in the lattice would not be occupied in the perfect lattice (interstitials).

A vacancy produces a fairly small distortion of the surrounding lattice but an interstitial has more effect on the positions of its neighbouring atoms. The interstitial position in a f.c.c. lattice is shown in Fig. 1a. An alternative lattice arrangement to accommodate an extra atom, however, has been put forward by Vineyard. In this case the interstitial atom and its neighbouring atom move such that they are symmetrically placed as in Fig. 1b, along a 100 direction. This is known as an interstitialcy and this form is accepted as being the stable configuration in copper[1].

An alternative form which has been suggested is that known as a crowdion. In this case a row of five or six atoms in a 110 direction have one extra atom over the normal number as in Fig. 1c.

of this arrangement is, however, doubtful[2].

If a vacancy and an interstitial are formed by displacing an atom from its normal lattice site to an interstitial position, the defect known as a Frenkel pair is formed. Other combination defects which can exist in the lattice are groups of two or three vacancies which are called divacancies and trivacancies respectively. In a f.c.c. lattice the trivacancy is suggested as having the form shown in Fig. 1d[3].

It has long been realised that such point defects can play an important part in the physical properties of solids. Self diffusion, for example, is a process which is dependent on the existence and movement of vacancies in the lattice. In this case the role played by the vacancies is well known, but in other phenomena such as strain enhanced diffusion, work hardening, and recovery, the effect of point defects is more obscure. It is important, therefore, that the properties of point defects should be studied in the hope that any information gained can be applied to help in the understanding of such phenomena.

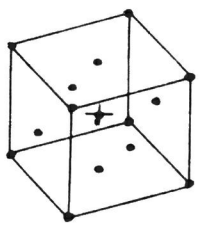

(a)

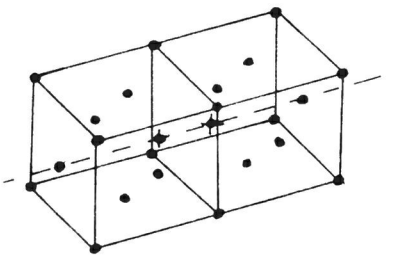

(b)

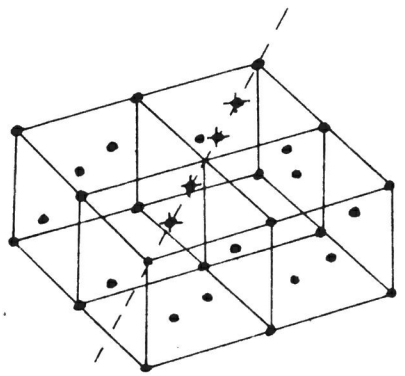

(c)

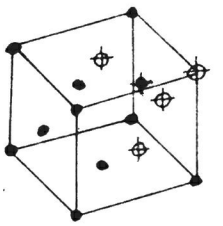

(d)

Figure 1.

1.2 Production of Point Defects for Study

1.2.1 Thermal production

In thermal equilibrium it can be shown[4] that the concentrations of monovacancies, divacancies, and trivacancies are given by the expressions

$$C_{1v} = \exp(S_{1v}^{f}/k) \exp(-E_{1v}^{f}/kT)$$

$$C_{2v} = 6C_{1v}^{2} \exp(B_{2v}/kT)$$

$$C_{3v} = 2C_{1v}^{3} \exp(B_{3v}/kT)$$

where S_{1v}^{f} is the vibrational entropy of formation of a monovacancy.

E_{1v}^{f} is the energy of formation of a monovacancy, and B_{2v} and B_{3v} are the binding energies of divacancies and trivacancies.

At high temperatures the total fraction of vacant lattice sites is of the order of 10^{-4}. This can be shown to be composed of about 90% monovacancies[5].

Since the formation energy of an interstitial is very high, very few interstitials will be produced thermally[6].

It is possible to produce extra defects in the lattice, therefore, by raising the temperature of a specimen, allowing the concentration of defects to reach the new higher equilibrium value, and then

quenching the specimen to a lower temperature. The excess defect population will then attempt to restore itself to the equilibrium value.

This excess makes itself evident in various properties of the material, for example it results in an increase of the electrical resistance. An opportunity therefore exists to study some of the properties of vacancies by this method. This technique has, with various refinements, been widely used.

1.2.2 Radiation Damage

Point defects are produced in a material subjected to radiation. The usual experiments bombard the test material with electrons or neutrons at very low temperatures. By raising the temperature the defects can anneal out and the changes in some physical property, usually the resistivity, observed. A full account of the information gained from this type of experiment is available for f.c.c. metals[7].

1.2.3 Production during deformation

When a material is deformed plastically the movement of dislocations can produce lattice defects. Fig. 2 shows two screw dislocations before and after they have intersected. The moving dislocation, B, has acquired a jog in intersecting with the fixed

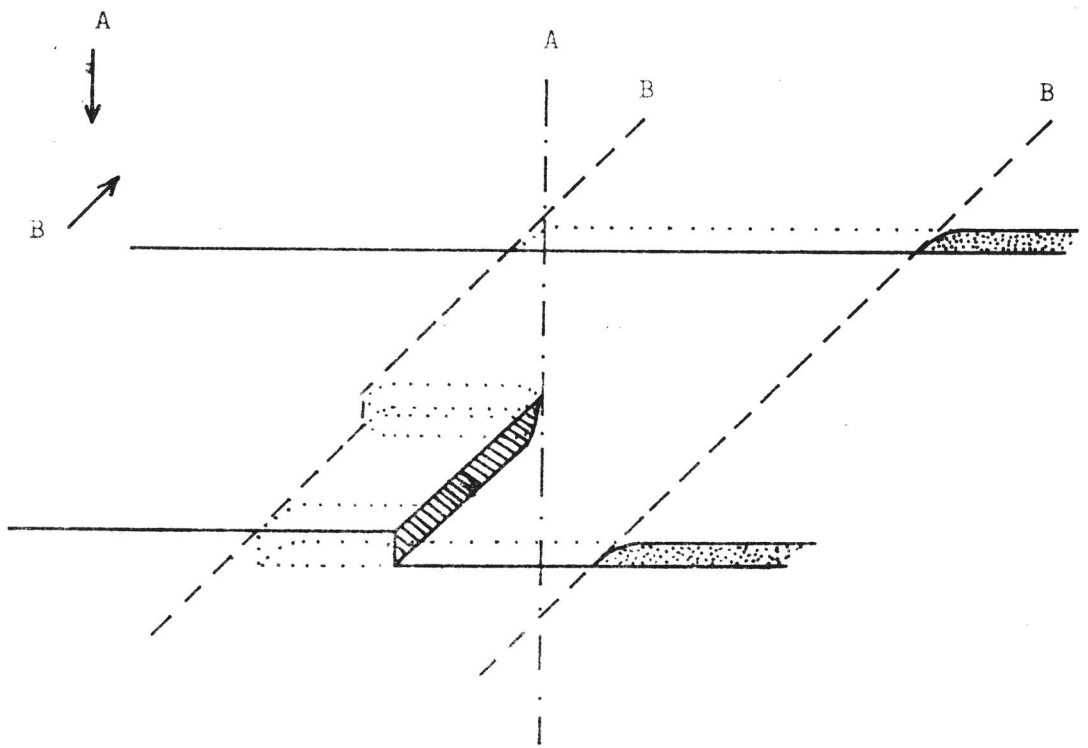

Figure 2.

dislocation A.

Since the jog can only move freely in the direction of the slip vector of B, that is by glide, it must climb to allow B to continue to move, leaving the void shown. If the slip vector of B is reversed, the string of vacancies must be replaced by a string of interstitials.

It is possible to imagine a series of such jogs on each dislocation, each one leaving a string of defects. Since energy must be supplied to form the defects, the dislocation must be deformed into a cusp at each jog when it is moving, as in Fig. 3. This situation can be seen as a possible series of Frank-Read sources.

The stress in the material causing the movement can, therefore, relieve itself, either by producing defects, or by propagating slip from Frank-Read sources. In the latter case the dislocations would bow out around the pinning points until the situation is reached where the edge components attract one another and annihilate, producing a row of point defects. It is conceivable that the energy released in the combination could produce some vacancy-interstitial pairs as well, but recombination would be likely if they did not diffuse away from each other quickly[8].

The strings of vacancies resulting from this process would appear to be more likely to break up

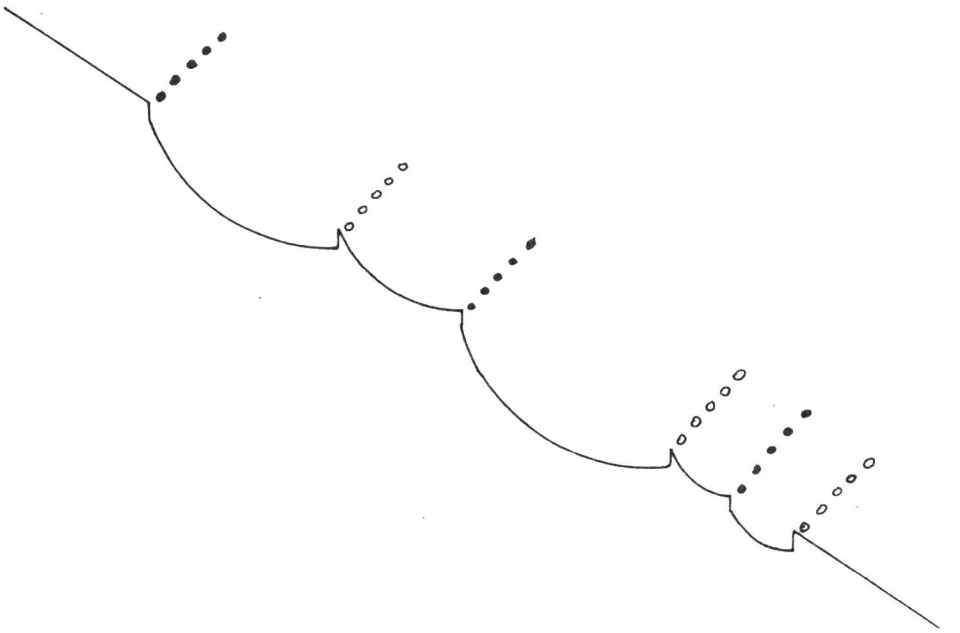

Figure 3.

in divacancies, which are more mobile then monovacancies. It is possible, however, that high enough local temperatures occur to break up the strings into single vacancies. Interstitials, being more mobile, will more easily escape from the strings.

In the case where the motion of the dislocation involves the production of point defects, the situation is complicated by the fact that unless the dislocations are moving very quickly, it is possible that the jogs could glide along the screw part of the dislocation until it reaches an edge part, where it would be ineffective in the production of point defects[9]. Seeger has discussed the motion of the jogs up and down the dislocation line, considering that during their random glide they jump forwards occasionally to produce a point defect[10].

It is probable, however, that a jog, which can be considered as a short dislocation, normal to the slip plane, can dissociate on close packed planes to lower its energy, forming stacking faults. Since the energy will increase linearly with the length over which the dissociation takes place, the equilibrium configuration will be partially constricted. The jog could form a low energy sessile configuration, that is, it would not be free to glide along the dislocation.

Hirsch and Warrington have shown that the flow stress of f.c.c. metals is at least partly controlled by the non-conservative motion of dislocations with sessile jogs[11]. A detailed analysis by Hirsch[12] shows that certain jogs are dissociated in such a way that they are sessile. In all cases for interstitial jogs, the activation energy for conservative motion (via constriction) was shown to be reduced indefinitely by stress, whereas for vacancy jogs the activation energy had to be supplied by thermal motion. Below a certain temperature, therefore, vacancy jogs will be sessile and non-conservative motion will occur. This is about 200°K for Aluminium, but in dislocation with edge components, the activation energies and hence the critical temperature will be higher. It is suggested that interstitial jogs would be expected to move conservatively since it would be easier to constrict the jog than to move it non-conservatively.

Weertman, on the other hand, using an extension of Hirsch's analysis, showed that if dislocations attached to double stacking faults are considered, interstitial producing jogs are possible[13].

At the present, no detailed analysis has been carried out for b.c.c. or h.c.p. crystals.

It would appear, therefore, that this mode of generation is more likely to occur when the slip vectors are such as to produce vacancies.

As the dislocation lines acquire an increasing ratio of edge to screw components, single defects would be produced.

Cottrell has shown that in most cases of two gliding screw dislocations intersecting the jogs formed are of the interstitial producing type[14]. This argument, however, does not apply to the case of a screw dislocation gliding through the forest dislocations, where jogs of both types would occur in equal numbers.

Of the other mechanisms which have been put forward, probably the most important is that suggested by Mott[15]. It is proposed that when a dislocation line forms a loop which almost closes, and this is cut by a screw, as in Fig. 4, a line of vacancies or interstitials will be formed, the number being of the order of

$$\frac{\varepsilon \ell b}{\lambda^2}$$

where ε is the strain

ℓ is the linear dimension of one of the loops

and λ is the distance between the loops formed by a single dislocation.

Mott puts this forward as probably the most important contribution to point defect production in stage III of work hardening.

D. Kuhlman Wilsdorf and H.G.F. Wilsdorf[16] have calculated the uncertainty in the position of a

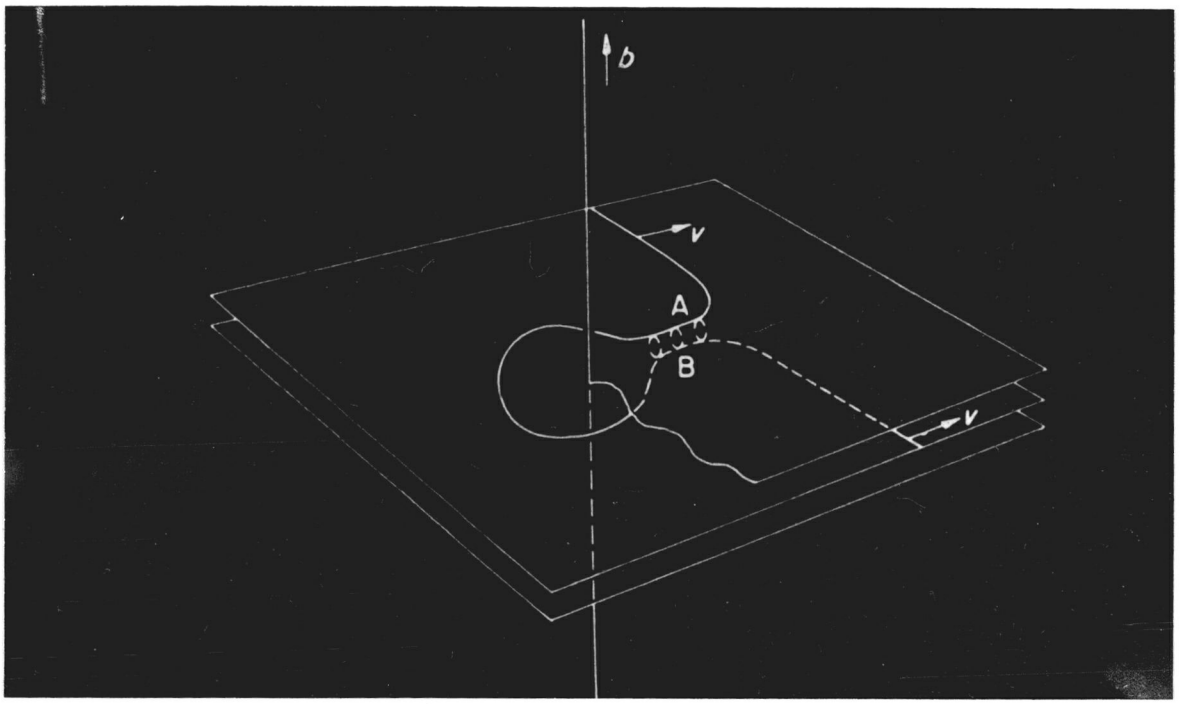

Figure 4.

dislocation due to thermal motion and have used this to put forward a mechanism for the production of point defects during motion of the dislocation.

The uncertainty in position is shown to be, in a direction normal to the dislocation axis, of the order of

$$U\left(\frac{8A}{\rho \tau_{crit}}\right)^{\frac{1}{2}}$$

where

- U is the mean displacement of the atoms due to thermal motion,
- ρ is the periodic lattice spacing on a slip plane normal to the dislocation axis,
- τ_{crit} is the highest shear stress which the lattice could support in the absence of dislocations, and
- A is a constant differing for edge and screw dislocations.

It is pointed out that this uncertainty is significant even down to the lowest temperatures in close packed metals.

Because of this uncertainty, therefore, it would seem reasonable that a dislocation line must transfer segments to adjoining planes, leaving the equivalent of an intersection jog in the transfer region. It is suggested that point defects are produced during the transfer as well as during non-conservative motion of the jogs.

There is some experimental evidence to support this mechanism. Peiffer[17] found a linear relationship between the number of point defects

produced during deformation of copper and the number of line defects by annealing out the point defects at room temperature, leaving the line defects. This relationship had previously been verified for aluminium. Such a relationship would occur if the defects were being produced by the dislocation uncertainty mechanism.

One mechanism which has not yet been mentioned is that of climb of edge dislocations. Normally, during deformation, a jog on a gliding edge dislocation is free to move conservatively with the dislocation. If, however, the dislocation comes up against an obstacle, climb forces can develop and in this case the jog can only move non-conservatively with the dislocation, creating or destroying defects according to the direction of climb.

Although it is now reasonably certain that point defects are created at jogs on dislocations during deformation by one or a combination of the above models, the details of the processes involved are still obscure since not enough is known about the jog structure or its dynamics.

1.3 Annealing of Point Defects

1.3.1 Point defect sinks

Various traps exist for point defects in a crystal lattice. It is possible to visualise point defects losing their identities in the following situations:-

1. at the surface
2. in a grain boundary
3. at jogs on dislocations
4. in the combination of vacancies and interstitials
5. in association with impurities
6. by combining with other defects and collapsing into dislocation loops
7. by combining with other defects and remaining in the lattice as some kind of cluster (e.g. voids)

There is also the possibility of a point defect being trapped on a dislocation, but retaining its identity.

Attempts to determine the nature of point defect sinks in metals have employed various experimental techniques. Recently these have been mainly concerned with the interaction of vacancies with dislocations.

Birnbaum[18] has employed a low temperature strain ageing technique on high purity, polycrystalline copper to study the formation and

annealing of point defects produced during plastic deformation.

After some prestrain the stress was dropped to a value low enough to prevent creep during ageing but not so low as to cause an unloading type of yield point. After ageing the increase in stress before yielding was measured ($\Delta\sigma$). The dependence of $\Delta\sigma$ on the time and temperature of the ageing was found to be of the form shown in Fig. 5.

Birnbaum indicates that the kinetics of the ageing process of peak I is due to pinning of the dislocations by an extremely mobile point defect, the calculated activation energy for movement being ·1 eV, and suggests tentatively that interstitials are responsible in this case.

Since for the process of peak II the activation energy could not be determined any more accurately than a value between ·4 and ·8 eV, the defect active in this process could be either a vacancy or a di-vacancy.

The temperature dependence of $\Delta\sigma$ is compared with that calculated by Hassen[19] and Nabarro[20], both of which are based on a dislocation-pinning point interaction of the form $U \propto \frac{1}{r}$ (U = potential, r = distance between dislocation and pinning point). Agreement is found with Nabarro's calculation at low temperatures and with Hassen's at

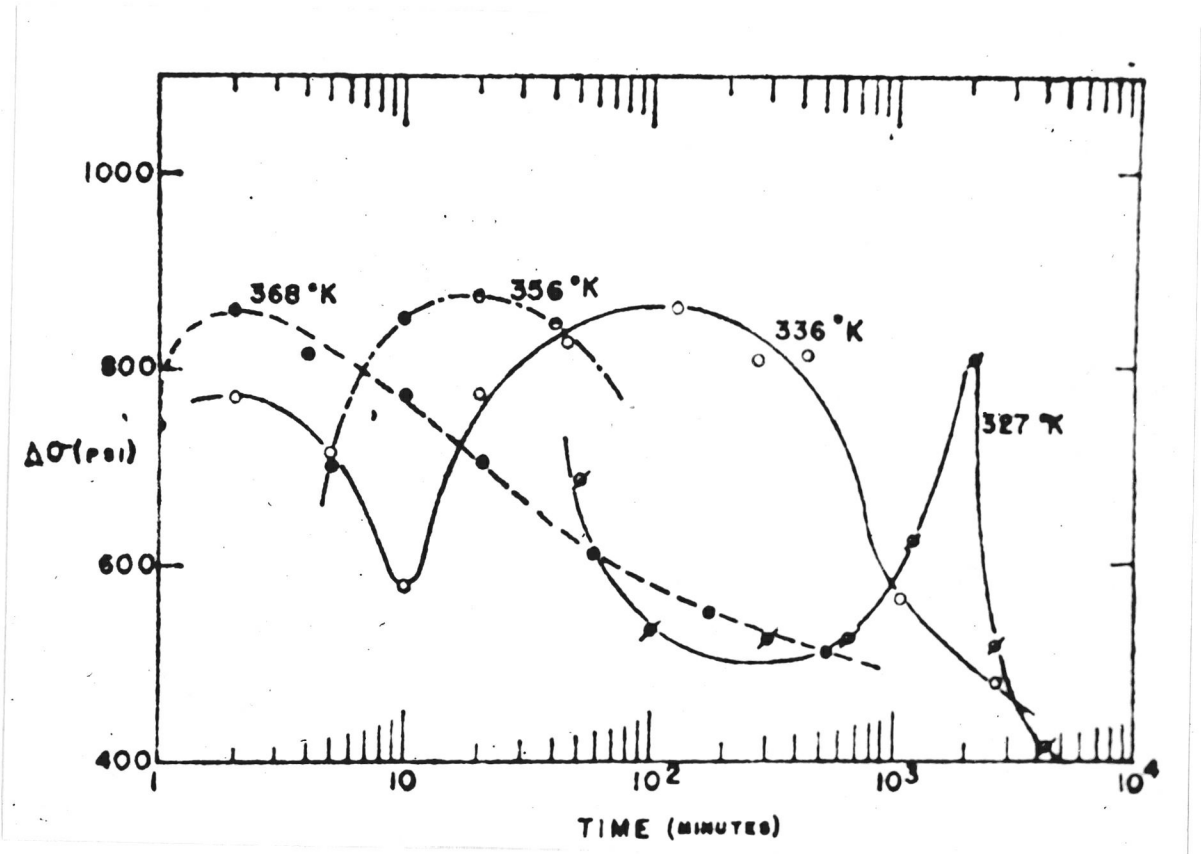
1000
800
600
400
ΔσCpsi)
368 °K
356 °K
336 °K
327 °K
1
10
10²
10³
10⁴
TIME (MINUTES)

Figure 5.

high temperatures.

Since this is the type of interaction to be expected between the stress field of a dislocation and that of a point defect, it is suggested that the point defects retain their identities at the dislocations.

The ageing kinetics are therefore taken as having the form of point defects migrating to the dislocations and acting as pinning points before diffusing along the dislocations to discrete sinks.

Other evidence for dislocations as sinks has been supplied by Cost[21] who examined the kinetics of formation and decay of thermal vacancies in a quenched Ag - Zn solid solution.

In this case the specimen was twisted elastically until all the anelastic strain appeared and then released, the decay of the anelastic strain being observed as a function of time.

The mean relaxation rate, τ^{-1}, can be shown to take the form[22]

$$\tau^{-1} = AC \exp\left(-\frac{E_m}{kT}\right)$$

where E_m is the energy of motion of a vacancy

A is a frequency factor

and C is the vacancy concentration

(which is proportional to $\exp -\frac{E_F}{kT}$, E_F being the energy of formation of a vacancy).

Thus τ^{-1} is sensitive to the vacancy annealing kinetics. Measurements were made on specimens relaxing isothermally (at 136°C) and on specimens which were up-quenched and down-quenched from the annealing temperature (by about 20 or 30°C). The processes of formation and decay of vacancies could then be compared.

Cost's conclusions are that first-order kinetics are obeyed for both formation and decay and that the time taken to reach equilibrium is that corresponding to $n_j \sim 10^7$ to 10^8, n_j being the number of jumps a vacancy makes in this time. This suggests that dislocations are acting as the sources and sinks. His analysis also indicates that vacancy diffusion along the dislocations, to and from discrete dislocation sites is the rate-controlling process. He also concludes that for this alloy, in the temperature range studied, vacancy annealing could be expected to be limited by dislocation diffusion if the jog spacing is greater than about 10^4 atom distances.

This concept of dislocations being the main sources and sinks of thermal vacancies is also held by Jackson and Koehler, following their quenching experiments on fine, pure, gold wires.[23] The specimens could be raised to the quench temperature, kept there for a given period, and then quenched, using a suitable control circuit. Annealing studies

could then be carried out on the specimens. These indicated that only lattice vacancies were present.

By comparing the quenched-in resistivity due to a given period at the quench temperature with that which would have been obtained if the specimen had been left at the quench temperature until the equilibrium concentration had been reached, it was possible to study the formation of the vacancies.

The ratio of the observed concentration of vacancies to the equilibrium concentration is, therefore, observed as a function of the time at the quench temperature. This ratio is then compared with that calculated due to the production of vacancies at the surface and it is found that for very short times about one quarter of the vacancies present are produced at the surface.

Since it was observed that the time taken to reach equilibrium concentration was approximately the same as that taken by vacancies to diffuse the distance between dislocations, it is suggested that dislocations are the main source of the vacancies. It is also concluded from these experiments that the vacancy production at the dislocations is rapid, consistent with a jog formation energy of less than 1.1 eV.

1.3.2 Annealing Kinetics

When the annealing of point defects in a material is to be examined, it is usual to study the annealing spectrum of some property of the material and attempt to ascribe the motion of point defects to sinks to explain some of its features.

Unfortunately, the kinetics of these annealing processes in deformed materials tends to be very complicated and this identification can often be suspect. In fact, Balluffi[7] claims that no point defect has been positively identified as taking part in the annealing spectrum of a cold-worked metal.

A defect annealing out by thermally activated motion is usually considered to follow the rate equation

$$-\frac{dn}{dt} = F(n, q_1, q_2 \ldots) \exp \frac{-E_m}{kT}$$

where n is the total defect concentration, the q's represent the distribution and types of sinks in the solid, E_m is the activation energy for motion, and $F(n, q_1, \ldots.)$ is some function dependent on the bracketed quantities.

If the physical property measured is a

function only of the defect concentration then it can be represented by a similar expression

$$-\frac{dp}{dt} = F'(p, q_1, \ldots) \exp \frac{-E_m}{kT}$$

assuming the q's are independent of temperature and time.

This expression is then usually integrated to give an expression of the form

$$-\int_{p_o}^{p} \frac{dp}{F'(p, q_1, \ldots)} = \int_{o}^{t} \exp\left(-\frac{E_m}{kT}\right) dt$$

Many experimenters have, therefore, measured the time taken to reach a given value of p on annealing isothermally for different temperatures, i.e.

$$t_1 \exp\left(\frac{-E_m}{kT_1}\right) = t_2 \exp\left(\frac{-E_m}{kT_2}\right)$$

from which the activation energy for movement, E_m, can be measured.

An alternative method has been to change the annealing temperature suddenly and measure the change in the annealing rate.

$$\left(\frac{dp}{dt}\right)_1 / \left(\frac{dp}{dt}\right)_2 = \exp \frac{-E_m}{k} \left(\frac{1}{T_1} - \frac{1}{T_2}\right)$$

In an experiment of this type, of course, the quantity E_m measured need not be simply the unique activation energy for motion of a point defect. Even if only one type of defect is

annealing out, several processes could be involved in the decay and the measured E_m could depend on the type of decay. If more than one defect is active in the temperature range being investigated then the measured E_m would have little meaning. It must also be noticed that if during its motion through the lattice, a defect comes in contact with an impurity atom, then the measured E_m would be larger by an amount corresponding to the binding energy between the defect and the impurity. By using very pure material, however, this effect can be overcome[24].

In general the annealing of defects to sinks can not be described by such a simple time dependence. Even in the simple case of one type of defect annealing to fixed inexhaustible sinks, the general solution is of the type

$$C(\underline{r}, t) = \sum_{i=0}^{\infty} a_i \phi_i(\underline{r}) e^{-\lambda_i D t}$$

where $C(\underline{r}, t)$ is the concentration of defects at a position $\underline{r}$ after time t, and the coefficients a_i are determined by the original distribution of defects[25]. Since the higher order terms damp more rapidly this reduces quickly to

$$C(\underline{r}, t) = a_o \phi_o(\underline{r}) \exp -\lambda_o Dt.$$

This can be seen to correspond, in the earlier notation, to

$$-\frac{dp}{dt} = A_o p \exp \frac{-E_m}{kT} \quad .$$

This asymptotic solution is reached more rapidly if the defects are uniformly spread throughout the material originally.

1.3.3 Scope of the present work

Most of the work to date on the annealing spectra of plastically deformed materials has been concentrated on f.c.c. metals. All this work has been concerned with annealing in the range up to room temperature of metals which have been deformed at low temperatures. Table 1 shows a selection of activation energies which have been measured for various annealing stages, mostly in f.c.c. metals. In each case the property measured during the annealing was resistivity.

It seems that in all these experiments point defect annealing processes do take place but in none of them is it possible completely to separate the annealing stages. In some cases, however, fairly accurately determined activation energies emerge which correspond quite closely with the expected activation energies for movement of point defects.

The only hexagonal material so far examined is Cadmium, in the experiments performed by Stevenson and Peiffer[24]. In this case one

Investigator	Material	Deformation	Deformation Temperature	Annealing Temperature	Activation Energy (eV)	Suggested Defect	Reference
Manintveld	Cu 99.94%	8% Tension	-183°C	-140°C to -70°C	.2	Vacancy aggregates	(26)
				-25°C to 40°C	.88	Vacancies	
Manintveld	Cu 99.94%	60% Rolling	-183°C	-180°C to -80°C	.25	Vacancy aggregates	(26)
				-70°C to 30°C	.82	Vacancies	
Berghout	Cu 99.97%	20% tension	-195°C	-80°C to 40°C	.65	Vacancies	(27)
Piercy	Pt.99.99%	8% tension	-195°C	0°C to 100°C	.73	Interstitials	(28)
				200° to 600°C	1.43	Vacancies	
Korevaar	Au - 7% Cu alloy	15% tension	-195°C	-40°C to 100°C	.60	Divacancies (very tentative)	(29)
Sosin and Brinkman	Ni 99.98%	10% tension	R.T.	70°C to 160°C	1.08	Interstitials	(30)
				170° to 350°C	2.5 + 1.0 overlapping	Vacancies and either divacancy or interstitial	
Kamel and Attia	Ag. (pure)	30% to 120% torsion	R.T.	20°C to 50°C	.7	vacancies	(31)
Johnson Peacock and Wronski	No	-	-	130°C to 170°C	1.0	vacancies	(32)
Johnson Peacock and Wronski	Nb	-	-	80°C to 120°C	1.3	vacancies	(32)
Peiffer and Stevenson	Cd 99.9999%	6% tension	78°K	in the region of 138°K	.24	vacancies	(24)

TABLE 1.

recovery stage is attributed to vacancy motion. During earlier experiments with less pure material, the same annealing characteristics emerged, apart from rather higher values of the activation energies. This was attributed to vacancy impurity binding.

No experiment has yet been attempted to study the annealing of defects produced mechanically at room temperature or above in low melting point metals. It was with this in mind that the present experiment was designed. Zinc was chosen as the experimental material since it is one of the very few metals which display the deformation characteristics necessary for the experiment. The fact that it is a h.c.p. metal, which have so far received the least attention in the field, is a coincidence.

Fig. 6 demonstrates the gap in the observations of point defect properties. It is seen that information is missing from the central region of the graph, i.e. at intermediate temperatures. This is the region which the present experiment is designed to cope with, at least in zinc.

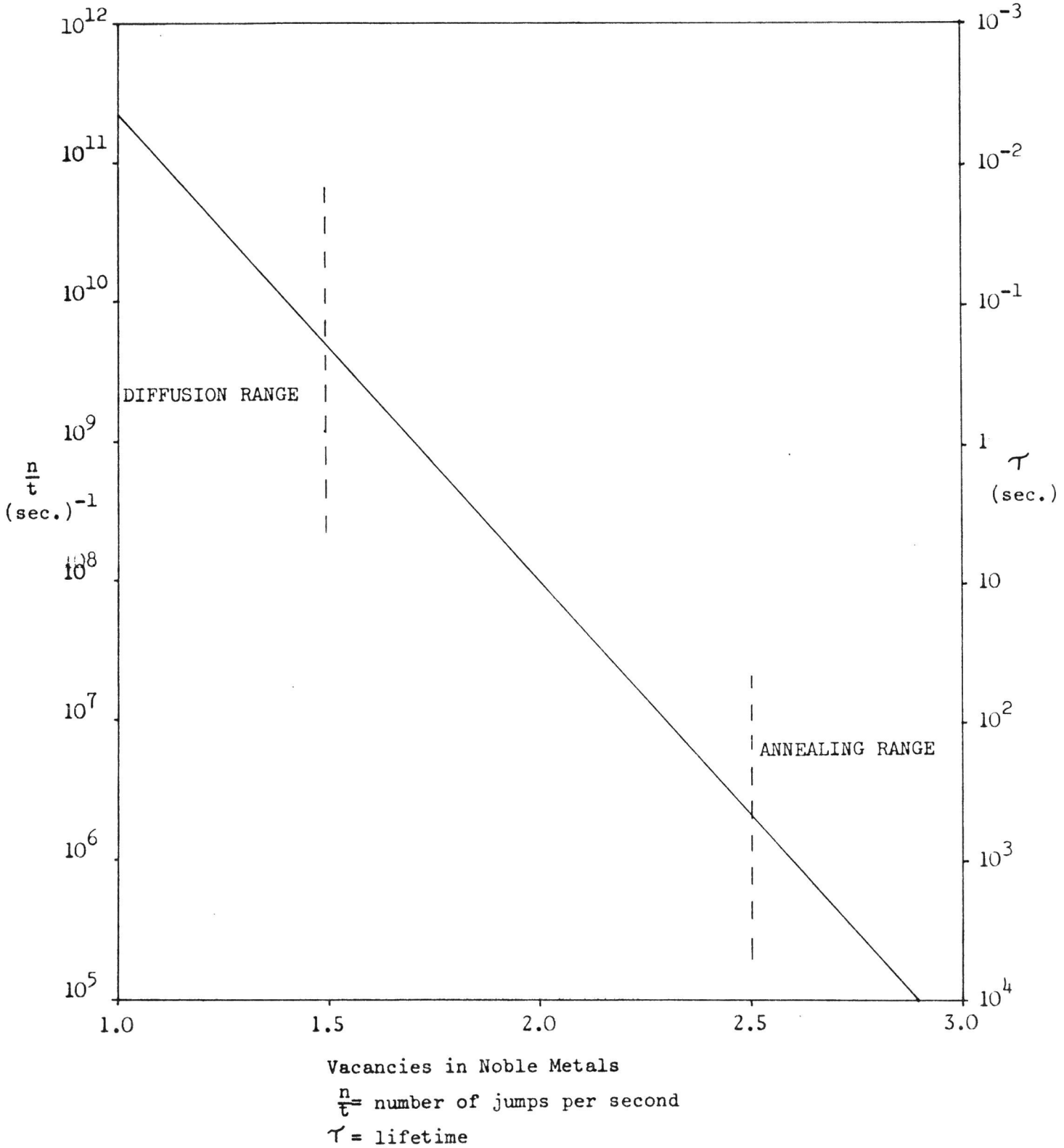
10^{12}
10^{11}
10^{10}
10^{9}
10^{8}
10^{7}
10^{6}
10^{5}
$\frac{n}{t}$ (sec.)$^{-1}$
10^{-3}
10^{-2}
10^{-1}
1
10
10^{2}
10^{3}
10^{4}
τ (sec.)
DIFFUSION RANGE
ANNEALING RANGE
1.0
1.5
2.0
2.5
3.0
Vacancies in Noble Metals
$\frac{n}{t}$ = number of jumps per second
τ = lifetime

Figure 6.

1.4 Resistance due to Point Defects

1.4.1 Experimental determination of vacancy resistance

Before the effect on the resistivity of a metal due to monovacancies can be determined experimentally some measure of the number of vacancies present must be obtained. The technique used is to measure the increase of lattice parameter $(\frac{\Delta a}{a})$ and the length expansion $(\frac{\Delta \ell}{\ell})$ of a specimen for various temperatures. The total defect concentration is then given by

$$(\frac{\Delta N}{N})_T = 3(\frac{\Delta \ell}{\ell} - \frac{\Delta a}{a})_T$$

Simmons and Balluffi[34] reported positive values for $(\frac{\Delta N}{N})$ at temperatures above 650°C. Below this temperature no difference between $\frac{\Delta \ell}{\ell}$ and $\frac{\Delta a}{a}$ could be detected. The experiments were carried out on gold using a filar micrometer microscope to measure the expansion, and a rotating single crystal method of X-ray diffraction to measure the lattice parameter.

Over the range 900°C to 1057°C it was observed that

$$\frac{\Delta N}{N} = \exp(1.0)\exp(-\frac{.94eV}{kT}) ,$$

with accuracies ranging from 8% to 25%.

Since the formation energy for vacancy interstitial pairs is high (4eV) it is unlikely

that the contribution to the equilibrium concentration of defects by interstitials is noticeable.

The measured $(\frac{\Delta N}{N})_T$ is not completely due to monovacancies however. Divacancies and trivacancies also contribute to its value. At temperatures near the melting point, however, clusters of more than one vacancy contribute only about 10% of the total number of vacant lattice sites[34].

By quenching metals from this temperature range to a much lower temperature, the excess vacancies produced at the higher temperature can be measured as an increase in the resistivity. Bauerle and Koehler[35], quenching gold wires from 900°C to 78°K at a rate of 3×10^4 °C/sec. obtained

$$\Delta\rho = 3.5 \times 10^{-8} \text{ ohm. cm.}$$

If

C_{1v} = monovacancy concentration

C_{2v} = divacancy concentration

C_{3v} = trivacancy concentration

and ρ_{1v}, ρ_{2v}, and ρ_{3v} are the corresponding resistivities, then

$$\Delta\rho = \rho_{1v} C_{iv} + \rho_{2v} C_{2v} + \rho_{3v} C_{3v} ,$$

the ρ's only depending weakly on temperature.

Now, according to Seeger and Bross[36]

$\rho_{1v} = \frac{1}{2}\rho_{2v} = \frac{1}{3}\rho_{3v}$ to within 20% or less.

$\therefore \Delta\rho = \rho_{1v}(C_{1v} + 2C_{2v} + 3C_{3v})_T$

$= \rho_{1v}\left(\frac{\Delta N}{N}\right)_T$

and for gold $\frac{\Delta N}{N} = 2.4 \times 10^{-4}$ at 900°C.

Hence $\rho_{1v} = (1.5 \pm .3)\mu$ ohm. cm/atomic% vac.

Other known results are given in Table 2.

1.4.2 Experimental determination of interstitial resistance

In annealing studies of electron irradiated copper (which should produce isolated interstitial vacancy pairs[37]), it has been observed that $\frac{\Delta \ell}{\ell}$ is very nearly equal to $\frac{\Delta a}{a}$ throughout the annealing range. This is what would be expected if equal numbers of vacancies and interstitials were being annihilated[31]. It is also found that the resistivity anneals in the same manner.

From work by Simmons and Balluffi, the ratio of the resistivity increment on irradiation, $\Delta\rho$, to $\frac{\Delta a}{a}$ is

$$\frac{\Delta\rho}{\Delta a/a} = 7 \times 10^{-4} \text{ ohm. cm.}^{(38)}$$

This corresponds to Vook and Wert's value for

$$\frac{\Delta\rho}{\Delta \ell/\ell} = 6.8 \times 10^{-4} \text{ ohm. cm.}^{(40)}$$

Metal	ρ_{lv} μ ohm cm./atomic %
Au	$1.5 \pm .3$
Ag	$1.3 \pm .7$
Al	$2.2 \pm .7$

After Simmons and Balluffi.

TABLE 2

Both these values are based on Cooper, Koehler & Marx's values for $\Delta\rho$, suitably normalised[41].

Hence $\frac{\Delta\rho}{\frac{\Delta V}{V}} = \frac{\Delta\rho}{3\frac{\Delta \ell}{\ell}} = 2.3 \times 10^{-4}$ ohm. cm.

Granato and Nilan[42] measured the energy release in deuteron irradiated copper and found a correspondence between their annealing curves and those for resistivity annealing.

Normalising their flux to 10^{17} deuterons/cm.^{2} (energy 10 MeV) the average energy release is then .83 calories/gm. Then using the resistance increment given by Cooper, Koehler and Marx and once again normalizing to the same deuteron flux and energy

$$\Delta(E/m)/\Delta\rho = 7.1 \text{ cal./gm./}\mu\text{ ohm.cm.}$$
$$= 1.9 \times 10^4 \text{ eV/atom/ohm. cm.}$$

If one atom in 100 is a defect then this can be written as

$$\Delta(E/m)/\Delta\rho = 100 \times 1.9 \times 10^4 \text{ eV/defect/ohm.cm.}$$

Then $E^f_{1v} + E^f_{1I} = \frac{\Delta(E/m)}{\Delta\rho}(\rho_{1v} + \rho_{1I})$

$$= \frac{\Delta(E/m)}{\Delta\rho} \times \frac{\Delta\rho}{\Delta V/V}(V^f_{1v} + V^f_{1I})/\Omega$$

where E^f_{1V} = energy of formation of 1 vacancy

E^f_{1I} = energy of formation of 1 interstitial

ρ_{1v} = resistivity increment for 1 atomic % of vacancies

ρ_{1I} = resistivity increment for 1 atomic % of interstitials

V^f_{1v} = volume of formation for vacancies

V^f_{1I} = volume of formation for interstitials

Ω = volume of given sample.

Hence using experimental values for E^f_{1v}, ρ_{1v}, $V^{f\,*}_{1v}$, and the theoretical value for E^f_{1I} (which is fairly precise)

$$\underline{\rho_{1I} = 1.0 \pm .6 \ \mu \text{ ohm.cm./atomic \%}}$$

and $V^f_{1I}/\Omega = .6 \pm .3$.

$\frac{V^f_{1v}}{\Omega}$ was measured by quenching and measuring the length contraction on subsequent annealing by Baurle and Koehler, thus obtaining a mean value of

$\frac{\Delta \rho}{\Delta V/V} = 3.3 \times 10^{-4}$ ohm. cm.

Combining this with $\rho_{1v} = 1.5 \ \mu$ ohm.cm./atomic%

gives $\frac{V^f_{1v}}{\Omega} = .45 \pm .1$.

---

* assuming they are similar for copper, silver and gold.

1.4.3 Calculated Values

Table 3 gives the calculated increase in resistivity due to vacancies and interstitials for copper. It is seen that the values for vacancies are in reasonable agreement with the experimental values but a wide variation in values exists for interstitials.

The reason for this is that while it is agreed that the relaxation of the lattice around the defect is of little importance in calculating the resistance due to vacancies, this may not hold when considering interstitials. Blatt argues, however, that Gorman and Overhauser overestimate the importance of this effect[43]. Certainly his value is in fair agreement with that given in 1.4.2.

Defects in Copper

Defect	Calculated Resistivity μ ohm cm./atomic %
Monovacancy	1 ± .5
Interstitial	2.9 ± 2.1
Divacancy	10% less than 2 monovacancies

after Blatt.

TABLE 3

CHAPTER 2

2.1 Jump Deformation

The present experiment involves investigating the phenomena of jump deformation in zinc single crystals. In Chapter 1 it was pointed out that no experiment to date had examined directly the annealing of mechanically produced defects, either at temperatures above room temperature, or of defects produced in this temperature range, in low melting point metals. By studying the phenomenon of jump deformation it is hoped that both these situations can be studied.

Normally, when a metal single crystal is extended in tension at room temperature the stress-strain curve takes the form shown in Fig. 7. If a careful examination is made of the surface of such a specimen, it is noticed that the slip making up the total deformation is confined to relatively few crystallographic planes. Fig. 8 shows one example of such "fine slip" as it is known, the size of individual steps ranging from several hundred to two thousand Angstrom units[44]. Normally these fine slip events occur uniformly throughout the specimen, contributing gradually to the total plastic extension.

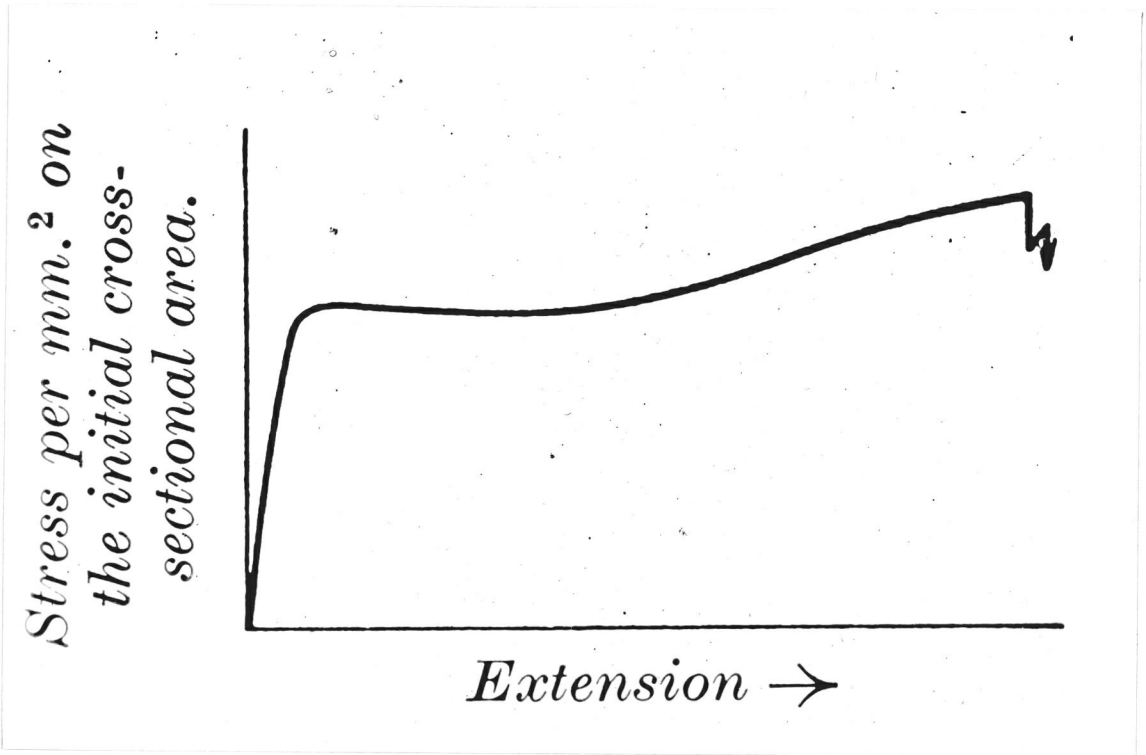
Stress per mm.² on the initial cross-sectional area.
Extension →

Figure 7.

Figure 8.

In certain cases, however, the fine slip events in a particular region of the material can occur one after the other in the form of an avalanche. This is quite a rare phenomenon, only occurring in certain materials, normally, rock salt, brass, and zinc single crystals. Although discovered by earlier investigators, the first full examination of this effect was carried out on zinc single crystals by Schmid and Valouch[45]. They repeated Orowan's tensile experiments on zinc when he reported such jump deformation, the jumps being of the order of several microns[46].

Schmid and Valouch investigated the effect of orientation, temperature, impurity content, surface condition, and the amount of deformation on jump deformation.

Their specimens were grown by the Czochvalski method of drawing from the melt, in this case the drawing rate being 60 cm./hr. The diameter of the crystals obtained varied between .7 and 1 mm. The crystals were then extended in a Polanyi testing machine at .0017 mm./sec., the load being monitored as the deflection on a steel beam attached to one end of the specimen. Typical examples of some of the stress-strain curves obtained are shown in Fig. 9.

Specimens of various crystallographic

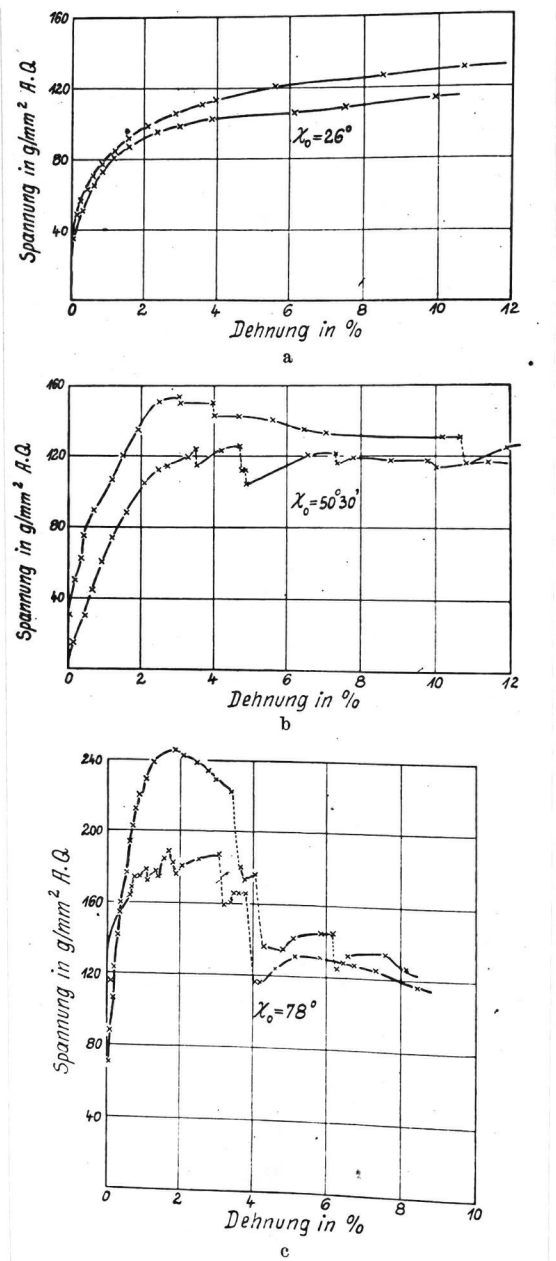
Spannung in g/mm² A.Q.
160
120
80
40
0
2
4
6
8
10
12
Dehnung in %
$\chi_0 = 26°$
a
Spannung in g/mm² A.Q.
160
120
80
40
0
2
4
6
8
10
12
Dehnung in %
$\chi_0 = 50°30'$
b
Spannung in g/mm² A.Q.
240
200
160
120
80
40
0
2
4
6
8
10
Dehnung in %
$\chi_0 = 78°$
c

Figure 9.

orientations were strained. It was found that jumps only occurred for orientations above $\chi_o = 38^\circ 30'$ (χ_o is defined in Fig. 10). The largest jumps appeared for $\chi_o > 60^\circ$.

Crystals were stretched at temperatures ranging from -185°C to 100°C. No jumps were observed at -185°C, but they did appear at 20°C and 100°C for suitably oriented specimens, although they were smaller at the higher temperature.

By employing a vacuum distillation method the impurity content was reduced to .0005 % Pb and .0005 % Cu. This was much purer than the zinc used by Orowan, whose jumps were, in fact smaller.

In an attempt to show that this was a volume effect, some specimens were extended while immersed in a solvent (20 cc. HCl in 300 cc. alcohol). No effect on the jump deformation was observed.

Jumping appeared at all parts of the deformation but generally, most occurred after the yield stress and after a few per cent elongation. The jumping disappeared after large strains.

It was stressed that this jump deformation was definitely associated with basal glide since not enough deformation occurred for twinning to have taken place. In any case, it was claimed that the orientation was only favourable for deformation twins which would shorten the specimen

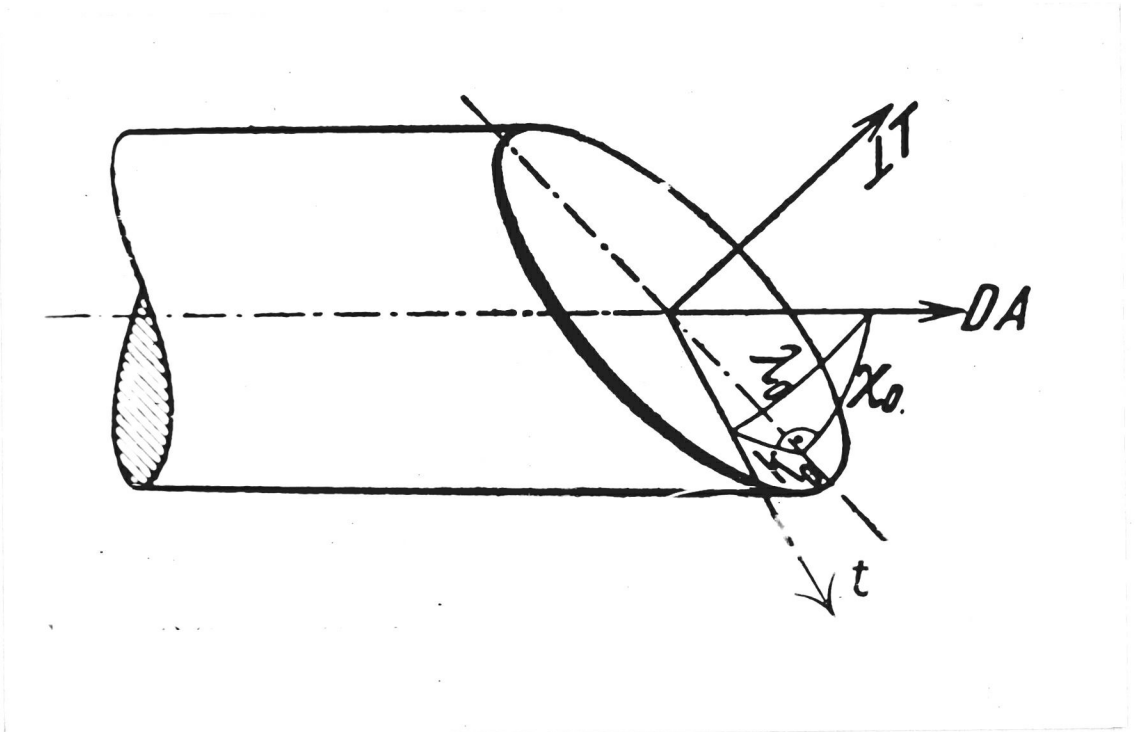

Figure 10.

in the longitudinal direction. Moreover, the external markings of basal glide were always apparent.

Adjacent sections of crystals which had displayed jumping were stretched under a microscope and the sudden appearance of both solid glide steps and a fine band structure in the basal plane were occasionally seen.

Schmid and Valouch suggested that the essential reason for the jump deformation was the recovery by thermal motion of pinned regions in the slip system. It was later suggested by Seitz and Read[47] that such small slip avalanches could be connected with local heating in the slip band, causing loosening of the structure and easier passage of the dislocations.

2.2 The Change of Resistance during Jump Deformation

The first attempts to follow the resistance of a specimen undergoing jump deformation were performed by Rozhanskii and his co-workers[48]. They also used single crystals of zinc as the specimens and strained them in tension. The purity of the zinc used is not mentioned.

The effect of orientation on the number of jumps and on the percentage of the total deformation due to jumps is illustrated in Fig. 11. It

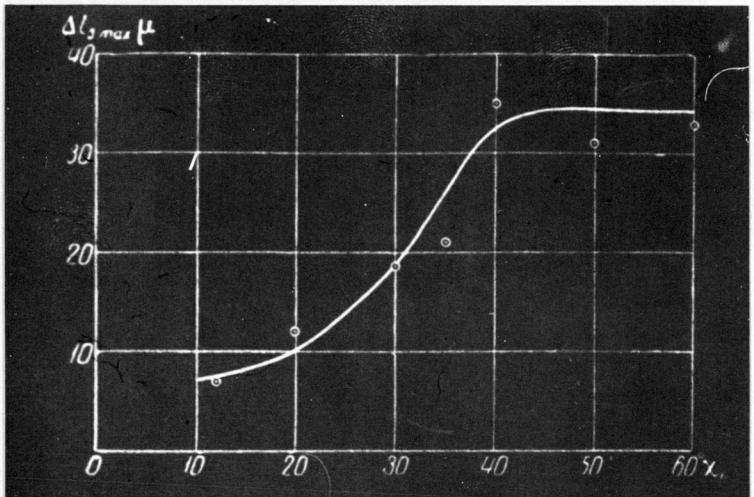

Рис. 9. Зависимость величины максимального скачка от ориентировки монокристаллов.

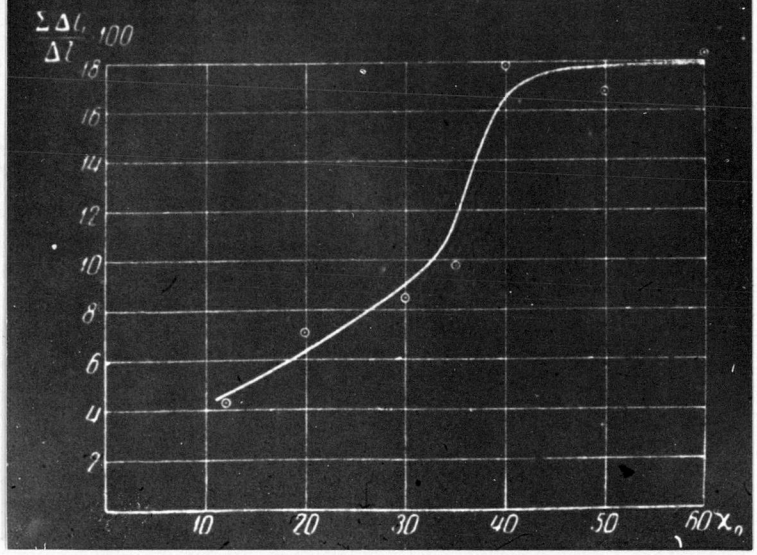

Figure 11.

It can be seen that jumping occurred for all orientations of χ_o greater than 45° and that the percentage of the total deformation due to jumps reaches a maximum of 18% at $\chi_o = 60^\circ$. The magnitude of the jumps varied between .5μ and 35μ, with durations between .01 and .1 seconds.

Some fine structure of the jumps could be detected by the strain measuring device used. This was a beam balance, one end of which was attached to the specimen, and the other to a shutter and photocell arrangement. Little could be said, however, except that the jumps appeared to be of a fairly complex nature.

By passing a D.C. current of about one ampere through the specimen, and using an amplifier with a bandwidth of 20 to 800 cps and with a 20 : 1 step-up transformer at the input, enough amplification was obtained to display some representation of the resistance changes of the specimen on an instrument known as a loop oscillograph. A modern version of this instrument is now available in this country which gives a good representation of signals up to 1 Kc./sec. The one used in these experiments, presumably, has the same sort of performance. The noise level at the specimen was very low, $\frac{1}{40}\mu V$, and very small changes in resistance could, therefore, be

resolved. The circuit of the amplifier used is shown in Fig. 12.

The structure of the resistance change during a jump of deformation always took the form of Fig. 13. The interpretation was that the leading edge was due to the increase in the specimen resistance and the trailing edge due to the amplifier's bandwidth characteristics. An initial fine slip event, triggering off the big jump, was used to explain the initial jumplet on the leading edge of the main pulse. In fact, by assuming

$$\Delta R = k \Delta \ell$$

where ΔR is the change in specimen resistance

k is a constant

and $\Delta \ell$ is the corresponding change in specimen length

and measuring ΔR and $\Delta \ell$ for the larger jumps to find k, $\Delta \ell$ for the small jumps turned out to be of the order of 2000 Å, the measured fine slip size.

It was pointed out that jump deformation produced slightly less change in resistivity than the equivalent amount of steady deformation.

In conclusion it was suggested that the slip zone did not melt, and that any heating of the slip zone could not be detected. In other words, the pulses mainly represented permanent changes in

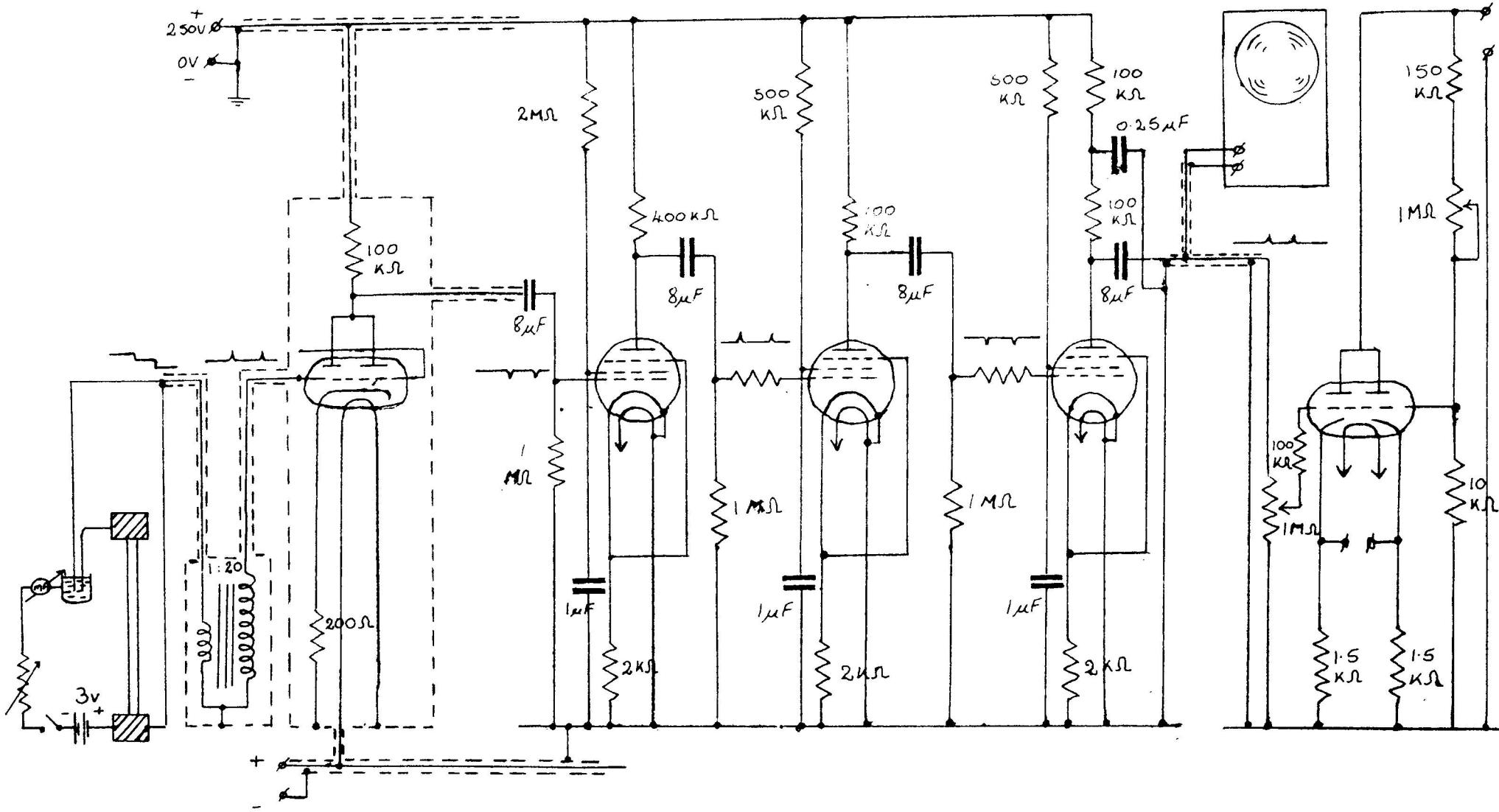
250V
0V
2MΩ
500 KΩ
500 KΩ
100 KΩ
0·25μF
150 KΩ
100 KΩ
400 KΩ
100 KΩ
100 KΩ
1MΩ
8μF
8μF
8μF
8μF
100 KΩ
1 MΩ
1 MΩ
1 MΩ
1μF
1μF
1μF
1:20
200Ω
2KΩ
2KΩ
2KΩ
100 KΩ
1MΩ
10 KΩ
1·5 KΩ
1·5 KΩ
3V
+
-

Figure 12.

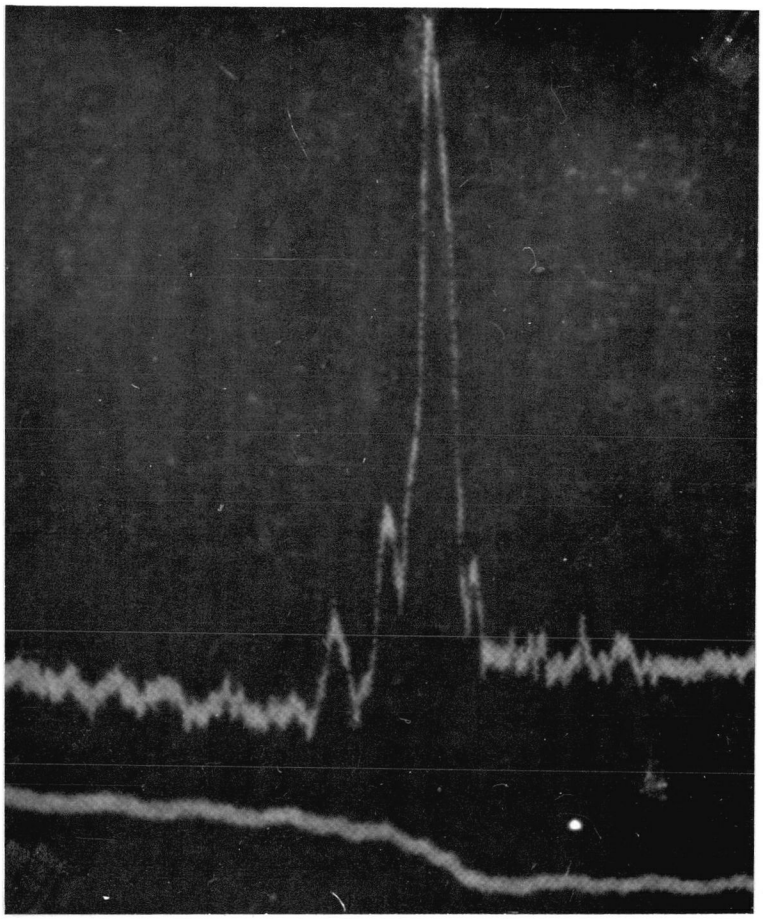

Figure 13.

resistance.

A close examination of one of the resistance pulses, however, shows that the fall time at the top of the pulse is comparable with the rise time, both being within the pass band of the amplifier used. Any attempt, therefore, to rule out a transient component of the pulse does not seem to be justified with the amplifier used, which was not D.C. sensitive.

The main reason for saying that the pulses represent a permanent change seems to be that even assuming they are wholly due to permanent changes of resistance, they are still smaller than the equivalent change due to steady deformation. Since the deformation process is different, however, one could hardly expect complete equivalence here.

The fact that two small pulses, similar to the initial jumplets, always appear in the trailing edge of the main pulses is not mentioned by Rozhanskii.

CHAPTER 3

3.1 Specimen Preparation

3.1.1 Material

The material used in the preparation of the single crystals was purchased from Johnson Matthey, the specification of purity being that listed in Appendix A. Some specimens were also grown from commercial zinc of unknown impurity content.

In both cases the material as supplied was in the form of 2mm. diameter wire, this being a suitable specimen diameter. Since some specimens of 1 mm. diameter were required, some of this wire was drawn out to the narrower section by pulling it through an ordinary wire drawing die using soap as a lubricant. It was found to be advisable to start off with the required specimen diameter since zinc does not flow well when molten because of the oxide film, even when under a reasonable vacuum.

3.1.2 Crystal Growing

Crystals were prepared in the two furnaces shown in Figures 14 and 15. The original furnace that of Figure 14, has, apart from minor alterations, been fully described elsewhere[49]. Briefly, it operates on the Bridgman principle, that of lowering a specimen, packed in a suitable crucible, through a region of a furnace at a

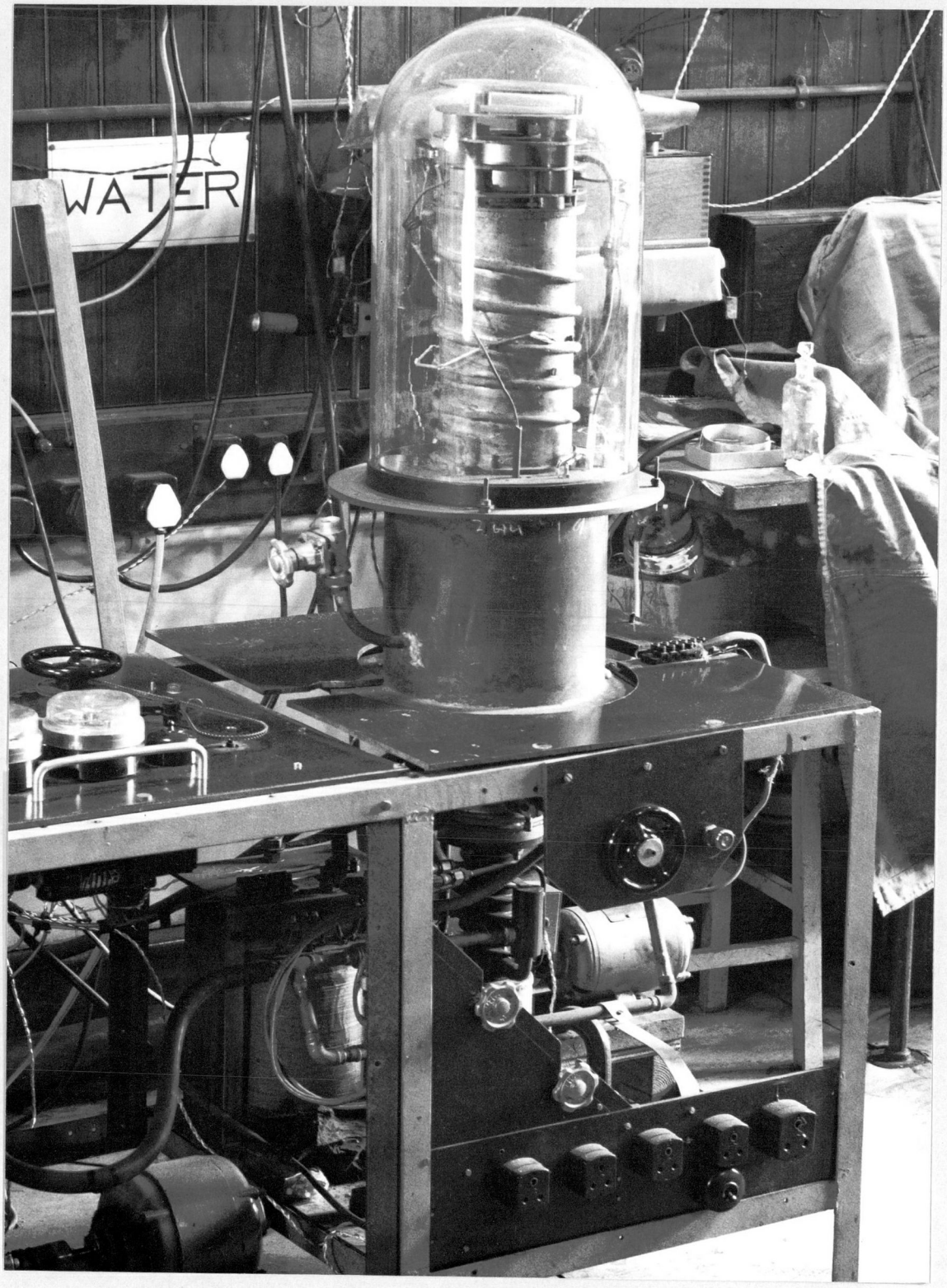

Figure 14.

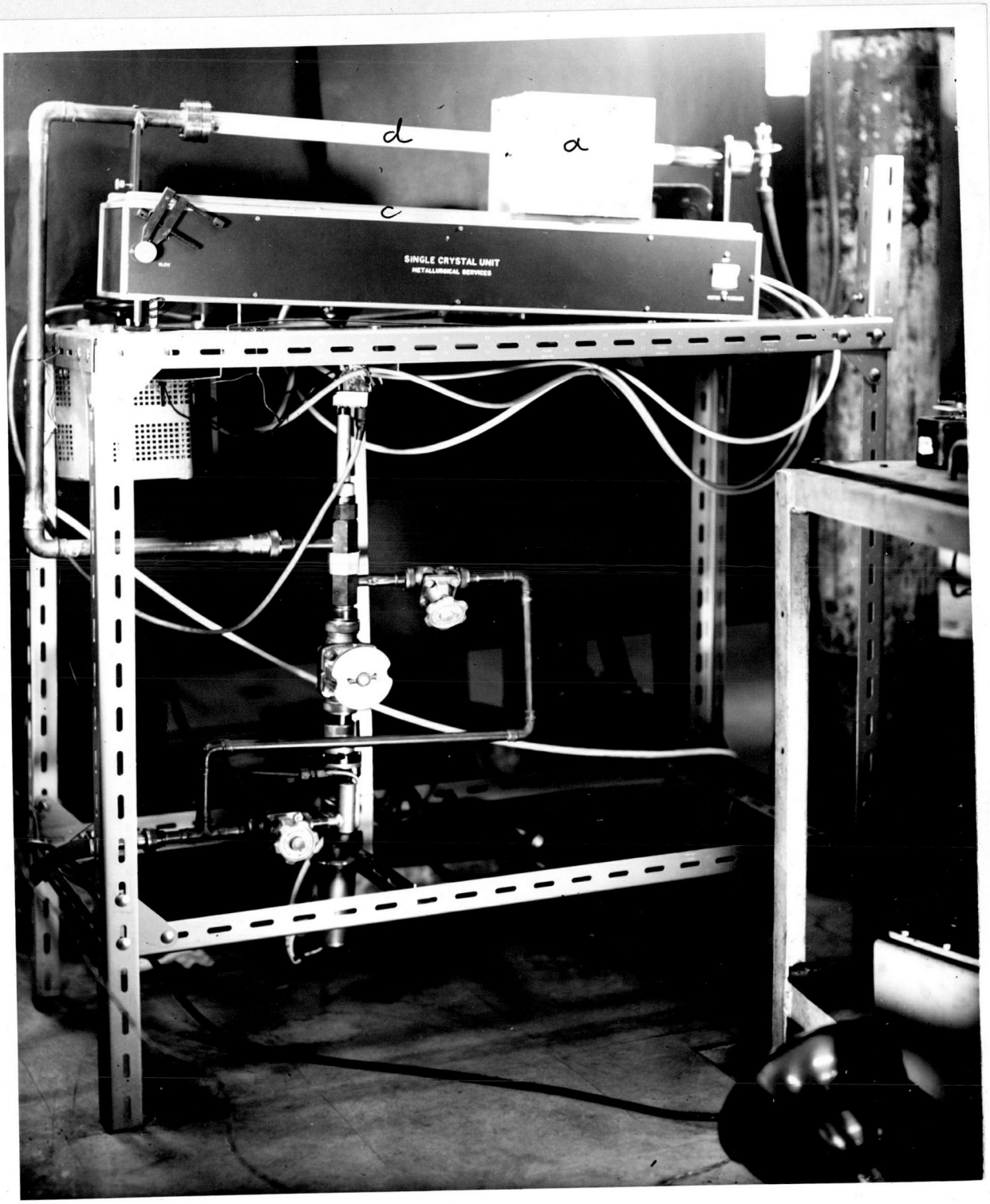

Figure 15.

temperature greater than the melting point of the specimen. Under suitable conditions crystal growth takes place from the bottom end of the specimen. This furnace is capable of running up to the correct temperature and switching on and off the dropping mechanism automatically.

Specimens were packed in fine alumina powder contained in a graphite tube, the tube being constructed in two halves to facilitate removal of the crystals, once grown. After raising the furnace temperature to 430°C the specimens were then lowered through the furnace at a rate of 2mm/min. By this means crystals of zinc 6 cm long were grown of random orientations.

This furnace did not survive transportation to a new laboratory site, however, and a new single crystal furnace was acquired which was felt to be more suited to the growth of low melting point metals.

The basic furnace was purchased from Metallurgical Services Ltd. It consists of a small, wire-wound furnace ("a" of Fig. 15) which can be clamped to an endless belt "b" which is driven by a synchronous motor through a two-speed gear box. This gives a smooth linear motion along the rails "c". The specimen, in a suitable crucible, is placed in the pyrex tube "d". This tube was normally evacuated by an Edwards water

cooled diffusion pump type 102 in conjunction with a Metrovac DRI rotary pump. Oxygen-free nitrogen was then admitted to the other end of the tube via an Edwards needle valve. By repeated flushing as much of the oxygen was removed from the system as possible, leaving a nitrogen atmosphere. This helped considerably in cutting down evaporation from the specimen surface.

The furnace is fed from a Variac variable transformer which allows the temperature to be varied up to a maximum of about 650°C, although at this temperature it is necessary to replace the glass tube with one made from silica.

After various trials the following was found to be the most consistent way of growing good single crystals with this apparatus. Specimens 8 cm long were cut from the zinc wire, straightened, and cleaned in a 50% solution of HCl. They were then contained in glass tubes of 3mm internal diameter which were sealed at one end before being placed in the furnace tube. After evacuating and filling the furnace tube with nitrogen at atmospheric pressure the furnace, which was already at the correct temperature, was placed over the specimen and left for half an hour. This was sufficient time to allow the specimen to melt. The driving motor was then started, moving the furnace at 3mm/min. The direction of growth was

"uphill", the specimen being tilted slightly by inserting the supports "e" under one end of the apparatus. Surface tension sufficed to keep the specimen cross section the original 2mm. in diameter.

Fig. 16 is a graph of the temperature along the length of the furnace with a current of 1.55 amps passing through the winding. The furnace was normally operated at this current setting.

Once grown, the specimens were removed from the tubes and dipped in liquid nitrogen. One end of the specimen was then broken off. Since zinc crystals normally fracture on the basal plane, recognizable as a very smooth cleavage surface, this gives an easy and accurate method of determining the orientation. The orientation was measured as in Fig. 17a. The reflection of a parallel beam of light from the cleaved surface was observed as shown. The orientation, χ_o, is then measured from the goniometer on which the crystal is mounted.

Since orientations $\chi_o > 45^\circ$ were required for the present experiments, crystals with $\chi_o < 45^\circ$ were regrown using the following procedure. After an exact determination of the orientation the crystal was bent 2 cm from one end as shown in Fig. 17b. The bent crystal was then loosely packed in fine alumina powder in an

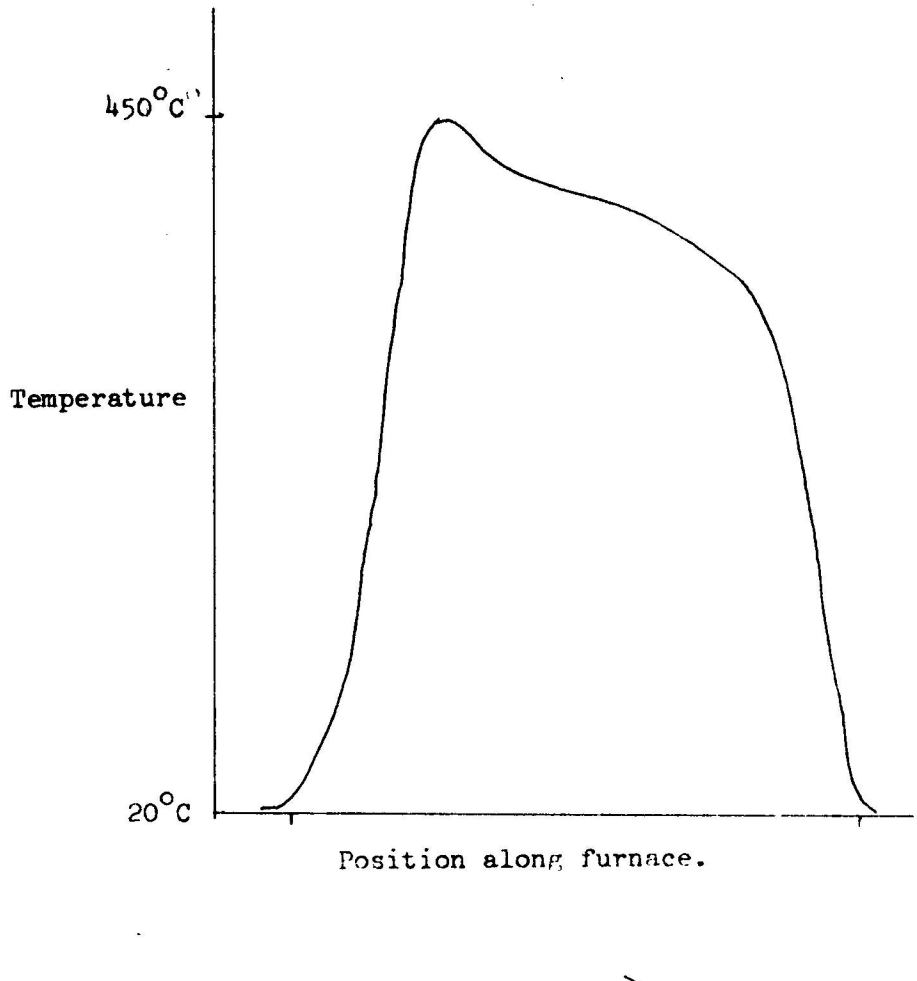
450°C
Temperature
20°C
Position along furnace.
Direction of furnace motion
over specimen.

Figure 16.

open graphite boat as in Fig. 17c, and regrown in the furnace using the short end as a seed. If regrown successfully the specimen could then be removed from the crucible and the part with the suitable orientation retained. In fact, even if all the specimen melted, the desired orientation was obtained, showing that some "memory" of the orientation must be retained by the oxide film.

3.1.3 Specimen "ends"

Since all attempts at growing zinc crystals with thicker ends were unsuccessful, it was necessary to solder ends on to each specimen for gripping in the tensile machine.

Fig. 18 shows a crystal, clamped in a split graphite crucible. A small gas flame was used to melt solder on to the zinc contained in the small cup at the top of the crucible. This was carried out for both ends of the specimen. By clamping the specimen very lightly (but for the support it would have slipped through the crucible) it was possible to put neat ends on the crystals with no more damage than that caused by normal careful handling. The specimens were then cleaned and polished.

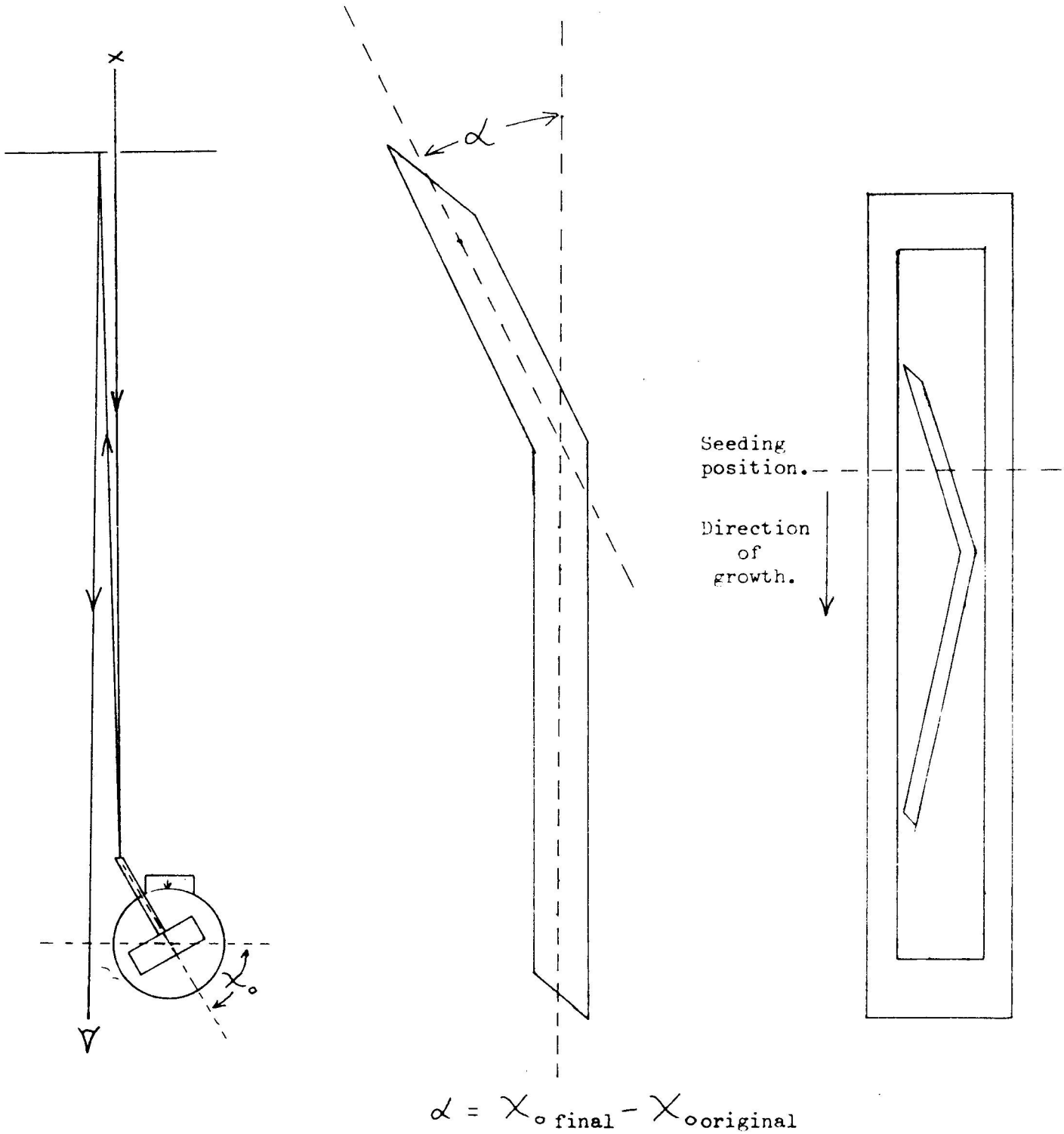
x
α
Seeding
position.
Direction
of
growth.
χ_o
$\alpha = \chi_{o\,final} - \chi_{o\,original}$
(a)
(b)
(c)

Figure 17.

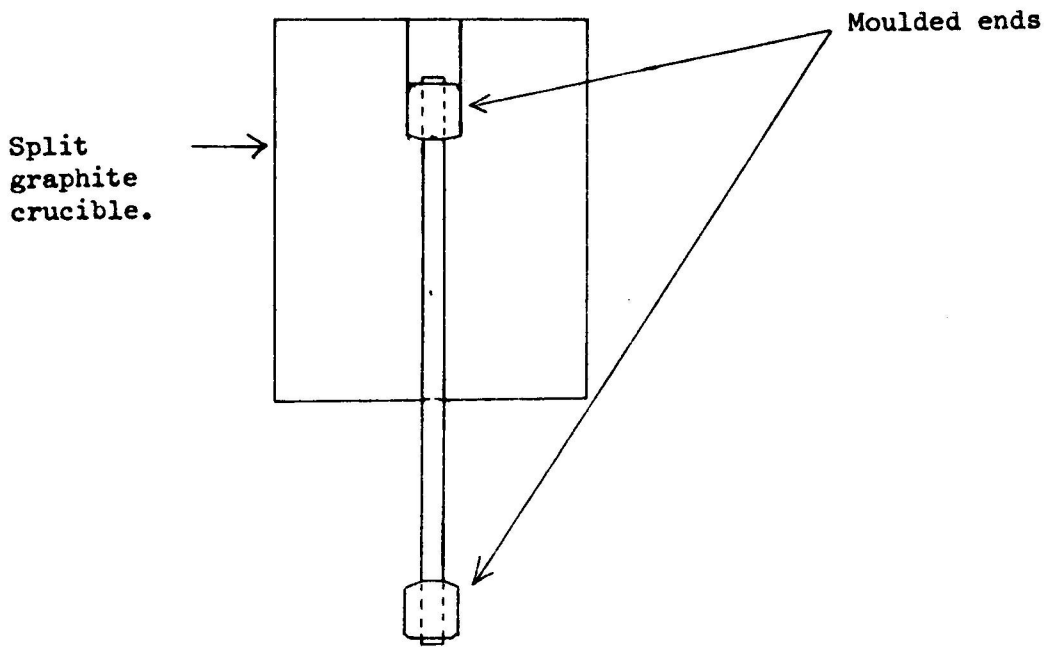

Figure 18.

3.2 Straining Machine

3.2.1 General construction

A Polanyi type of testing machine was constructed to subject the crystals to the necessary deformation. The basic form is shown in Figs. 19 and 20. The body was manufactured by the Newpark Engineering Co. Ltd. to specification. Struts "a" of Fig. 19 were machined with the shoulders accurately spaced to ensure that the sliding frame was rectangular when assembled, thus ensuring that the phosphor-bronze bushes "b" would run smoothly on the chromium plated uprights "c".

A precision thread "d" of 20 turns per inch is anchored in the sliding frame and vertical movement introduced by the nut "e", whose housing can rotate on two ball races, one taking the thrust. This nut is rotated by the worm gear "f". An NBD motor-generator type 126/54451, "a" of Fig. 20, is used to drive the worm via a series of gear boxes, "b" and "c", allowing reduction ratios from 108/1 to 5832/1. The motor generator is controlled by a Servomex Unit MC43, allowing speeds varying between 0 and 6000 R.P.M. The rate of revolution of the motor generator can be read on a built-in meter, correct to 1.5%. Variation in mains voltage up to 7% is compensated for by the unit.

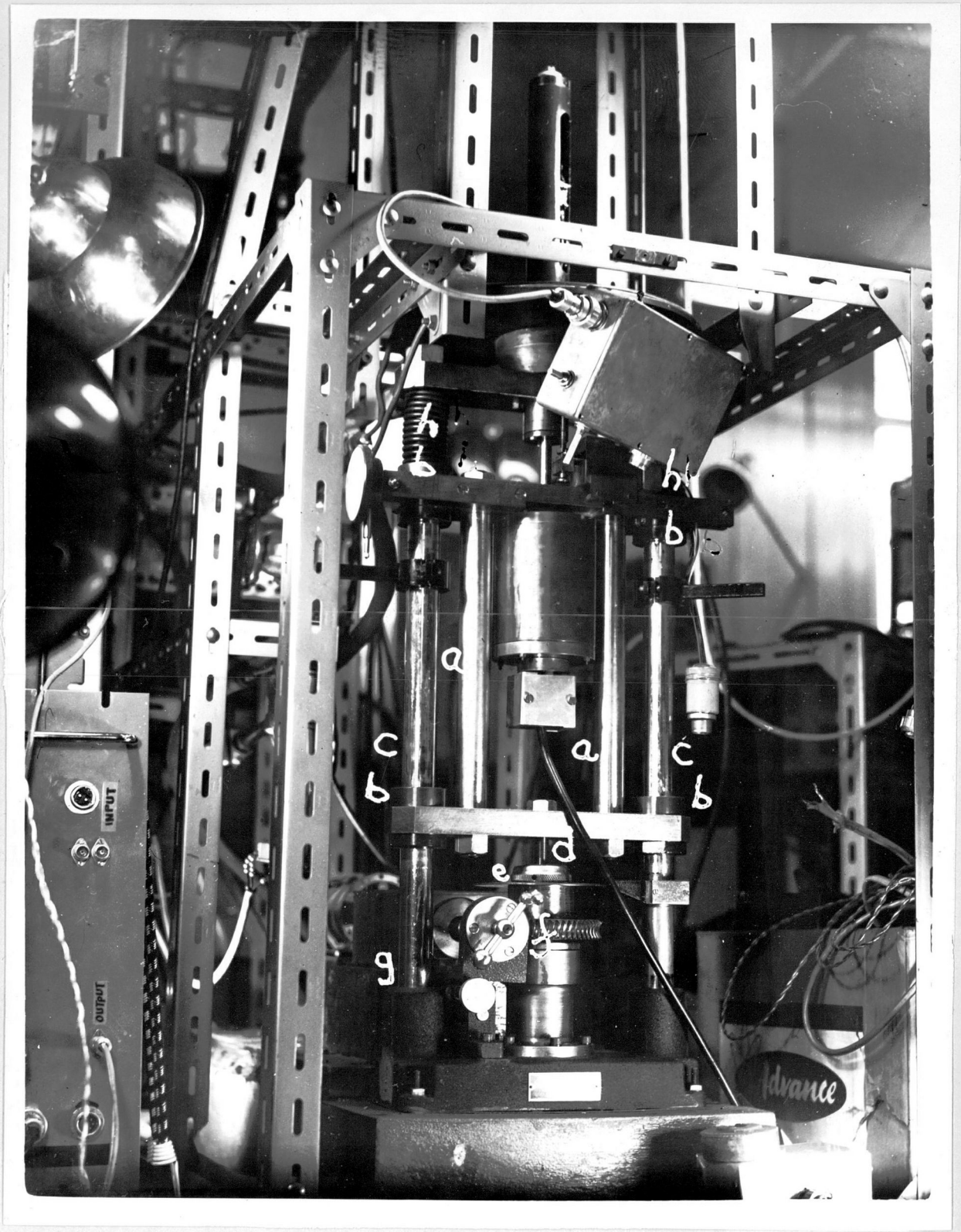

Figure 19.

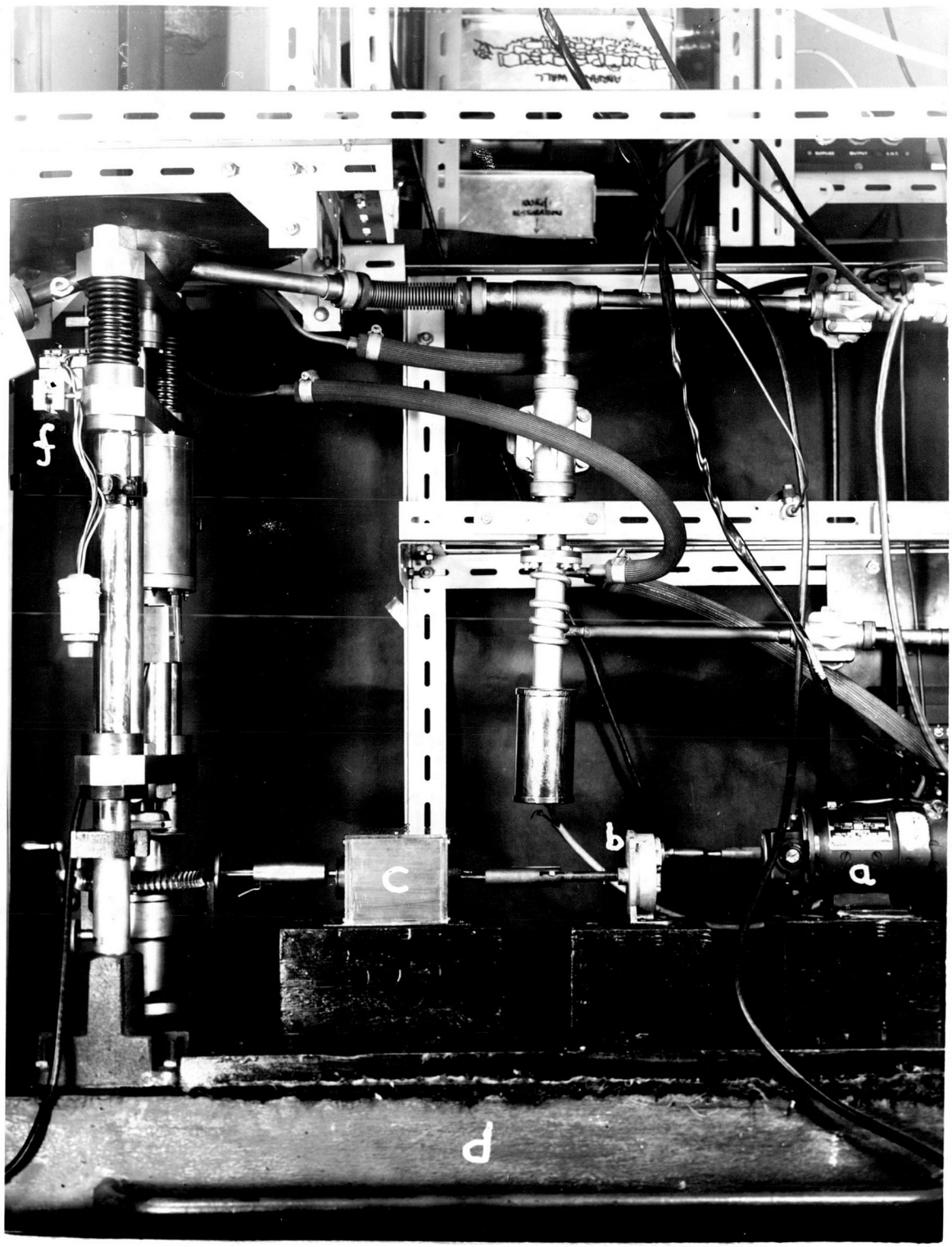

Figure 20.

The machine is bolted to the concrete block, "d" of Fig. 20, which in turn rests on a felt pad on a specially constructed part of the laboratory floor. This consists of a concrete block separated from the rest of the floor, which rests on a rubber mat placed in the foundations of the building. A wooden slab and a felt pad separate the motor and gear box from the rest of the machine.

3.2.2 Crosshead construction

Fig. 21 is a drawing of the crosshead of the tensile machine. The double "O-ring" seal "a" allows the working section to be evacuated but does not interfere with the rod connecting the specimen's lower grip, which is contained in the tube "b", with the stress measuring beam, which sits in the brass cylinder "c". The tube "b" is constructed in Nimonic 75 with cut-outs as shown, which give access to the specimen grips. The tube which carries the electric leads into the working section is not shown in the drawing but it can be seen at "e" in Fig. 20. The leads pass through a neoprin seal at the end of the tube.

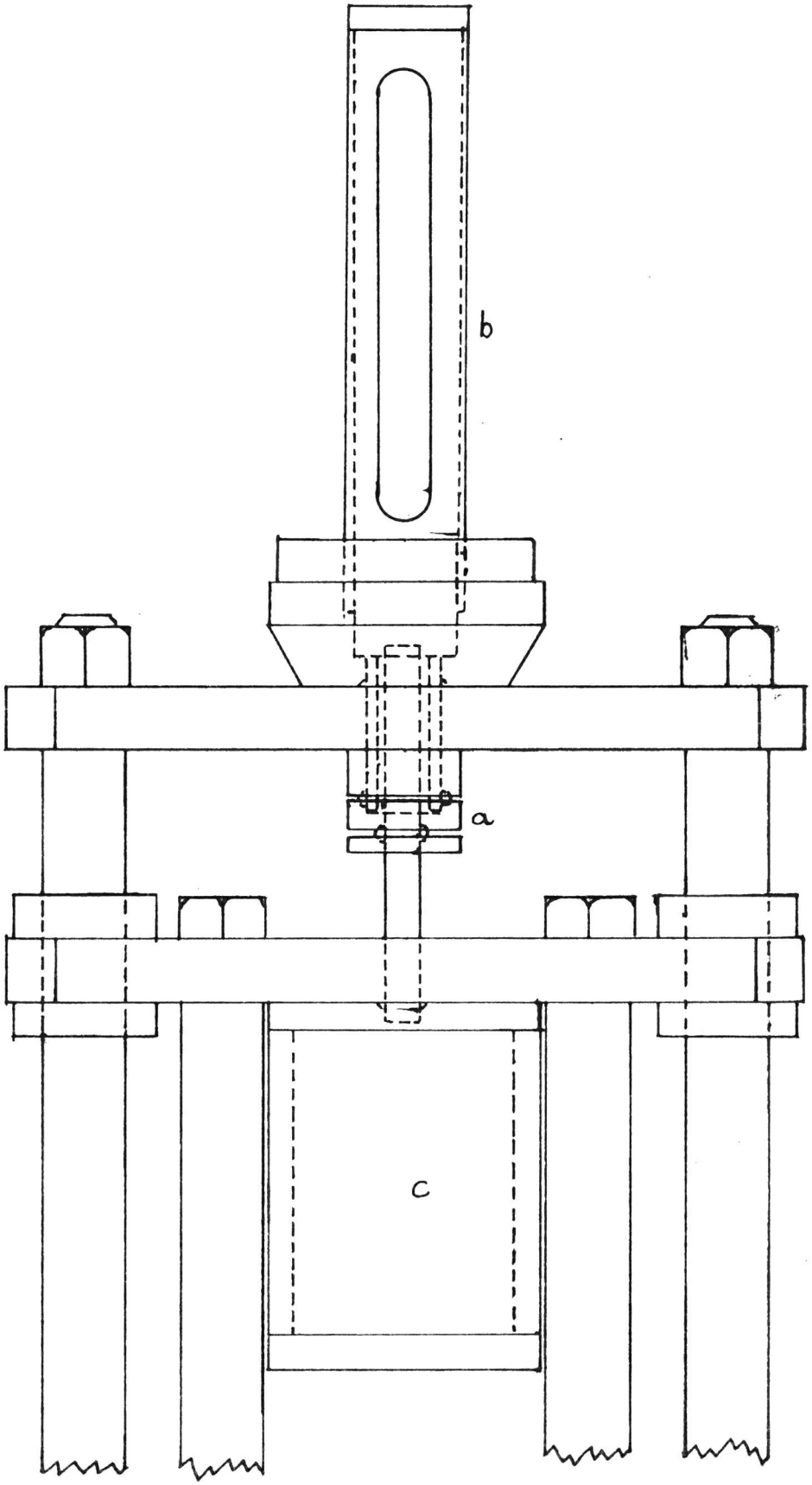

Figure 21

3.2.3 Performance of the basic testing machine

The smoothness and linearity of the motion of the testing machine was examined by positioning dial gauges at positions "g" in Fig. 19 and an electrical strain gauge bridge at position "f" in Fig. 20. This bridge consists of a spring steel cantilever beam with Tinsley wire strain gauges mounted, two on the top surface and two on the bottom surface. The tip of the beam is connected to the centre of the upper metal strut "d" of Fig. 21 and the clamped end to the moving crosshead. Since the strain gauges were attached to the beam at the position of maximum curvature, that is at the clamped end, this is a sensitive monitor of the crosshead position over a long range of movement (about 1.5 cm.). Using a similar circuit to Fig. 24 movements of the crosshead down to less than $\frac{1}{4}\mu$ could easily be followed.

With these instruments it was found that the motion of the machine, as it was delivered, was not linear. In other words during one rotation of the worm gear the crosshead did not move at a constant rate. This was overcome by grinding the worm gear with carborandum powder until the "high spots" were removed. To ensure that the positions of the worm and gear were fixed at the time of the grinding and during all subsequent occasions, a

block, "g" in Fig. 19, was placed in a machined niche between the base casting and the movable worm housing. (This was movable to allow disengagement of the worm and gear for rough setting of the crosshead).

A major defect in the machine originally was an aptitude for "walking" of the crosshead down the chromium uprights. This was easily detected on the dial gauges. In other words, one side of the crosshead tended to move several microns down the upright on that side to be followed a few seconds later by the other side. This was particularly evident at slow speeds. The effect was completely eliminated by introducing the springs "h" of Fig. 19 above the crosshead. These required a force of about 100 lbs. to compress them 1". Since they are normally compressed about two to three inches the motor now only acts to release the spring pressure.

The method of mounting of the testing machine seems to be effective in protecting the machine from any vibrations or shocks. Even jumping on the floor of the laboratory, next to the machine, produces no measurable signal from any of the stress or strain measuring instruments on it.

3.2.4 Gripping the specimens

Various designs of grips were tried, the most effective being that shown in Fig. 22. Since this does not allow rotation of the specimen it is by no means ideal, but the most important consideration is that of good electrical contact. Provision is made in the lower grip for the clamping of a "dummy" specimen "a". The specimen "b" and the dummy are firmly clamped in the lower grip and the specimen only in the upper grip by means of the screws "c". The metal strip "d" is used to protect the specimen from distortion while it is being placed in the testing machine. Taper pins "e" firmly attach the grips to the top of the working tube and to the stress measuring beam, which is attached to the silver-steel rod "f". Electrical leads are taken to the specimen at the upper grip at position "g" and to the dummy at the small block "h", this being separated from the upper grip by an air space. The upper grip is insulated from the stainless steel cap "i", which sits in a recess in the top of the working tube, by means of a series of ceramic washers "j".

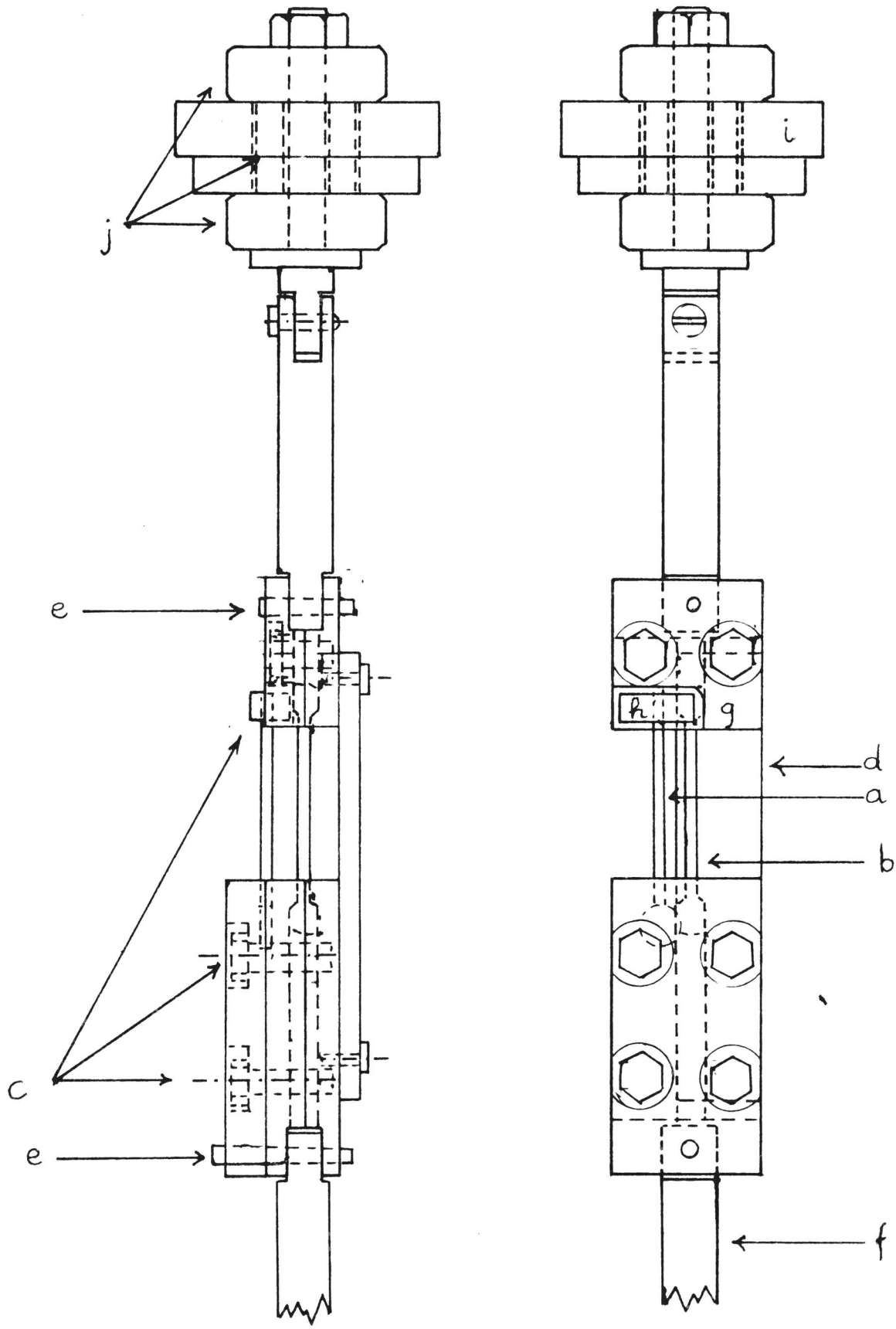

Figure 22

3.2.5 Measurement of strain

In addition to the instruments used to measure the movement of the cross-head, it is possible to measure the strain at the specimen. This can be monitored by attaching a differential transformer to one grip and a special core, mounted on a screw, to the other. The transformer and core were manufactured by Schaevitz Engineering, the type being 005 MS-L. A differential transformer consists simply of an arrangement of primary and secondary coils with some method of altering the amount of flux linkage between them. In this case, two primary coils are placed on either side of the secondary coil, colinear with it. The core can move up and down a hole through all three. A signal of 20 Kc/sec is supplied to the primary coils from a Tectronix "Q" unit and the signal from the secondary fed back to the "Q" unit where it is amplified and detected before being displayed on the screen of an oscilloscope.

The maximum sensitivity of this arrangement is such that a relative movement between transformer and core of .1μ can be detected. In practice it is difficult to use since only a very small range of movement can be tolerated and frequent balancing is necessary.

3.2.6 Measurement of Stress

Because of the difficulty of measuring the strain at the specimen, especially at temperatures above room temperature, when the differential transformer could not be used, (being insulated with pitch) it was decided that a very sensitive stress measuring beam would be the best means of detecting jump deformation of the specimen.

Conventional wire grid strain gauges have a gauge factor (defined as $\Delta R/R / \Delta \ell/\ell$ where R and ℓ are the resistance and length of the gauge wire and ΔR and $\Delta \ell$ are the corresponding changes in these quantities) no higher than 2. It was decided, therefore, to employ the silicon strain gauge elements manufactured by Century of Tulson, obtainable through Cossar Instruments in this country. These consist of silicon single crystals, 20μ thick by 1 cm long by .5 mm wide, into which some boron has been diffused. The elements are then "n" type semiconductors, whose resistance is extremely sensitive to any applied strain, the gauge factor being 140.

Since these strainistors are very fragile they can not be used in an unbonded type of transducer. They were, therefore, bonded to a clamped beam in the pattern shown in Fig. 23. For an upwards deflection of the centre of the beam, in

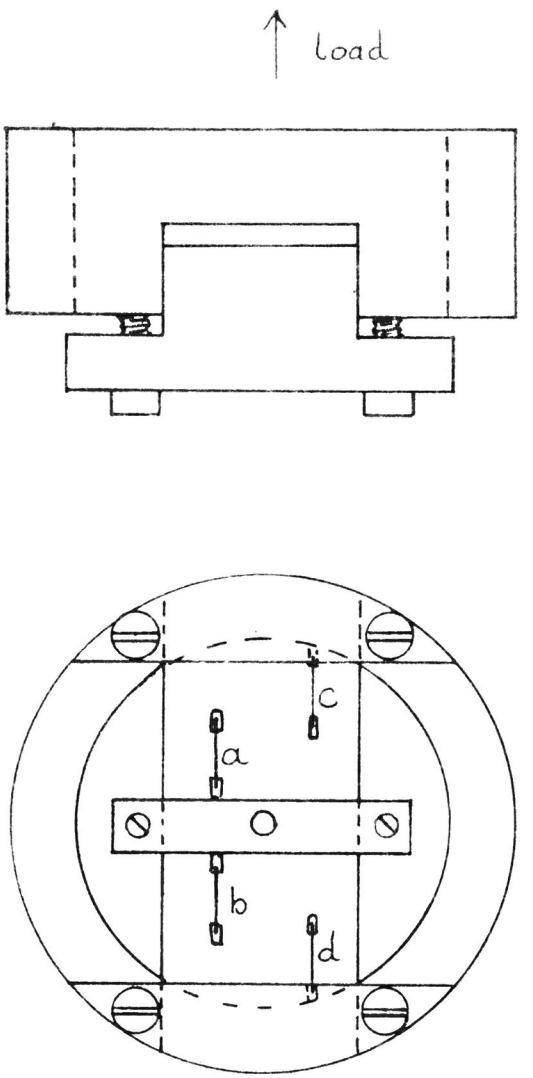

Figure 23

this case corresponding to a tensile load on the specimen, strainistors "a" and "b" are compressed and "c" and "d" stretched. The recommended adhesive not being available for bonding the strainistors to the beam, Araldite was used, proving satisfactory.

The beam was machined from a low hysteresis aluminium alloy, Hiduminium 72 to dimensions 4.9 cm x 2.54 cm x .35 cm. This, by calculation, deflects $\frac{1}{2}\mu$ for a load of 1 Kg. With the strainistors placed as shown the linear extension or compression of any one is $\frac{1}{6}\mu$. Since the maximum strain they can take without damage is 17μ, they are, therefore, always worked well within their limit.

Although matched in resistance before bonding, it was found that the strains imposed by the setting adhesive caused various changes in resistance, of the order of a few ohms, in the individual strainistors. The circuit of Fig. 24 compensated for this, as well as giving a method of balancing the bridge roughly over large variations in load. The output from the bridge can be fed either to a Tectronix "Q" unit or to a Sefram recording galvanometer. A measuring potentiometer is normally used in conjunction with the recorder for backing-off purposes.

The sensitivity of the transducer is compared

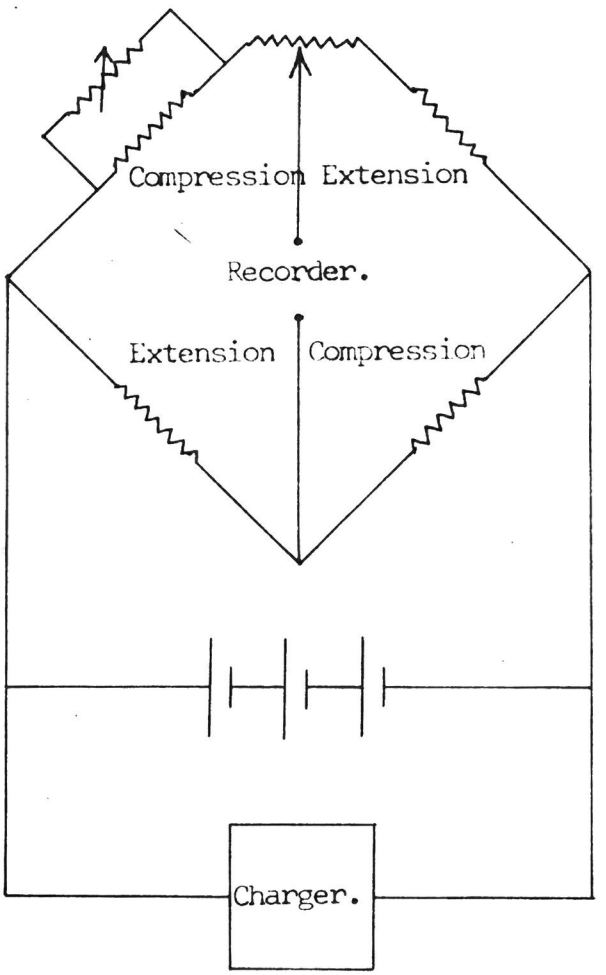
Compression Extension
Recorder.
Extension Compression
Charger.

Figure 24.

with other, more conventional types, in Table 4. In each case the transducer is used in conjunction with a Tectronix "Q" unit plugged into a Tectronix "555" oscilloscope. Columns 1 and 2 refer to a "soft" and a "hard" beam of similar construction to the strainistor beam but using Tinsley wire grid strain gauges. Column 3 refers to a UF2 transducer manufactured by J. Langholm Thomson. It gains its sensitivity by using an unbonded strain gauge element. the 4th column refers to the strainistor beam.

Since the bandwidth of the "Q" unit is 6Kc/sec. a deflection of the beam lasting longer than .2m sec. and of magnitude greater than 10^{-6} cm could easily be detected by the strainistor beam. This is slightly less than the variations of stress on a specimen due to the running of the testing machine.

When the transducer is used with the recording galvanometer the effective sensitivity is the same but the bandwidth is, of course, much less.

3.2.7 Temperature control

It had been experienced with an earlier machine that the presence of a furnace on a Polanyi type of testing machine could impair the performance by distorting the various members.

	1	2	3	4
Load	50 gm.	1 Kgm.	50 gm.	17 gm.
Deflection of beam	.3μ	.6μ	.02μ	.01μ
Deflection of C.R.O. beam	1 cm.	.8 cm.	.4 cm.	.8 cm.

TABLE 4

As seen in Fig. 25 this has been avoided in the present machine by keeping the working tube outside the main framework and bringing the furnace down on to a water-cooled plate ("i" in Fig. 19) as shown.

The temperature of the furnace can be controlled using a conventional arrangement, employing a Sunvic RT2 proportional controller with a platignum resistance thermometer. The controller is used to switch a resistance in and out of the furnace circuit, in a sequence which keeps the temperature constant. Large variations in mains voltage (up to 15%) can be coped with by the controller. Using a Platinum - Platinum/ -13% Rhodium thermocouple to measure the temperature, no variation in temperature could be detected.

Although designed for testing at room temperatures or above, provision was made for working at lower temperatures using the lagged jacket shown in Fig. 26. This fits over the working tube. When this is filled with liquid nitrogen the temperature of the specimen is a fairly constant -70°C. Liquid nitrogen must be regularly pumped from a dewar into the jacket, however, since the rate of loss is high.

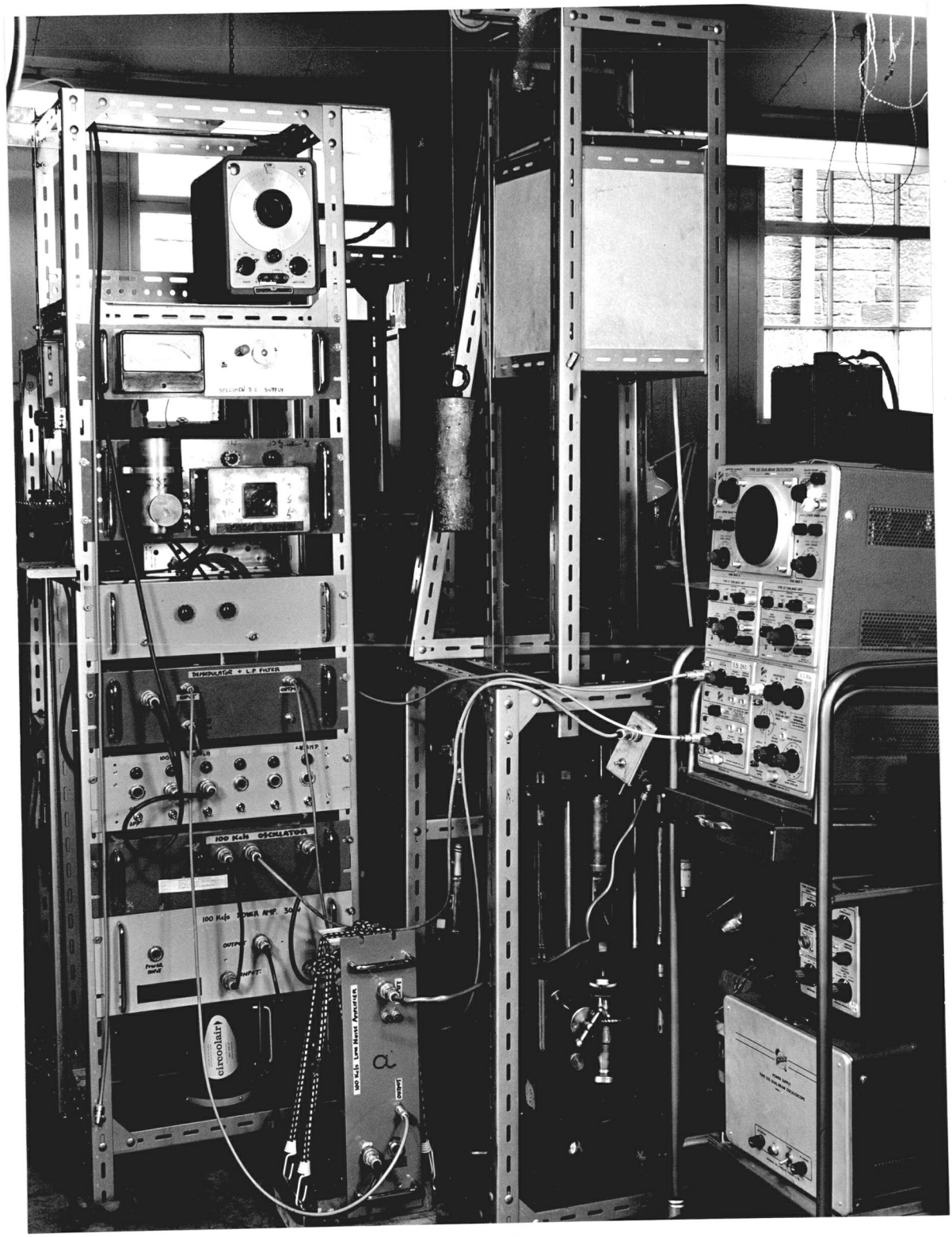
DEMODULATOR + L.P. FILTER
100 Kc/s OSCILLATOR
100 Kc/s POWER AMP. 30W
100 Kc/s Low Noise Amplifier
circoolair

Figure 25.

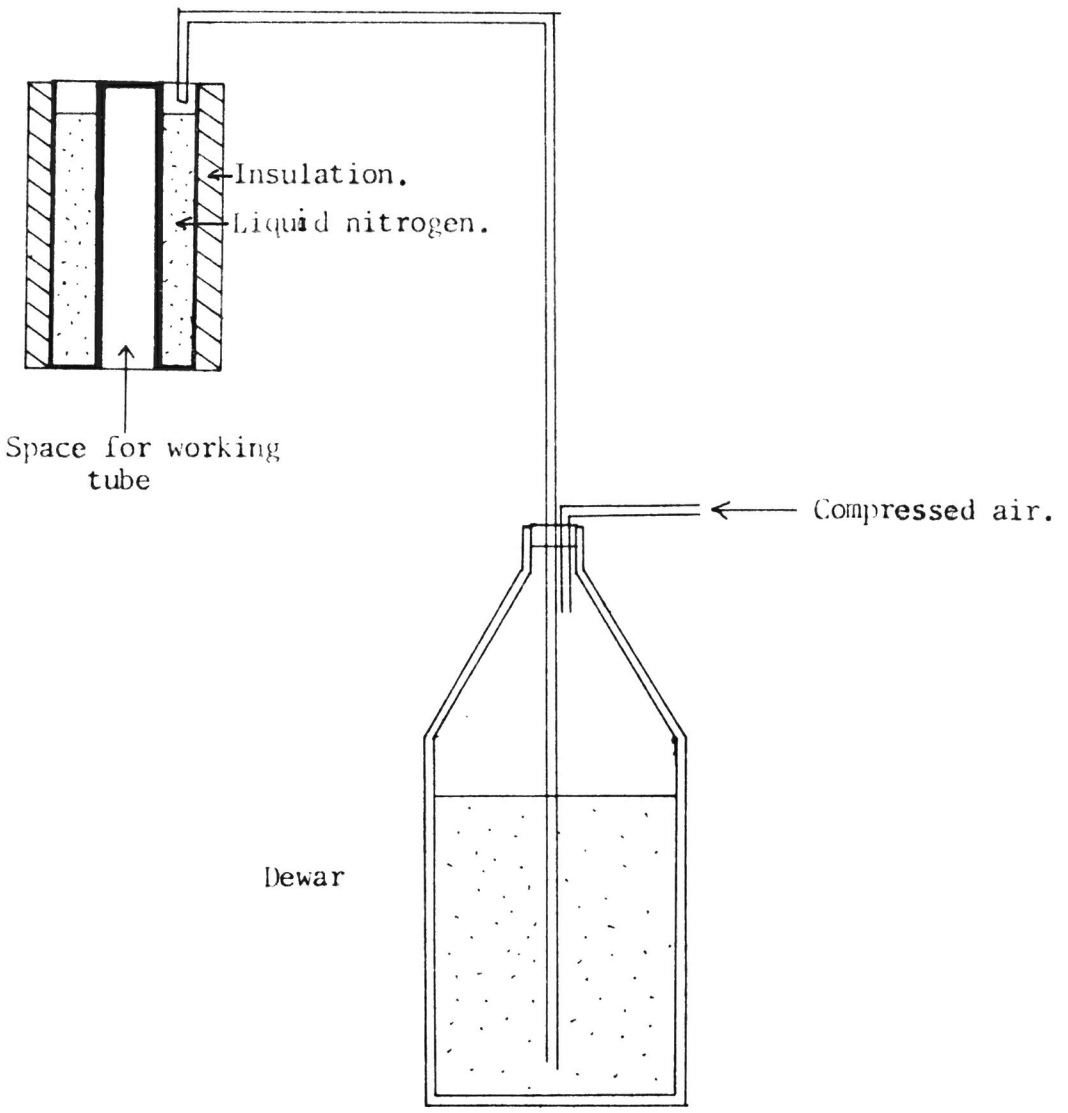
Insulation.
Liquid nitrogen.
Space for working tube
Compressed air.
Dewar

Figure 26.

3.2.8 Vacuum system

The whole system is capable of being evacuated as is seen in Fig. 20. A Metrovac DR1 rotary pump combined with an Edwards type 102 diffusion pump can pump the system down to a pressure of about 5×10^{-6} mm. Hg. The pressure can be measured using an Edwards ionisation gauge and control unit. Since the pumping system is not mounted on the concrete block, it is joined to the testing machine by a flexible vacuum tube to avoid the transmission of vibrations. A needle valve, which can be used to bleed gas into the system, is included.

3.3 Resistance Measurement System

3.3.1 Preliminary considerations

Since the present experiment involves the measurement of small, fast changes in resistance, the main problems in the design of suitable measuring equipment are the following.

1. A high gain is necessary for the presentation of the pulses on an oscilloscope screen.
2. The noise level of the electronics must be kept well below the amplitude of the pulses.
3. The bandwidth of the system must be adequate to follow the pulses.

The first of these problems is the most easily solved. A few amplifier tubes can easily be linked up to give a gain of 10^6 or so, which is adequate for the input of even the most unsophisticated oscilloscope.

The difficulties arise when the last two points come under consideration. The noticeable noise will be that which arises at the grid of the first amplifying tube. It is usual to compare the "shot" noise produced in a vacuum tube with what is referred to as its equivalent resistance, R_{eq}. One can then calculate the noise level in the tube as being equal to that of the thermal noise produced in a resistance R_{eq}, at room temperature, placed at the grid of the tube. The noise level can then be written in the usual form

$$E^2 = 4kT \int_{f_1}^{f_2} R \, d \, f \quad ,$$

where E^2 is the square of the effective value of the voltage components lying between the frequencies f_1 and f_2.

If R_{eq} is assumed to remain constant over the frequency range f_1 to f_2 then

$$E^2 = 4kT \, R_{eq} \, (f_2 - f_1) \quad .$$

R_{eq} has been calculated by North[50] for a space charge limited triode and for a pentode.

He has demonstrated that the noise energy from a pentode is from three to five times greater than that from a triode at the same gain. It would seem advisable, therefore, that the first stage of the amplifier should be based on a triode circuit.

Since the total noise produced can be seen to be dependent on the pass band of the amplifying system, this must obviously be limited to keep the noise level down. This can be seen to be at the expense of the third point in the design considerations.

An amplifier fulfilling the necessary conditions could be designed either as a D.C. amplifier with a pass band of 0c/sec. to 2 Kc/sec or as an intermediate frequency amplifier. In the second case a suitable carrier frequency current would have to be passed through the specimen. Resistance changes in the specimen would then cause the amplitude of the signal across the specimen to vary and would also alter the frequency spectrum of the carrier frequency. The information would then be contained in the "side bands" grouped on either side of the carrier frequency. The pass band in this case, therefore, must be 4 Kc/sec if both side bands were to be included. By using a single side band mode of operation, however, the pass band could be cut to 2 Kc/sec without loss of information.

The second method has three main advantages.

1. The design is simpler.

2. Some application could be made use of the "skin" effect by examining the resistance changes of the specimen according to depth.

3. A step-up transformer can be used at the input to the amplifier without introducing distortion to the signal.

This third consideration is probably the most important because of the very small signals involved in the experiment.

Initially, experiments were attempted with an old communications receiver type R1155A, of which only the intermediate frequency and detector stages were used. This employed a carrier frequency of 565 Kc/sec, supplied by the oscillator of Fig. 27. Unfortunately the noise level in the I.F. (intermediate frequency) stage was of the order of several microvolts and tended to mask any detail in even the largest pulses.

After further development work an amplifier working at 465 Kc/sec with a noise level of about $\frac{1}{10}$ microvolt emerged. The pass band, however, was less than 1 Kc/sec. It was also felt that the skin depth at this frequency, .2 mm, was too small to give a fair representation of the change of resistance of the whole specimen.

The design which shall now be discussed has

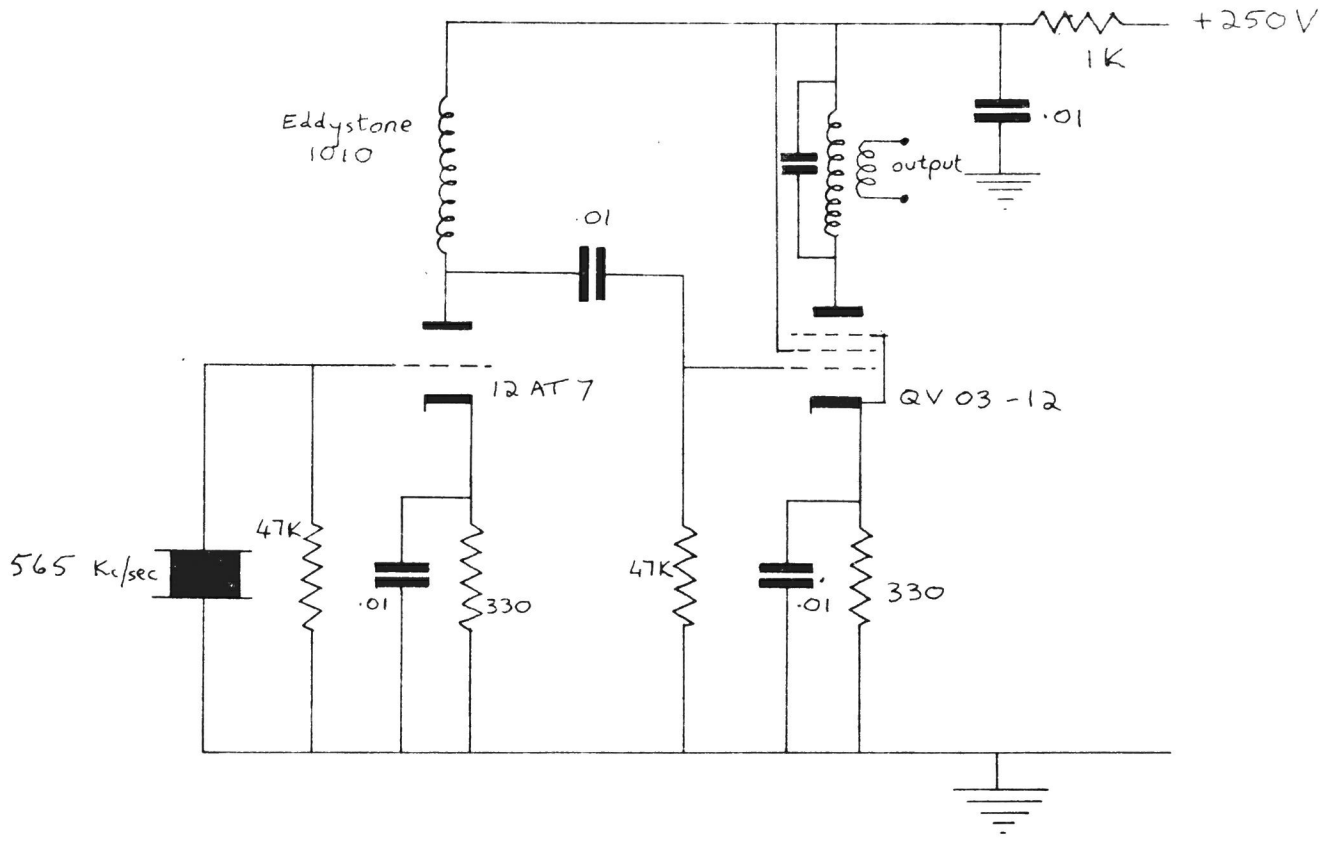
+250V
1K
.01
Eddystone
1010
output
.01
12 AT 7
QV 03 -12
565 Kc/sec
47K
.01
330
47K
.01
330

Figure 27.

been the one used in the present experiment. It employs a carrier frequency of 100 Kc/sec, giving a skin depth of .4 mm.

3.3.2 Outline of the system

Fig. 28 is a block diagram of the measuring system. An oscillator "a", working at 100 Kc/sec, feeds a signal to a power amplifier "b". This, in turn, supplies a current of several amps to the bridge "c" containing the specimen. The out of balance signal from the bridge is then fed to the low noise amplifier "d" and "e". The carrier frequency is then subtracted by the detector "f" and only the modulation displayed on the oscilloscope "g".

3.3.3 Design of the oscillator

The oscillator was built to a design recommended by the Quartz Crystal Company, with several modifications and additions, for use with their crystals. The circuit is shown in Fig. 29.

At 20°C this circuit, using a crystal rated at 100.0 Kc/sec should be correct in frequency to within .01%. By varying the capacitance "A" a slight variation in frequency can be obtained.

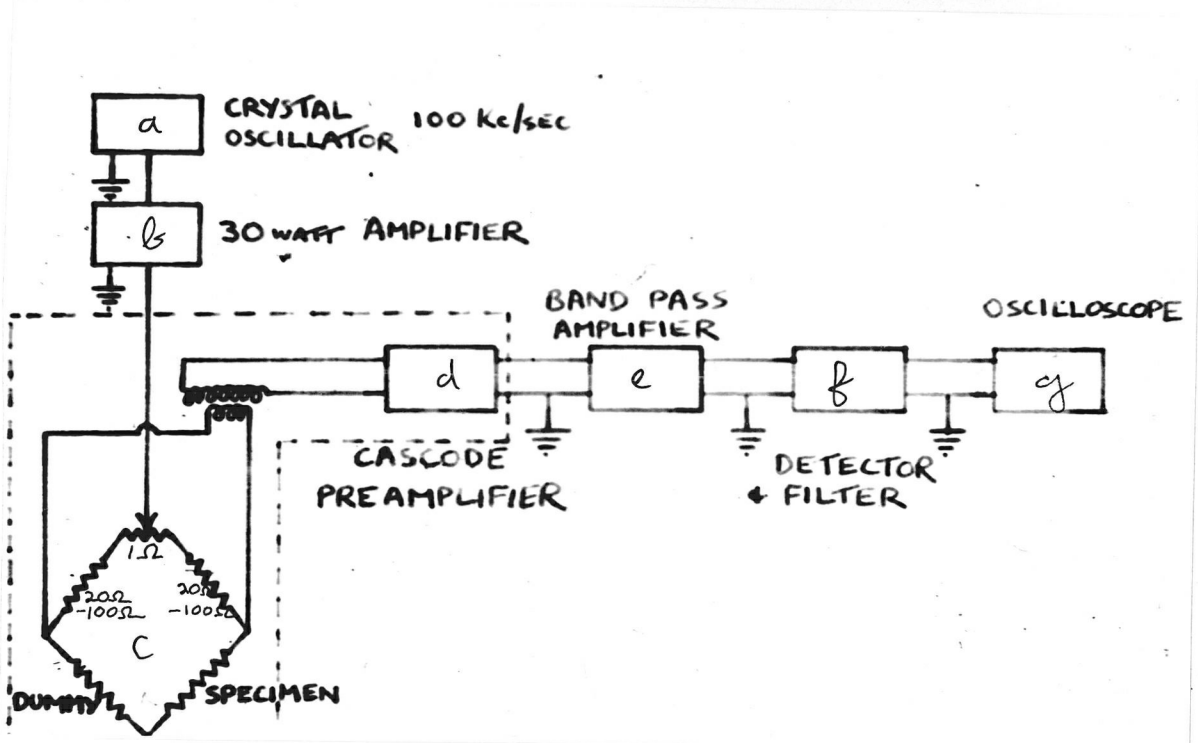
a
CRYSTAL OSCILLATOR
100 Kc/sec
b
30 WATT AMPLIFIER
BAND PASS AMPLIFIER
OSCILLOSCOPE
d
e
f
g
CASCODE PREAMPLIFIER
DETECTOR & FILTER
1Ω
200Ω
100Ω
200Ω
100Ω
C
DUMMY
SPECIMEN

Figure 28.

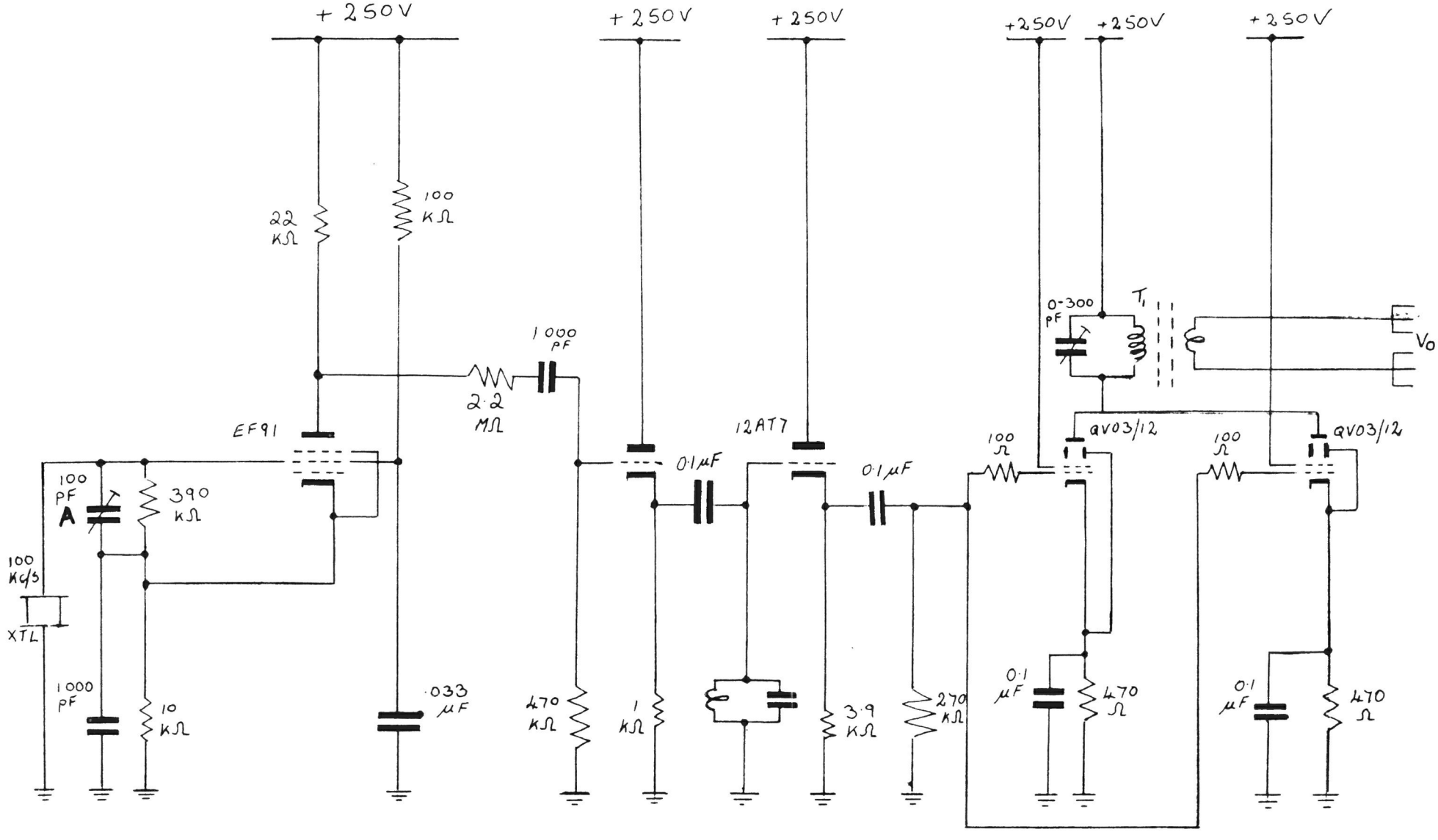

100 Kc/s OSCILLATOR

Figure 29.

Since the shape of the signal was found to be very dependent on the loading conditions a cathode follower stage was included after the basic oscillator. This consists of the two halves of a 12AT7, one used as a filter, and the other as an extra guarantee against loading the oscillator. The filter was included to improve the shape of the signal.

A current of at least one ampere through the specimen and dummy specimen is required. In Fig. 28 it can be seen that this must also pass through two 50 Ω resistors. The minimum power requirement from the oscillator is, therefore, 25 watts.

This is achieved by passing the signal through the power amplifier whose circuit is shown in Fig. 30. This consists of a push-pull amplifier stage made up from two 5B/254M vacuum tubes. The output transformer consists of windings on a cylindrical ferrite rod, which was used because of the bulk of the wire required for the output winding. Control of the power fed into the bridge is effected by a potentiometer control at the input of this amplifier. Up to 30 watts can be fed into the bridge using this system.

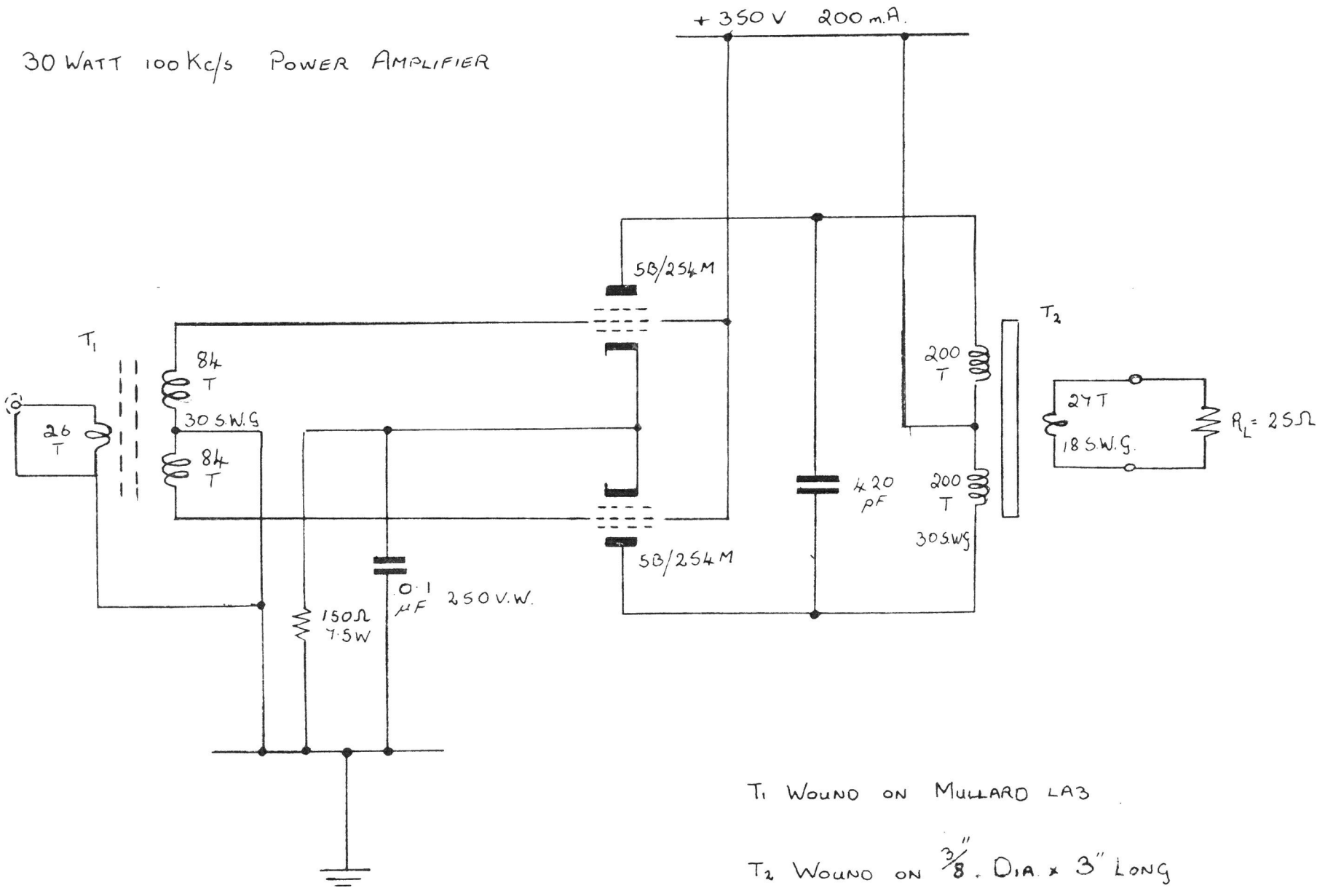
30 WATT 100 Kc/s POWER AMPLIFIER
+350 V 200 m.A.
5B/254M
T1
84 T
30 S.W.G
26 T
84 T
150Ω 7·5W
0·1 μF 250 V.W.
5B/254M
420 pF
T2
200 T
200 T
30 S.W.G
27 T
18 S.W.G.
RL = 25Ω
T1 WOUND ON MULLARD LA3
T2 WOUND ON 3/8". DIA. x 3" LONG
FERRITE ROD

Figure 30.

3.3.4 Specimen bridge

The proper design of a radio frequency bridge involves special techniques. Dye and Jones[51] have demonstrated the suitability of a Schering bridge, with Wagner earthing, for frequencies up to one megacycle. Many other designs have been successfully used, all with one thing in common - very elaborate shielding and careful lay-out has to be provided. This is necessary because at frequencies above 3000 cycles/second the inter-bridge element capacities become important.

The present experiment, however, has not been designed to measure accurately the magnitude of the resistance changes. In fact, with the available bandwidth, it is doubtful if the peaks of the transient parts of the resistance changes could be observed in any case. The space available for the bridge network is also very limited, being confined to the working tube of the testing machine. In this case, therefore, the bridge is extremely simple.

The grips, which have been described, hold two similar specimens, one under tension, the other a dummy. The grip which clamps both specimens is earthed. The current is fed into the unclamped end of the dummy specimen and to the tensile specimen via the upper grip, which is insulated.

The current reaches the working tube by a two strand screened cable 2 mm. in diameter. Since the insulation consists of packed alumina powder, this cable is unaffected by high temperatures. The 50 Ω resistances in series with the specimens are mounted outside the working region in the box containing the 1 Ω balancing potentiometer seen in Fig. 28.

An identical screened cable brings the potential leads into the two specimens.

With this system it was possible to keep the out of balance voltage down to about 10^{-4} volts. This is sufficient to avoid saturation of the low noise amplifier.

3.3.5 Low noise amplifier

In the initial considerations it was pointed out that a triode has a lower equivalent noise resistance than a pentode at the same gain. Tuned voltage amplifiers, however, usually employ pentodes since they have negligible grid-plate capacity, give an effective "Q" of the amplifier which is almost that of the resonant circuit, and give more gain per stage than a triode.

With a triode the grid-plate capacitance is large, causing regeneration. This must, therefore be neutralized at every stage. If a triode is to

be used for the first stage of the amplifier, therefore, a cascode circuit must be employed. This gives the characteristics of a pentode, while retaining the low noise level of a triode.

The triodes used are low noise level, low distortion S.T.C. valves type 3A/167M. These were incorporated in a circuit recommended in an S.T.C. applications report, modified to allow the use of a step-up transformer at the input. In practice, this stage proves to be critically dependent on lay-out. Careful shielding as indicated in the circuit of Fig. 31 had to be included to prevent the amplifier going into oscillation.

The shaping of the pass-band of the amplifier was built into the design of the next stage. This is a selective band pass I.F. amplifier built using the design procedure of Belrose[52]. High attenuation outside the desired frequency range and a level bass band within it is attained.

The feature of the design is the inclusion in the cathode circuits of two parallel tuned circuits, one tuned to a frequency above that of the carrier, the other to one below. These supply negative feedback with large attenuation at the resonant frequencies. If the tuned circuits in the anode circuits are over-coupled, causing a trough in the pass band level, then by appropriate

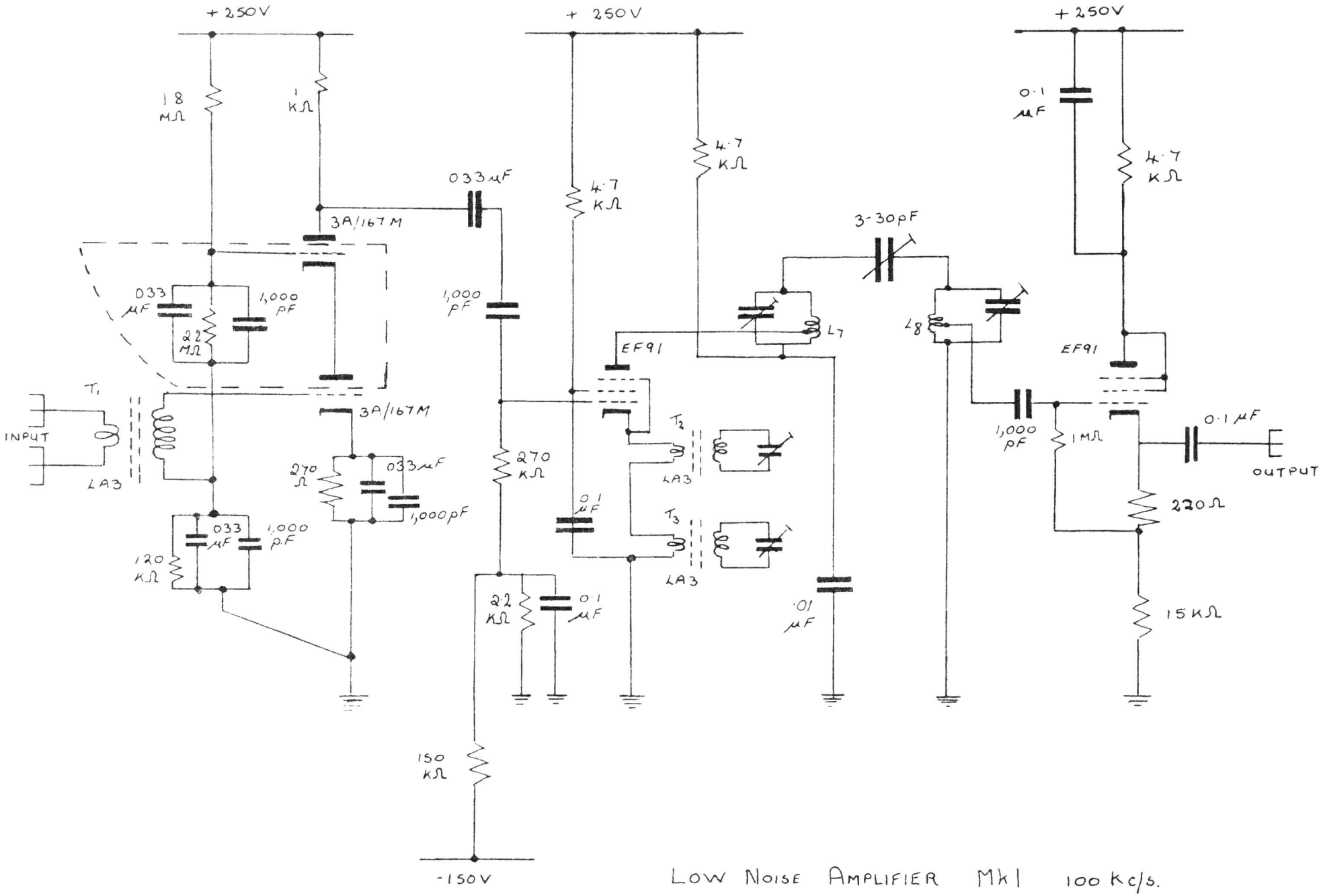

LOW NOISE AMPLIFIER Mk I 100 Kc/s.

Figure 31.

design the overall effect on the amplifier of the combination of the two effects can be that of a level pass band, with sharp attenuation at the chosen frequencies.

This is demonstrated in Fig. 32, where the cathode response curve is plotted on the same sheet as the over-coupled anode response.

The resultant amplifier behaves well in practice, the noise level being in the region of $\frac{1}{100}$ μV and bandwidth being 3 Kc/sec.

3.3.6 Demodulator

Originally a simple diode detector was used to eliminate the carrier frequency before the signal was displayed on an oscilloscope. This, however, introduced distortion. The detector eventually used is that shown in Fig. 33.

The first stage, a CV 138, is used to amplify the signal to approximately 10 volts. The resulting signal is then fed into the grid of an EF 184, causing a variation of the current through the 10K ohm cathode resistor, which is common to the next EF 184. The second EF 184 is normally drawing current, but the resulting swing in the cathode voltage can take it into the cut-off region. By varying the voltage on the grid of the second EF 184, the signal can then be rectified to the

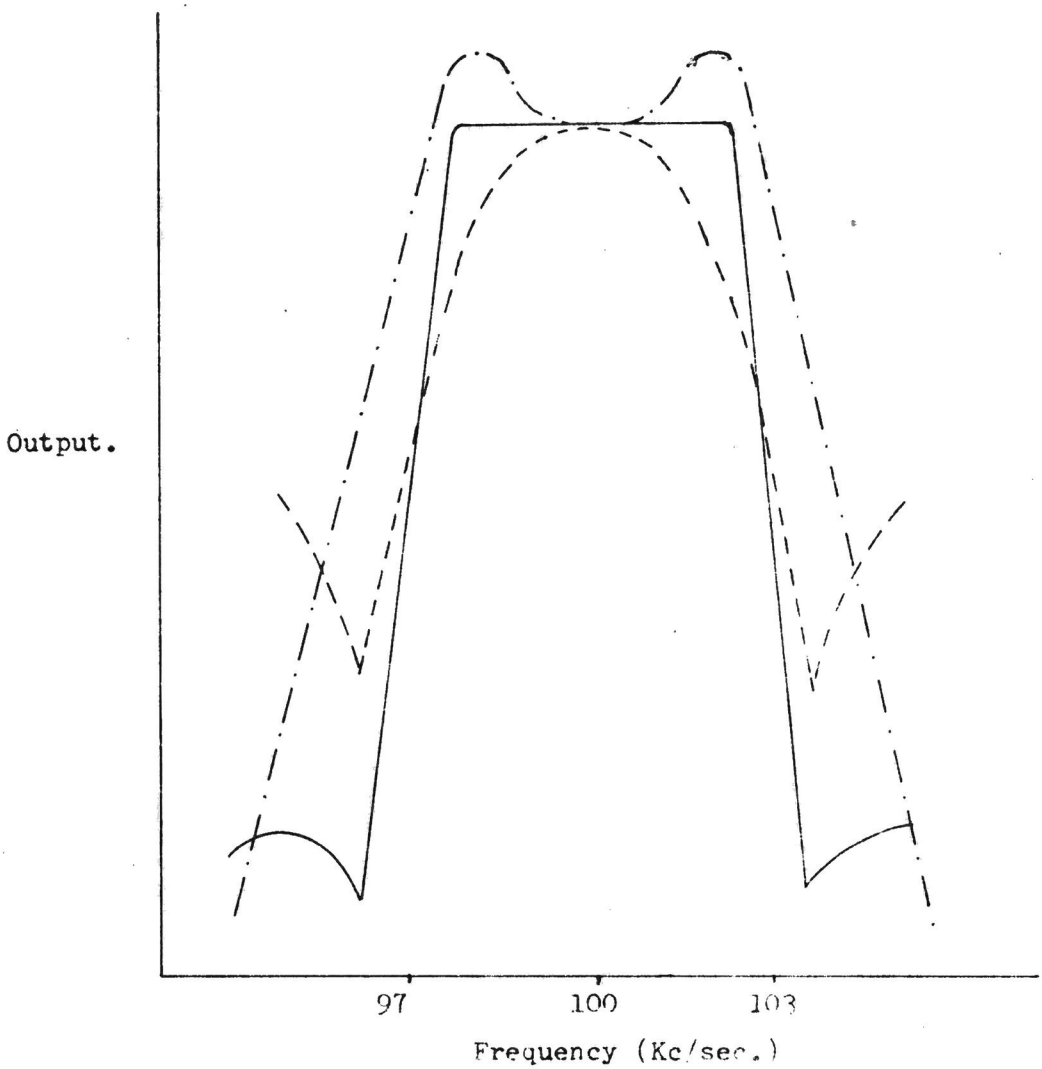
Output.
97
100
103
Frequency (Kc/sec.)
Amplifier response.
Anode circuit responce.
Cathode circuit responce.

Figure 32.

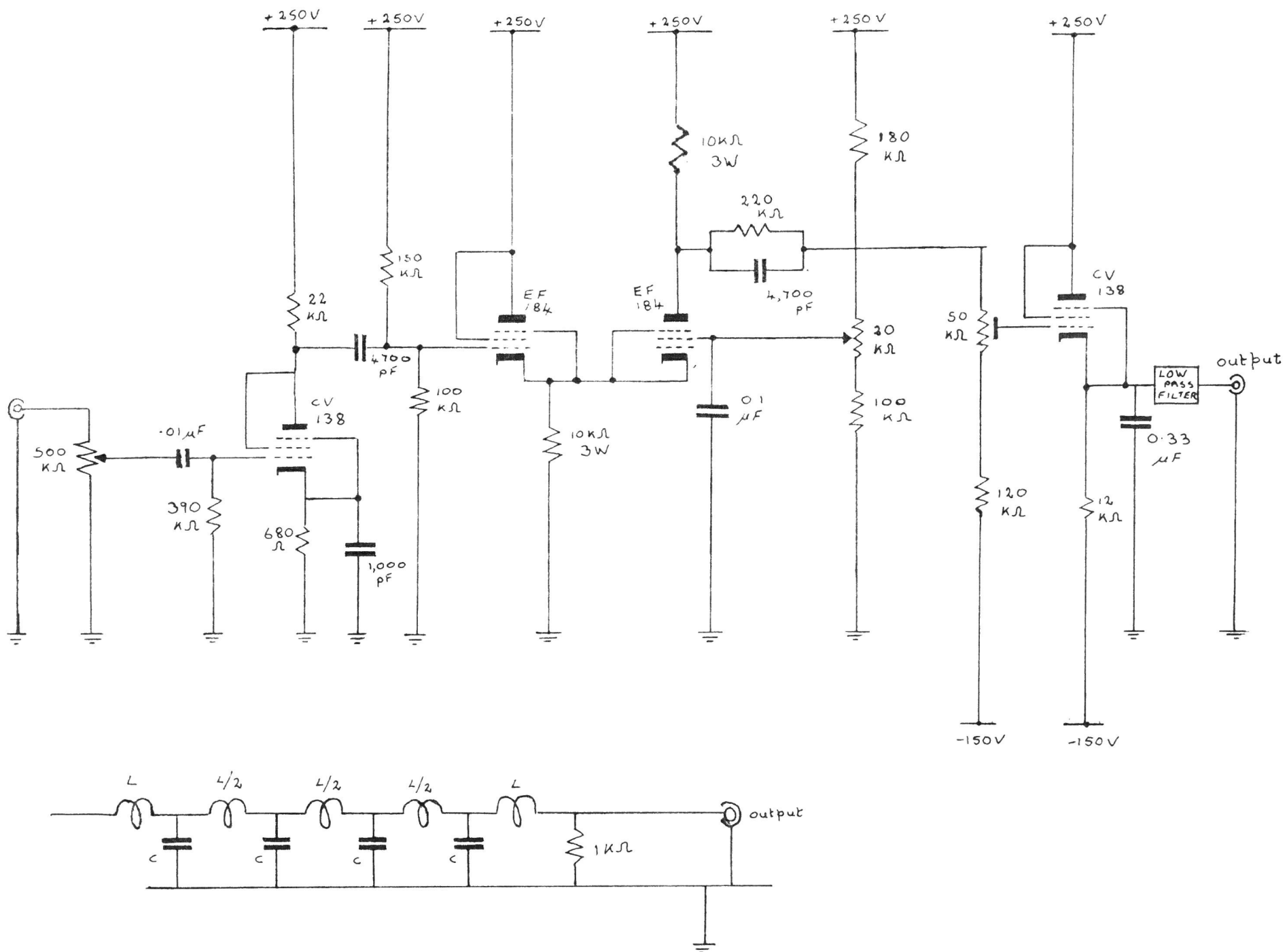
+250V
+250V
+250V
+250V
+250V
+250V
10KΩ 3W
180 KΩ
220 KΩ
4,700 pF
150 KΩ
22 KΩ
EF 184
EF 184
CV 138
50 KΩ
4,700 pF
20 KΩ
100 KΩ
.01μF
CV 138
500 KΩ
390 KΩ
680 Ω
1,000 pF
10KΩ 3W
.01 μF
100 KΩ
LOW PASS FILTER
output
0.33 μF
120 KΩ
12 KΩ
-150V
-150V
L
L/2
L/2
L/2
L
C
C
C
C
1KΩ
output

Figure 33.

required extent.

The signal is then fed through a cathode follower into the properly terminated filter as shown. This eliminates the carrier frequency but allows through all modulation signals up to 3 Kc/sec.

3.3.7 Display

The system described is capable, therefore, of detecting any change of resistance of the specimen greater than 10^{-8} ohms (with one amp. through it), lasting longer than $\frac{1}{3}$ millisecond.

A permanent record of any resistance change of the specimen is obtained by displaying the changes on a Tektronix 555 oscilloscope and photographing them with a Tektronix C12 camera with a Polaroid-Land film back. The camera shutter is left open and the oscilloscope allowed to trigger at some predetermined level.

The gate output from the oscilloscope is used to switch in a solenoid which sets off an electric bell whenever a resistance change is photographed.

3.3.8 Power supplies to electronics

Each section of the electronics is fed from a separate Solartron power pack, AS517 types being

used for the low noise amplifier and detector stages and type AS956 for the oscillator and power amplifier. In addition it was found to be necessary to use 6 volt car batteries for the heater supplies to the low noise amplifier and the detector. These are continuously trickle charged and require very little attention.

CHAPTER 4

4.1 Crystals Exhibiting Jump Deformation

4.1.1 The conditions governing jumping

The parameters determining whether or not any zinc crystal will display jump deformation can be expected to be orientation, impurity content, growing conditions, previous deformation history and the temperature. Schmid and Valouch showed that the orientation of the crystals was important but the impurity content relatively unimportant in this respect[45]. On the other hand, in similar tensile experiments on zinc single crystals, Wain and Cottrell[53] found yield points when using commercial zinc but no yield points when using pure zinc. If, however, nitrogen was introduced into the pure zinc by melting in air for 30 minutes prior to growing the crystals, yield points could be induced. No orientation dependence was observed. Jump deformation was not observed in these experiments, only conventional, single yield points.

Ardley and Cottrell[54] did, however, notice jump deformation, or jerky flow as they called it in single crystals of β-brass grown in a nitrogen atmosphere. These experiments were also aimed at finding the effects of nitrogen impurity atoms on

the yielding properties of the material. Jump deformation was not observed in a brass, nor has it been observed in any f.c.c. metal.

Bullen[55] has observed jump deformation associated with slip on the basal plane in zinc single crystal specimens. The jumps were only seen with specimens deformed at -196°C after some prestrain at room temperature. These specimens had no nitrogen impurities.

In the present experiments zinc crystals were grown both in vacuum and in a nitrogen atmosphere, using both pure and commercial zinc. Out of fifty crystals tested only six have shown a strong tendency towards displaying jump deformation. Of the six, four were grown in vacuum using pure zinc, one was grown in a nitrogen atmosphere using pure zinc, and one was grown in a nitrogen atmosphere using commercial zinc. The four crystals which were grown in vacuum were grown in the vertical furnace described in 3.1.2, the other two being grown in the horizontal furnace described in the same section. Other crystals showed some slight tendency to jump but the six crystals mentioned were the only ones from which it was possible to get recordings of resistance pulses.

In an attempt to get some nitrogen into the crystals, the zinc was left in a molten state in an oxygen-free nitrogen atmosphere for 30 minutes

prior to growing. This, however, seemed to have little effect on the tendency to jump. A further attempt to get impurity atoms into the material was attempted by diffusing lead into a zinc crystal from the surface. Lead was evaporated onto the surface and the crystal was annealed for one week at 300°C. At the end of this time lead was still visible on the surface. In this time, therefore, and at this temperature, lead must have diffused into the surface to a depth corresponding to $\sqrt{Dt} = 100\mu$. This specimen showed no tendency to jump on subsequent straining.

It would seem, in fact, that any tendency to jump deformation in a zinc crystal depends as much on the growing conditions as on the impurity content. The four crystals grown in the vertical crystal furnace probably were less perfect than those grown on the horizontal furnace. This vertical furnace, designed for use at high temperatures had a very low temperature gradient when used at low temperatures, as in growing zinc crystals. The crystals were also grown in a constrained manner, packed firmly in alumina powder enclosed in a split graphite crucible. This probably imposed high stresses during cooling. The crystals grown in the horizontal furnace at the rate of 3.5 mm./min. showed no tendency to jump. The two which did jump were grown at

7 mm./min. Once again, the crystals could be expected to be less perfect.

The crystals used by Schmid and Valouch were prepared by drawing from the melt. This also would impose high strain during cooling. The cross sections of these crystals were not uniform and it is possible that this could have some effect on the jumping properties. Some crystals were grown, therefore, on the horizontal furnace, of uneven cross section of about 1 mm. diameter by simply growing them in air, the oxide film rumpling the surface. These still showed no tendency to jump. The crystals used by Bullen were grown constrained in pyrex tubes (coated with graphite) in a vertical crystal furnace. These could, therefore, have growth defects.

It should be pointed out that the stress beam used in these experiments is capable of detecting jumps as small as .05μ, in other words, it is much more sensitive than any previously used.

Specimens which exhibited jump deformation continued to do so when the temperature was varied over the range 18°C to 100°C. On lowering the temperature to 273°K and 200°K fracture occurred very early, on the basal plane, after steady slip. Some twinning was observed at these lower temperatures, giving apparent jump deformation.

4.1.2 Observations of jumping

In 3.2.6 it was mentioned that the stress beam could be used with a recording galvanometer. Since the beam only deflects $\frac{1}{2}\mu$ for a load of 1 Kg. any jump of a size of interest in the present experiments will completely relax the beam. The size of the jumps, therefore, can conveniently be measured by measuring the time taken for the load to reappear on the beam, as read from the recording galvanometer. This was found to be, in practice, a much more convenient way of measuring the size of the jumps than using the differential transformer described in 3.2.5. This system has the disadvantage, however, of not recording the change in strain on the same recorder (i.e. the oscilloscope camera) as the change in resistance.

Although the response of the recording galvanometer is slower than the alternative display it is still fast enough for these experiments. At the strain rates used, 2μ/sec., the stress takes about 10 seconds to reappear, which is well within the response of the galvanometer. A typical recording of the stress-time curves obtained is shown in Fig. 34.

Table 5 includes the measured size of the jumps for the corresponding approximate changes in resistance.

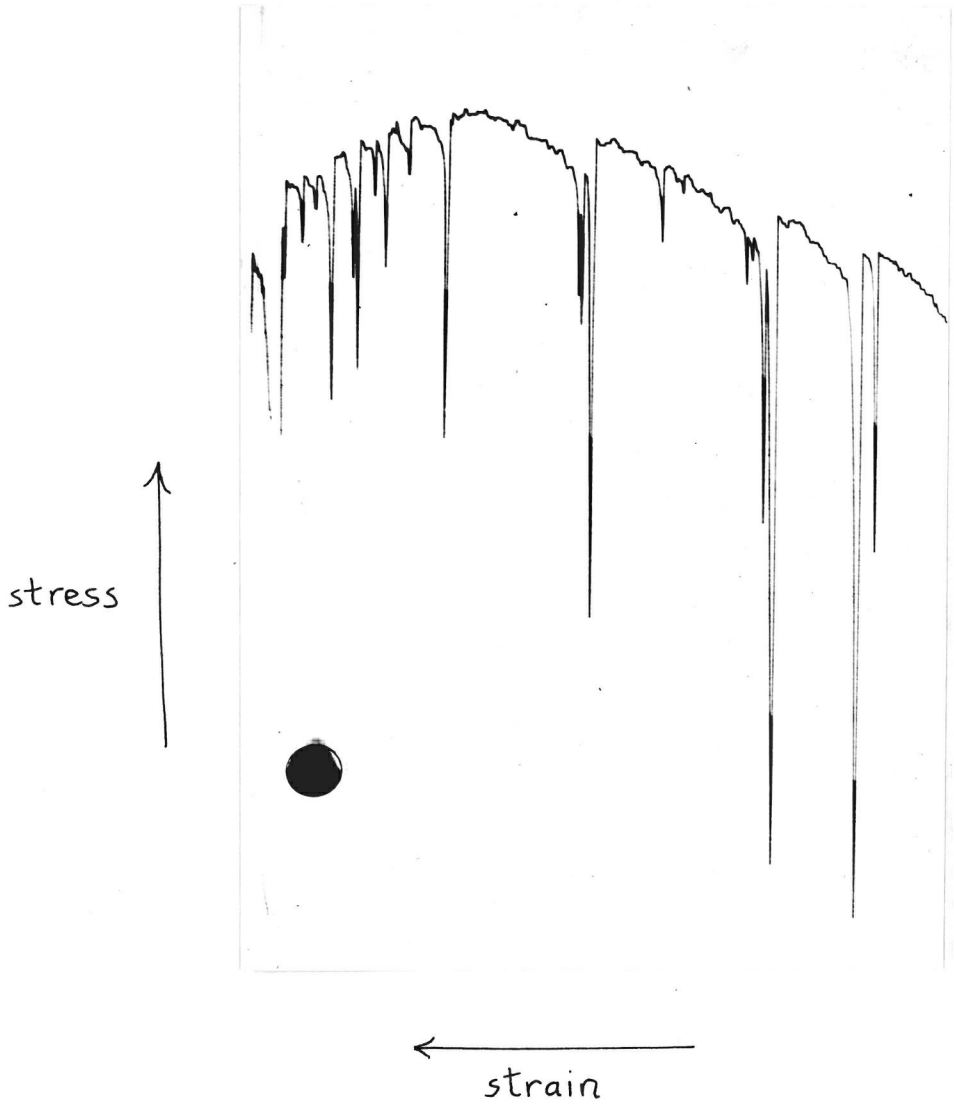

Figure 34.

Specimen	χ_o	Temp. °C.	No. of jumps	Approximate Size microns	Approximate Resistance μ ohm.	Time to 1/3 max. height (m.sec)	E_m (eV)	n_j
Zn 9	45°	18	24	-	.1	3.0	-	10^6
Zn 25	70°	18 65 77	1 2 1	-	.05 .1 .05 .05	7 2.3 1.2	.30 ± .05	2×10^6
Zn 26	12°	27 47 66 88	3 3 3 3	-	.1	.8	-	-
Zn 35	20°	18	2 1	15	.05 .05	1.9 .7	-	5×10^5
Zn 40	40°	18 77	1 2 1 1	20	.05	3.1 .6 .8 .4	.30 ± .05	10^6
Zn 43	42°	18 40 100	3 3 3	30	.1	11.0 5.1 .6	.32 ± .01	3×10^6

TABLE 5

4.1.3 The appearance of crystals after deformation.

Crystals which had not displayed jump deformation always had the appearance of Fig. 35. It is seen that no coarse slip bands are visible on the surface.

Fig. 36, on the other hand, is a photograph of a crystal which has displayed jumping. It is seen that the surface is covered with coarse slip bands or slip clusters. The number of coarse slip bands appearing corresponds roughly to the number of jumps which are observed.

This is in accordance with Schmid and Valouch's observations on zinc[45] and with Ardley and Cottrell's observations on β brass[54].

4.2 Observation of Sudden Changes in Resistance

4.2.1 Recording of changes of resistance

Due to the rarity of the specimens which showed jump deformation, the random appearances of the pulses, and the random size of the resistance changes, very large numbers of photographs had to be taken to obtain even a few good recordings. For convenience, therefore, "Polaroid" film was used in recording the pulses. This also gave an immediate indication of when to change the temperature, i.e. on obtaining a few suitable pictures at any one temperature.

Figure 35.

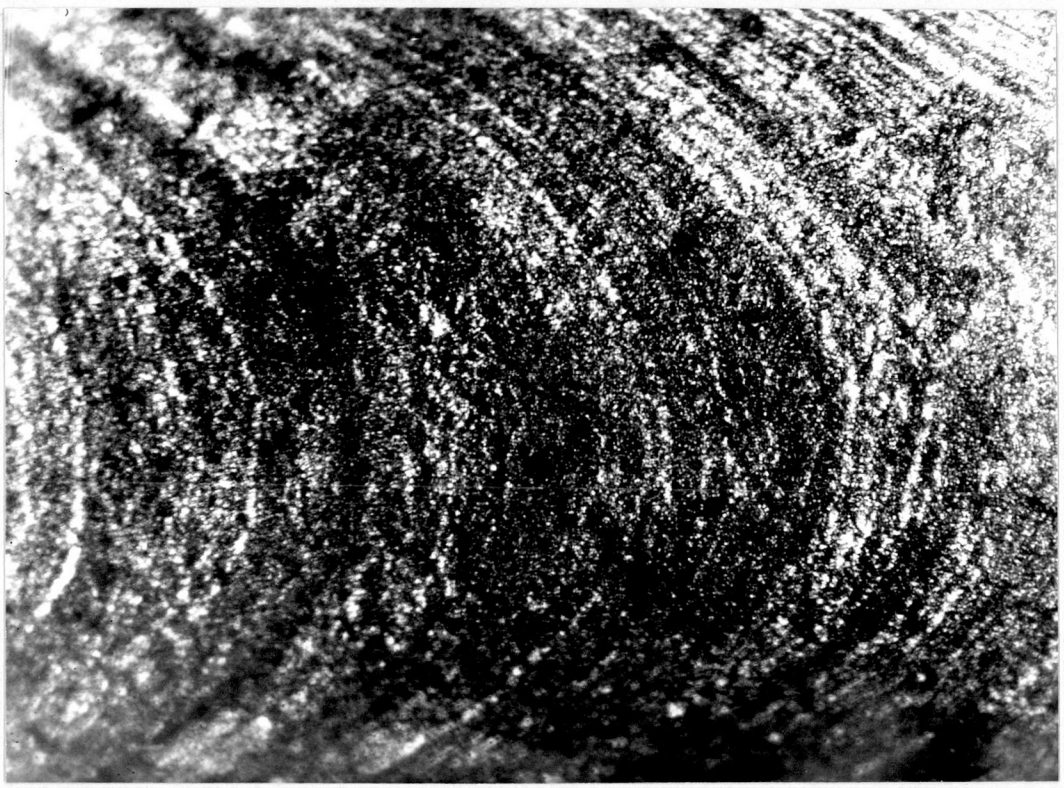

Figure 36.

Enlargements were then taken from the Polaroid prints by rendering them translucent with the following solution:-

Tricresyl Phosphate	-	50 parts
Acetone	-	1 part
Petrol	-	49 parts

4.2.2 The types of resistance changes observed

Coinciding with every large jump in deformation, a resistance change occurred in the specimen. This is illustrated in graph 2 where a transient part of a resistance change is photographed at the same instant as the appearance of the trace due to the sudden change in stress.

The change in resistance consists of a permanent part with a superimposed transient part. The permanent part of the pulses is due to permanent structural changes, change of crystal cross-section and the apparent alteration of resistivity due to the difference in specific resistance as measured perpendicular or parallel to the basal plane. The transient part, which could be resolved on most of the pulses, is the part which is of interest in the present work.

The permanent changes were of the order of $2 \times 10^{-6} \Omega$ for jumps of about 20μ. Due to change in cross-section one would expect a change

of resistance of about 1.5μ ohm. assuming the jump occurs in a region of the crystal 50μ long. The effective change in resistivity would be expected to contribute less than .1μ Ω .

The decay time of the observed transient can be seen from Table 5 to vary from less than the amplifier can resolve, i.e. $\frac{1}{3}$ m. sec. to greater than10 m. sec. Some decays appeared to be much longer than this, of the order of seconds, but since this could be affected by the lack of long term stability in the electronics, and since these were only observed in small pulses , no quantitative observations could be made on them with the present apparatus.

Generally the short duration pulses, which were near the limit of the amplifier's pass band, appeared to have little dependence on temperature.

The longer decaying peaks were, however, temperature dependent in the specimens with which it was possible to obtain observations at different temperatures. The range of temperatures can be seen to be limited by the pass band of the amplifier.

4.3 The Observed Activation Energies

4.3.1 Annealing kinetics

If the transients are assumed to be dependent on some thermally activated rate process, it was earlier mentioned that the simplest form the decay could take would be

$$-\frac{d\rho}{dt} = A_o \rho \exp\left(-\frac{E_m}{kT}\right) ,$$

in this case ρ being the resistivity.

For most annealing processes in metals this is only an approximation. If, however, it is possible to fit the observed decay curves to this form, it is reasonable to use it in the subsequent calculation of the activation energy E_m.

Integrating the expression at constant temperature gives

$$-\int_{\rho_o}^{\rho} \frac{d\rho}{\rho} = (A_o \exp \frac{-E_m}{kT}) \int_o^t dt$$

$$\therefore \quad \text{Ln} \frac{\rho_o}{\rho} = (A_o \exp \frac{-E_m}{kT})t ,$$

where ρ_o is the maximum value of the resistance transient.

Graphs 1 to 6 illustrate how closely the observed decays approximate to this type of relationship over the temperature range 18°C to 100°C.

4.3.2 Determination of activation energies

Assuming that the expression

$$\text{Ln}\frac{\rho_o}{\rho} = (A_o \exp\frac{-E_m}{kT})t$$

describes each decay curve, E_m can be determined by measuring the time taken to reach a certain value of $\frac{\rho_o}{\rho}$ for different temperatures by writing

$$\exp - \frac{E_m}{kT} = K\frac{1}{t} \quad ,$$

K being a constant.

A graph of $\text{Ln}\frac{1}{t}$ against $\frac{1}{kT}$ will then have a slope whose value is E_m.

The present measurements were simply made by measuring, from enlargements, the time taken to reach $\frac{1}{3}$ of the maximum height in the case of specimen Zn 25 and $\frac{1}{10}$ of the maximum height in specimen Zn 43, the results being plotted in graphs 7 and 8.

These two specimens were the only two in the present experiments with which it was possible to record resistance changes at three different temperatures before the specimen stopped jumping.

Point 1 of graph 7 is measured from one pulse but is confirmed to within 20% by another recording of poorer quality. Point 2 is measured for one pulse. The third point, measured at room temperature has a large error since the tail-end is missing from the recording. It must be within the indicated error, however.

The slope of the graph corresponds to

$E_m = .30 \pm .05$ eV.

Specimen Zn 43 resulted in a much better set of recordings. Readings at three temperatures were again possible, each point being the mean of three recordings. In this case the slope corresponds to

$$E_m = .32 \pm .01 \text{ eV}.$$

4.3.3 Sources of error in measuring the decay time.

The measured decay time of the resistance transient can differ from the true decay time due to distortion of the pulse by the amplifier. The simplest way to allow for this is to pass pulses of known decay constants through the amplifier and detector and compare the result with the original.

A pulse generator which could produce pulses of 1μ sec. rise time and $\frac{1}{10}$ to 50 m. sec. fall time was used to modulate a carrier signal of 100 Kc./sec. The modulated signal was then passed through the amplifier and detector. The original modulated signal and the final detected signal were then displayed on the same screen. A recording of such a trace is shown in Fig. 37. By measuring the time taken for both signals to reach .1 of the

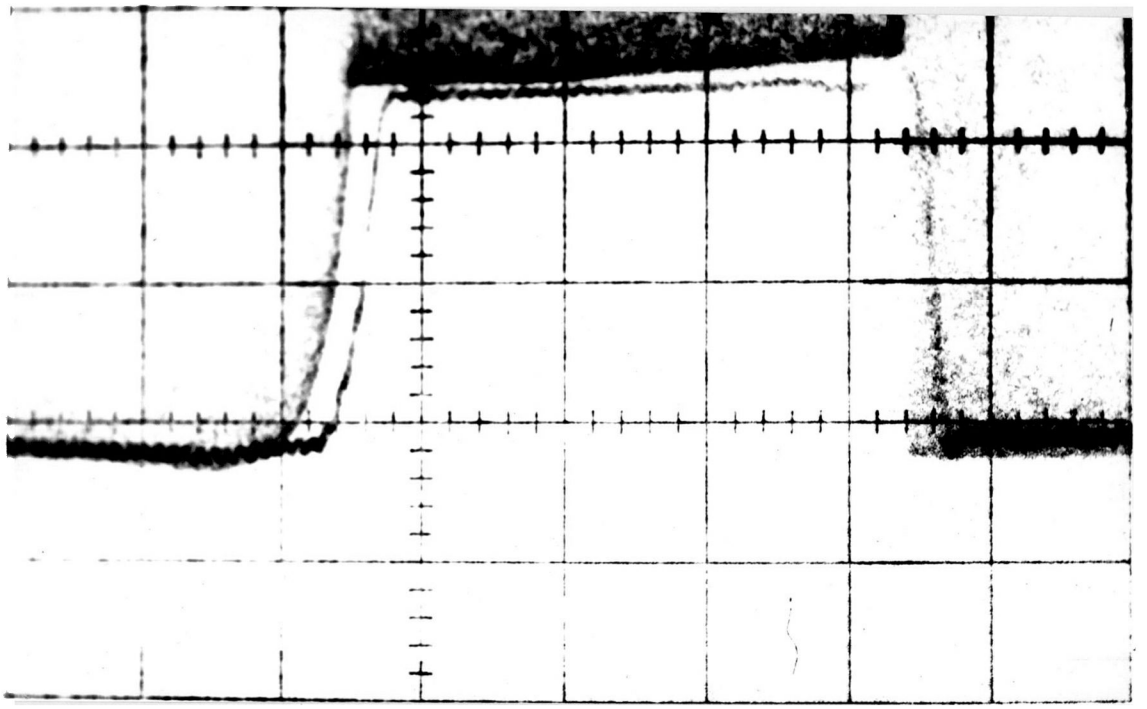

Figure 37.

original height a calibration curve for the amplifier was drawn. As seen from Fig. 38 the error introduced by the amplifier is quite small. It was allowed for, however, in calculations involving short decay times.

Errors in the calibration of the oscilloscope used are usually less than 1% according to the manufacturers.

4.4 Discussion of Results

4.4.1 Source of the transients

Since various causes could be put forward for the explanation of the transients observed in these experiments it is as well to examine them individually. The most obvious objection in any experiment of this nature, where very small voltage pulses are being examined, is that spurious pulses due to such causes as pick-up, slipping in the grips, and rupturing of the oxide-film would also be recorded as transient changes.

Any changes due to actual e.m.f.'s produced at the contacts or on the specimen are, of course, avoided by the use of a carrier frequency method. This also helps in eliminating pick-up to a large extent. In fact, the only serious pick-up

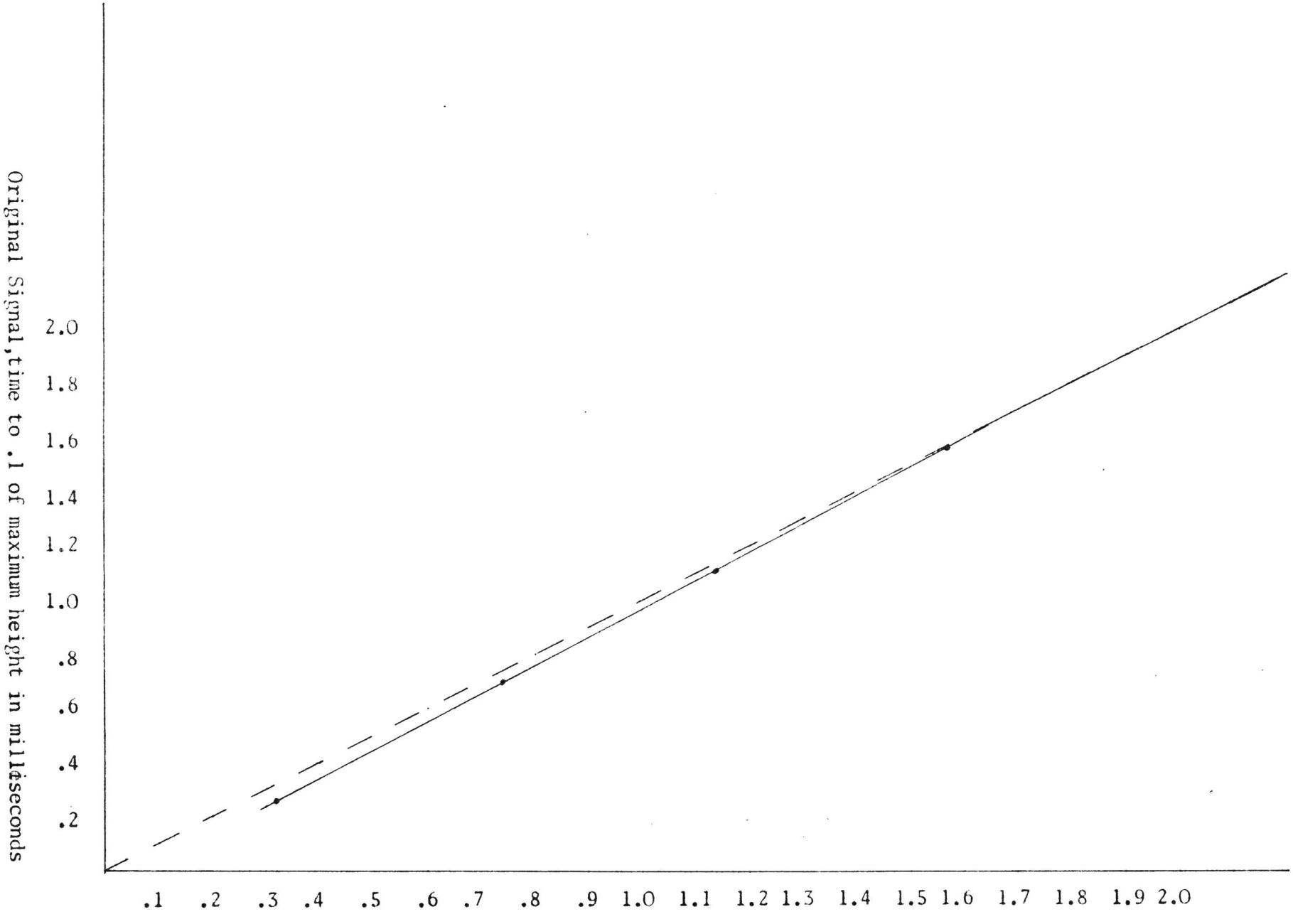
Original Signal,time to .1 of maximum height in milliseconds
2.0
1.8
1.6
1.4
1.2
1.0
.8
.6
.4
.2
.1 .2 .3 .4 .5 .6 .7 .8 .9 1.0 1.1 1.2 1.3 1.4 1.5 1.6 1.7 1.8 1.9 2.0
Amplified Signal,time to .1 of maximum height in milliseconds.

Figure 38.

detected was mains hum which for some reason occasionally appeared at the detector stage (as a modulation signal) when the two EF 184 valves were being over-run. This could be avoided by changing the valves and resetting the voltages whenever it appeared. Other spurious pick-up pulses were not observed, even if the equipment was set up for 12 hours (the specimen not being strained) at its most sensitive setting. Microphony was eliminated by mounting the amplifier on blocks of lead in the manner illustrated in Fig. 25 at position "a".

The design of the grips used seemed to eliminate the possibility of slipping. Although a number of copper crystals were strained (copper not showing jump deformation) in no case was any evidence of slipping in the grips evident from the stress-time graph.

Three other possible explanations for the transients exist. They could be caused by:-

1. Dislocations
2. Heating
3. Point defects.

These will be discussed in turn.

1. It is possible that, during a jump of deformation, some dislocations last slightly longer than others in the crystal. In other words, towards the end of the avalanche process, the last

of the dislocations which terminate at the surface could be evident as a transient increase in resistance, the lifetime being of the order of the time it takes a dislocation to traverse the specimen.

Assuming that the screw dislocation velocity is of the order of 30 metres/sec.[56], a transient due to this cause would last $\sim \frac{1}{10}$ m. sec. It is possible, therefore, that this could be an explanation for the short lifetime transients, but an unlikely reason for the longer lived ones.

2. As mentioned in 2.1 it has been suggested that slip avalanches could be connected with heating of the slip region[47]. This would, of course, be recorded as a transient increase of resistance. A temperature rise of 30°C would be required in the region of the slip avalanche to explain the size of a resistance transient of .1μ ohm. The corresponding energy concentrated in the region is then 10^{-2} joules. The total energy available, however, can be estimated as a maximum of 10^{-3} joules by considering the force on the specimen and the distance slipped during an avalanche. This explanation of the transients is, therefore, unlikely.

It can also be shown (Appendix B) that a temperature rise of this size, concentrated in a region of the specimen 50μ in length would be seen

as an increase in resistance which would decay in a time of several seconds to .1 of its original value. This is two orders of magnitude longer than the observed transients.

Any melting in the avalanche region due to very high local temperatures at intersecting dislocationswould not be discernible since Seitz has shown that the original energy would be shared with all the atoms up to 30 atomic distance in a time of the order of 10^{-14} seconds[8]. This would then represent only a small rise in temperature.

3. Since no detailed low temperature annealing experiments have been performed on plastically deformed zinc crystals, it is not possible to compare the observed activation energy with a known value. Experiments are going on in this laboratory with this in view. It is possible, however, to compare the result with that which would be expected from the empirical relationship due to Thompson[57]

$$E_m = 5.0 \times 10^{-4} T_m \text{ eV},$$

T_m being the melting temperature. This holds for various f.c.c. and b.c.c. metals.

For zinc this gives $E_m = .35$ eV, which compares reasonably with the observed activation energy of .32 eV.

The agreement is not so favourable with that

derived from the results of Gertsriken and Slysar[58]. Assuming that $E_{sd} = E_M + E_F$ where E_{sd} is the activation energy for self diffusion and using their values for E_{sd} and E_F of 23.1 and 8.7 K cal./g. atomic respectively, one obtains

$$E_M = 14.4 \text{ K cal./g. atomic}$$
$$= .62 \text{ eV.}$$

A higher value could be expected since it is probable that impure zinc was used in these experiments. According to Peiffer[24] the vacancy impurity binding energy in cadmium is at least .1 eV. It must also be noted that the value of E_F used above is a mean value of results obtained from quenching and equilibrium experiments, the individual results differing by 60%. Using the value obtained from the equilibrium experiment, and allowing for an impurity binding effect, one obtains

$$E_m = .44 \text{ eV.}$$

4.4.2 Feasibility of the vacancy mechanism

Since no observations on the effect of deformation produced vacancies on the resistivity of zinc have been performed, the following discussion uses Peiffer's results on cadmium[24] for

comparison purposes.

Peiffer observed an increase in resistance of 15μ ohm due to vacancies produced by 5% deformation of a specimen 10 cm. long by .1 cm. diameter. This corresponds to an increase in the resistivity of

$$\triangle s = 2 \times 10^{-9} \text{ ohm cm.}$$

for 1% deformation.

In the present experiments an average transient corresponds to an increase of the order of .1μ ohm in a region of the specimen 50μ long by .2 cm. diameter after 50% deformation.

This corresponds to

$$\triangle s = 10^{-8} \text{ ohm cm.}$$

for 1% deformation

- a rather greater increase.

No value for the resistance due to vacancies in a hexagonal metal has been calculated. A value must, therefore, be assumed before an approximate calculation of the vacancy concentration can be made.

It can be assumed with some justification (see Appendix C) that the resistivity increase in zinc due to one atomic per cent of vacancies is

$$\triangle s = 4\mu \text{ ohm cm.}$$

This implies that .1 atomic per cent of

vacancies are present in the avalanche region during a transient of .1μ ohm in a region of the specimen 50μ long. The total number of vacancies in the region will then be about 10^{16}. The energy required to produce this number, if the energy of formation of a vacancy is .4 eV[58] is of the order of 10^{-3} joules. This is approximately the total amount of energy which is available due to the deformation.

In other words, an extremely high proportion of the available energy is required to explain the vacancy concentration. This suggests that either vacancies in a hexagonal metal have a higher resistance than would be thought, at least when present in high concentrations, or that the presence of the vacancies plays a fundamental part in the avalanche process.

Since an extension increase of 20μ can be considered to be caused by 10^5 cm. of unit dislocation line it is possible to calculate the vacancy production per centimeter of dislocation line. This is $10^{16}/10^5 = 10^{11}$ vacancies/cm. in moving .2 cm., i.e. across the specimen, or 5×10^{11} vacancies/cm. in moving unit distance. The value calculated by Seitz[11] is 5×10^{11} vacancies/cm. (This was calculated using data on observed resistivity increase as a function of strain. Seitz, in fact, probably overestimated

the resistance due to vacancies and 5×10^{12} vacancies/cm. would be more reasonable.)

It is possible to estimate the number of jumps a vacancy makes to a sink from the relationship

$$n_j = 10^{14} \tau \exp(-\frac{E_m}{kT}) \qquad (59)$$

τ being the approximate relaxation time for the annealing.

This parameter can be seen from Table 5 to vary from specimen to specimen at the same temperature. If the vacancies were forming into clusters, randomly spaced, it seems unlikely that such a variation in sink spacing would be evident. If, however, dislocations are acting as sinks, the variation can be explained since the jumps take place at different stages of the deformation for different specimens, and the dislocation density will vary.

The dislocation spacing, as implied by this parameter, n_j, is about 1μ, which is not unreasonable for such a heavily deformed region.

4.4.3 The mechanism of jump deformation

In all observations of jump deformation the surfaces of the specimens have exhibited coarse slip bands. The formation of coarse slip bands in

f.c.c. metals is, according to Seeger[60], connected with the observed fragmentation of the slip lines. Cross slip of screw dislocation would push dislocations on the edge of the coarse band out into regions where further slip was possible. This is a gradual process in f.c.c. metals and it is not normally observed in h.c.p. metals. An excess of vacancies would help this process but it is difficult to see how, if this were the cause of the jump deformation, the process could occur so quickly.

Ardley and Cottrell[54] pointed out that a slip avalanche would be large if the stress needed to start it was high since, according to Fisher, Hart and Pry[61] the number of dislocations formed in one avalanche increases exponentially with the amount of stress that has to be relaxed in order to stop it. In their experiments the high stress necessary to explain the size of the avalanches was attributed to the segregated impurity atoms.

It was suggested earlier that, since a very high proportion of the available energy is necessary to create the number of vacancies observed, the defects themselves may play an important part in the avalanche mechanism. They could do this in two ways, by being absorbed at jogs and enabling pinned dislocation to climb over obstructions, or by supplying energy during annihilation which "loosens" the lattice and makes it easier for the

dislocations to tear loose. Since all the deformation takes place in a very short time, of the order of a few milliseconds, and since the transients last for a time of the same order, one could consider that vacancies produced early in a small slip process could spread out and help to propagate slip in other planes.

In the number of jumps observed a vacancy could be expected to travel a distance of the order of 1μ before reaching a sink, this being greater than the distance between elementary slip planes[44]. Thus although this could be an important contributory factor towards slip avalanches it does not seem likely that it is the only one. It is possible, however, that an initial slip process could spread over a small region by this method. The resultant local increase in orientation could then assist nearby pinned dislocations in breaking loose under the applied stress and the process could be repeated until all the more loosely pinned dislocations in the avalanche region were free.

This would require particular conditions in the specimen before jumps could be observed, in other words jump deformation would only be observed if suitable pinned regions existed in the crystal. The scarcity of the jumps and the dependence on growing conditions lends some weight to this argument.

APPENDIX A

Zinc rods supplied by Johnson, Matthey & Co. Ltd. contained the following impurities as determined by a spectrographic examination.

Iron	< 0.001 %
Copper	< 0.0005 %
Calcium	< 0.0001 %
Magnesium	< 0.0001 %
Cadmium	< 0.0001 %
Silicon	< 0.0001 %

APPENDIX B

Since the problem is to calculate how long a resistance transient due to a heated region in a crystal will last, each mode of dissipation of heat energy will be considered separately.

1. Radiation

The highest rate of loss of energy due to radiation will occur when the heated region is at its highest temperature, i.e. when all the energy is concentrated in the original slip region, causing a temperature rise of 30°C. At this time the rate of loss of heat energy is

$$< 10^{-4} \text{ joules/sec.}$$

from the surface of the region which is 10^{-3} cm.^{2}. This, therefore, will take a time of about 10^2 seconds to dissipate the energy (10^{-2} joules).

2. Convection

If, once more, the loss is calculated at the beginning of a transient, then using the notation of Roberts and Miller's "Heat and Thermodynamics", p. 297, the quantity $\log_{10} \frac{\theta d^3}{\nu} = .2$ in this case, θ being the excess temperature, d the specimen diameter, and ν a quantity read from the table provided.

From the graph provided, the quantity $\log_{10} H/K$ can then be measured as .5 where H is the heat loss per second per cm.^{2} in calories, and K is read from the table. H is then calculated as 2×10^{-4} joules cm.$^{-2}$ sec.$^{-1}$. The rate of loss from the heated region is, therefore, 2×10^{-7} joules/sec.

If the calculation is repeated at a later stage, when the energy has spread out over a larger volume of the specimen by conduction, this is found to increase to a maximum of about 2×10^{-4} joules/sec., and a time of about 2×10^{1} seconds is required to dissipate the energy.

3. Conduction

If the specimen is considered as an infinite rod whose original temperature distribution is given by

$$T = f(x)$$

where x is measured along the rod, then the equation of conduction is

$$\frac{\partial T}{\partial t} = K \frac{\partial^2 T}{\partial x^2}$$

where $K = \frac{C}{ds}$

with C = conductivity

d = density

and s = specific heat.

The solution for this equation is

$$T = \frac{1}{2\sqrt{\pi K t}} \int_{-\infty}^{\infty} f(x') e^{-(x-x')^2/4Kt}\, dx' \qquad (62)$$

at time t.

If the original temperature distribution is considered as

$f(x) = 0$ outside the region $-\frac{h}{2} < x < \frac{h}{2}$

and

$f(x) = 30$ inside the region $-\frac{h}{2} < x < \frac{h}{2}$

this reduces to

$$T = \frac{30}{2\sqrt{\pi K t}} \int_{-\frac{h}{2}}^{+\frac{h}{2}} \exp\frac{-x^2}{4Kt} \exp\frac{+2xx'}{4Kt} \exp\frac{-x'^2}{4Kt}\, dx'$$

$$= \frac{30}{2\sqrt{Kt}} \exp\frac{-x^2}{4Kt} \int_{-\frac{h}{2}}^{+\frac{h}{2}} \exp\frac{+2xx'}{4Kt}\, dx'$$

since the term in $x'^2 \simeq 1$ for small x' .

$$T = \frac{30}{2\sqrt{\pi K t}} \exp\frac{-x^2}{4Kt} \left[\frac{4Kt}{2x}\left\{\exp + \frac{2xx'}{4Kt}\right\}\right]_{-\frac{h}{2}}^{\frac{h}{2}}$$

$$= \frac{30}{2\sqrt{Kt}} \exp\frac{-x^2}{4Kt} \left[\frac{4Kt}{2x}\left\{1 + \frac{2x}{4Kt}\frac{h}{2} - 1 + \frac{2x}{4Kt}\frac{h}{2}\right\}\right]$$

$$= \frac{30h}{2\sqrt{\pi K t}} \exp\frac{-x^2}{4Kt}$$

Now consider a small region of length dx at a distance x from the original heated region after time t. The change of resistance of this region due to heating up will then be

$$R = \frac{\rho}{A} \frac{30h}{2\sqrt{\pi K t}} \alpha \exp \frac{-x^2}{4Kt} \, dx \, .$$

where ρ = resistivity

A = cross-sectional area

and α = temperature coefficient of resistivity.

The change in resistance of the whole specimen will therefore be

$$R = 2 \frac{\rho}{A} \frac{30h\alpha}{2\sqrt{\pi K t}} \int_0^\infty \exp \frac{-x^2}{4Kt} \, dx \, .$$

Consulting the table in Weatherburn's "Mathematical Statistics", p. 56 and putting $\sigma = \sqrt{2Kt}$ gives, for $x = 1$ cm., this function as decaying with time in the following manner.

.46 R_{max} at $t = \frac{1}{10}$ sec.

.21 R_{max} at $t = 1$ sec.

.07 R_{max} at $t = 10$ sec.

A time of several seconds is therefore required to reach .1 of the original increase in resistance.

APPENDIX C

The resistivity of a metal can be written as

$$\rho = \frac{m^*}{Nq^2\tau_T} + \frac{m^*}{Nq^2\tau_V} + \frac{m^*}{Nq^2\tau_I} + \text{.... etc.}$$

where τ_T is the relaxation time due to phonon collisions

τ_V is the relaxation time due to collisions with vacancies

τ_I is the relaxation time due to collisions with impurities

etc.

m^* is the effective mass of an electron

N is the number of valence electrons per cubic meter

and q is the electronic charge.

Considering only the second term

$$\rho = \frac{m^*}{Nq^2\tau}$$

$$= \frac{m^* v_F}{Nq^2 \Lambda}$$

where v_F is the velocity of an electron at the Fermi level

and Λ is a measure of the distance an electron travels between collisions.

Hence $$\frac{(\rho_v)Zn}{(\rho v)\,Cu} = \frac{(m^* v_F)_{Zn}\, N_{Cu}}{N_{Zn}\,(m^* v_F)_{Cu}}$$

for the same vacancy concentration.

i.e. the same value of .

$$\text{i.e.} \quad \frac{(\rho_v)_{Zn}}{(\rho_v)_{Cu}} = \frac{\mu_{Cu} \cdot R_{Zn}}{\mu_{Zn} \cdot R_{Cu}}$$

where $R = \frac{1}{Nq}$, the Hall constant

and $\mu = \frac{q \Lambda}{m^* v_F}$, the Hall mobility.

Using values for R and μ from Seitz's "Modern Theory of Solids" gives

$$\frac{(\rho_v)_{Zn}}{(\rho_v)_{Cu}} = 4.$$

Hence using the recognised value for $(\rho_v)_{Cu}$ of $1\mu\Omega$.cm. for 1 atomic per cent vacancies gives

$$(\rho_v)_{Zn} = 4\mu\Omega.\text{cm./atomic per cent vacancies.}$$

REFERENCES

1. L. Tewordt, Phys. Rev. 109, 61 (1958).

2. R.A. Johnson & E. Brown - not yet published.

3. A.C. Damask, G.J. Dienes, & V.G. Weizer, Phys. Rev. 113, 781 (1959).

4. R.O. Simmons and R.W. Balluffi, Phys. Rev. 125, 862 (1962).

5. R.W. Balluffi, J.S. Koehler & R.O. Simmons, Symposium on "Recovery and Recrystallisation of Metals", A.I.M.E. Annual Meeting Feb. 1962.

6. A.B. Huntington, Phys. Rev. 61, 325 (1942)
" " 91, 1092 (1953).

7. R.O. Simmons, J.S. Koehler & R.W. Balluffi, I.A.E.A. Symposium on Radiation Damage in Solids and Reactor Materials, Venice, May 7-11, 1962.

8. F. Seitz, Advances in Physics I, 43 (1952).

9. J. Freidel, "Les Dislocations", Paris, 1956.

10. A. Seeger, Phil. Mag. 46, 1194 (1955).

11. P.B. Hirsch & D.H. Warrington, Phil. Mag. 6, 735 (1961).

12. P.B. Hirsch, Phil. Mag. 7, 67 (1962).

13. J. Weertman, Phil. Mag. 967 (1963).

14. A.H. Cottrell, "Dislocations and Mechanical Properties of Crystals", John Wiley & Sons Inc., New York, 1957.

15. N.F. Mott, "Dislocations & Mechanical Properties of Crystals", John Wiley & Sons Inc., New York, 1957.

16. D. Kuhlman Wilsdorf & H.G.F. Wilsdorf, Acta Met. 10, 584 (1962).

17. H.R. Peiffer, Acta Met., May 1963.

18. H.K. Birnbaum, Jour. Appl. Phys., Aug. 1963.

19. P. Haasen, "Internal Stresses and Fatigues in Metals", Elsevier Publishing Co. Inc., Amsterdam, 1959, p. 205.

20. F.R.N. Nabarro, Adv. Phys. 1, 271 (1952).

21. J.R. Cost, Acta Met., Dec. 1963.

22. A.S. Nowick & R.J. Sladek, Acta Met. 1, 131 (1953).

23. Jackson & J.S. Koehler - not yet published.

24. F.R. Stevenson & H.R. Peiffer, Phys. Status Solidi, 4 2 (1964).

25. G.J. Dienes & G.H. Vineyard, Radiation Effects in Solids, Vol. 11, Interscience 1957.

26. J.A. Manintveld, Nature 169, 623 (1952).

27. C.W. Berghout, Acta Met. 6, 613 (1958).

28. G.R. Piercy, Phil. Mag. 5, 201 (1960).

29. B.M. Korevaar, Acta Met. 6, 572 (1958).

30. A. Sosin & J.A. Brinkman, Acta Met. 7, 478 (1959).

31. R. Kamel & E.A. Attia, Acta Met. 9, 1047 (1961).

32. A.A. Johnson, D.E. Peacock & A. Wronski, S.2.52 Fifth International Congress & Symposia of International Union of Crystalography Cambridge, Aug. 1960.

33. F.R. Stevenson & H.R. Peiffer, Jour. of Appl. Phys. 34, 9, 2804 (1963).

34. R.O. Simmons & R.W. Balluffi, Phys. Rev. 125, 857 (1962).

35. J.E. Bauerle & J.S. Koehler, Phys. Rev. 107, 1493 (1957).

36. A. Seeger & Bross, J. Phys. and Chem of Solids 6, 324 (1958).

37. J.W. Corbett, R.B. Smith & R.M. Walker, Phys. Rev. 114, 1452, 1460 (1959).

38. R.O. Simmons & R.W. Balluffi, J. Appl. Phys. 30, 1249 (1959).

39. R.O. Simmons & R.W. Balluffi, Phys. Rev. 109, 1142 (1958).

40. R. Vook & C. Wert, Phys. Rev. 109, 1529 (1958).

41. H.G. Cooper, J.S. Koehler & J.W. Marx, Phys. Rev. 97, 599 (1955).

42. A.V. Granato & T.G. Nilan, Phys. Rev. Letters 6, 171 (1961).

43. F.J. Blatt, Solid State Physics 4, 322 (1957).

44. A.F. Brown, Adv. Phys. I, 427 (1952).

45. E. Schmid & N.A. Valouch, Zs. f. Phys. 75, 531 (1932).

46. E. Orowan, Diploma Arbeit Technische Hoch-Schule, Berlin, 1929.

47. F. Seitz & T.A. Read, J. Appl. Phys. 12, 470 (1941).

48. V. Rozhanskii et al., Physics of Metals and Metallography Vol. III, Part 1, (1956).

49. D.A. Blackburn, Thesis, University of Edinburgh, 1961.

50. North, R.C.A. Revue 4, 441 (1940)
" " 5, 244 (1940).

51. Dye & Jones, Journal I.E.E. 72, 169 (1933).

52. J.S. Belrose, Wireless World, Sept. 1956.

53. H.L. Wain & A.H. Cottrell, Proc. Phys. Soc. B63, 339.

54. G.W. Ardley & A.H. Cottrell, Proc. Roy. Soc. 219 (1953).

55. F.P. Bullen, Phil. Mag. 7 (1) (1962).

56. N.K. Chen & R.B. Pond, Trans. A.I.M.E. 194, 1085 (1952).

57. M.W. Thompson, Phil. Mag. 5, 278 (1960).

58. S.D. Gertsriken & B.F. Slysar, Phys. Metals & Metallography 6, (1958), part 6, p. 103.

59. W.M. Lomer & A.H. Cottrell, Phil. Mag. 46, 711, (1955).

60. A. Seeger, Phil. Mag. (1957), 323.

61. J.C. Fisher, E.W. Hart & R.H. Pry, Phys. Rev. 87, 958.

62. H.S. Carslaw & J.C. Jaeger, Conduction of Heat in Solids.

Zn 25,18°C.

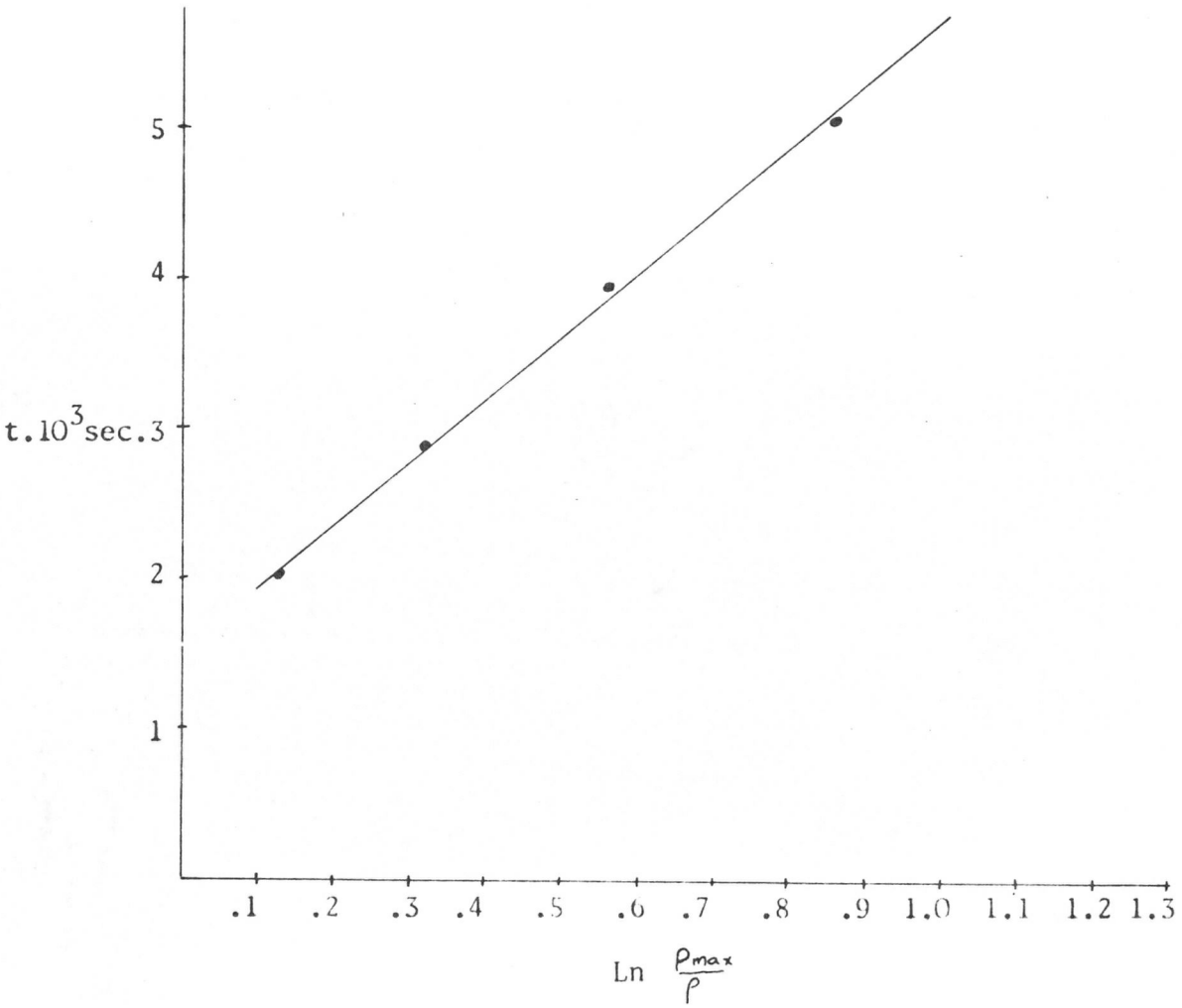

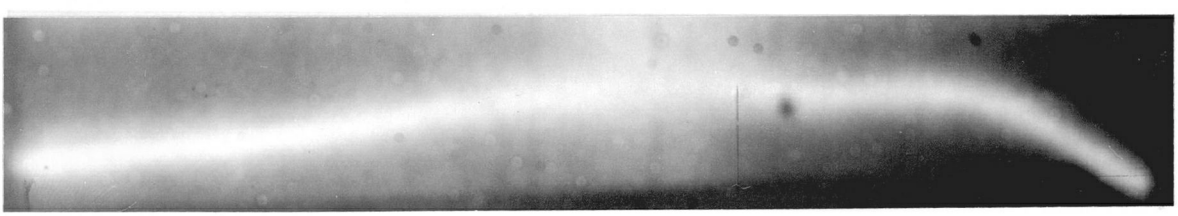

Graph 1.

Zn 25,65°C.

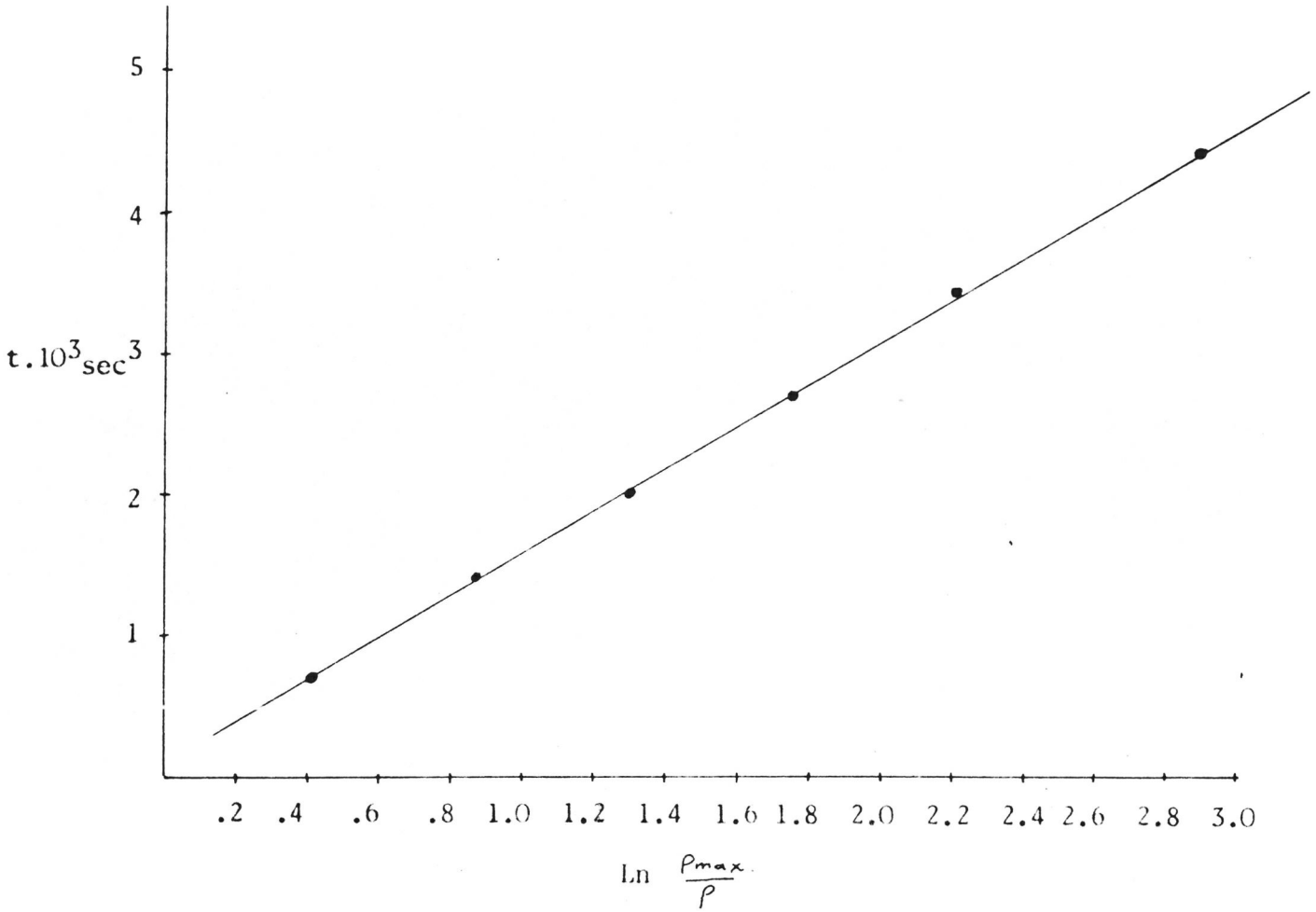

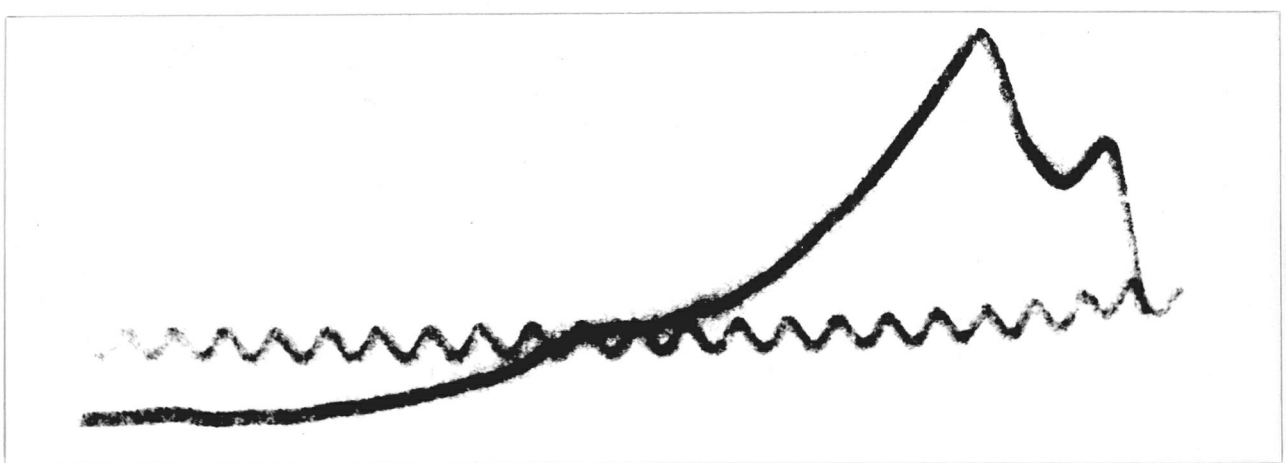

Graph 2.

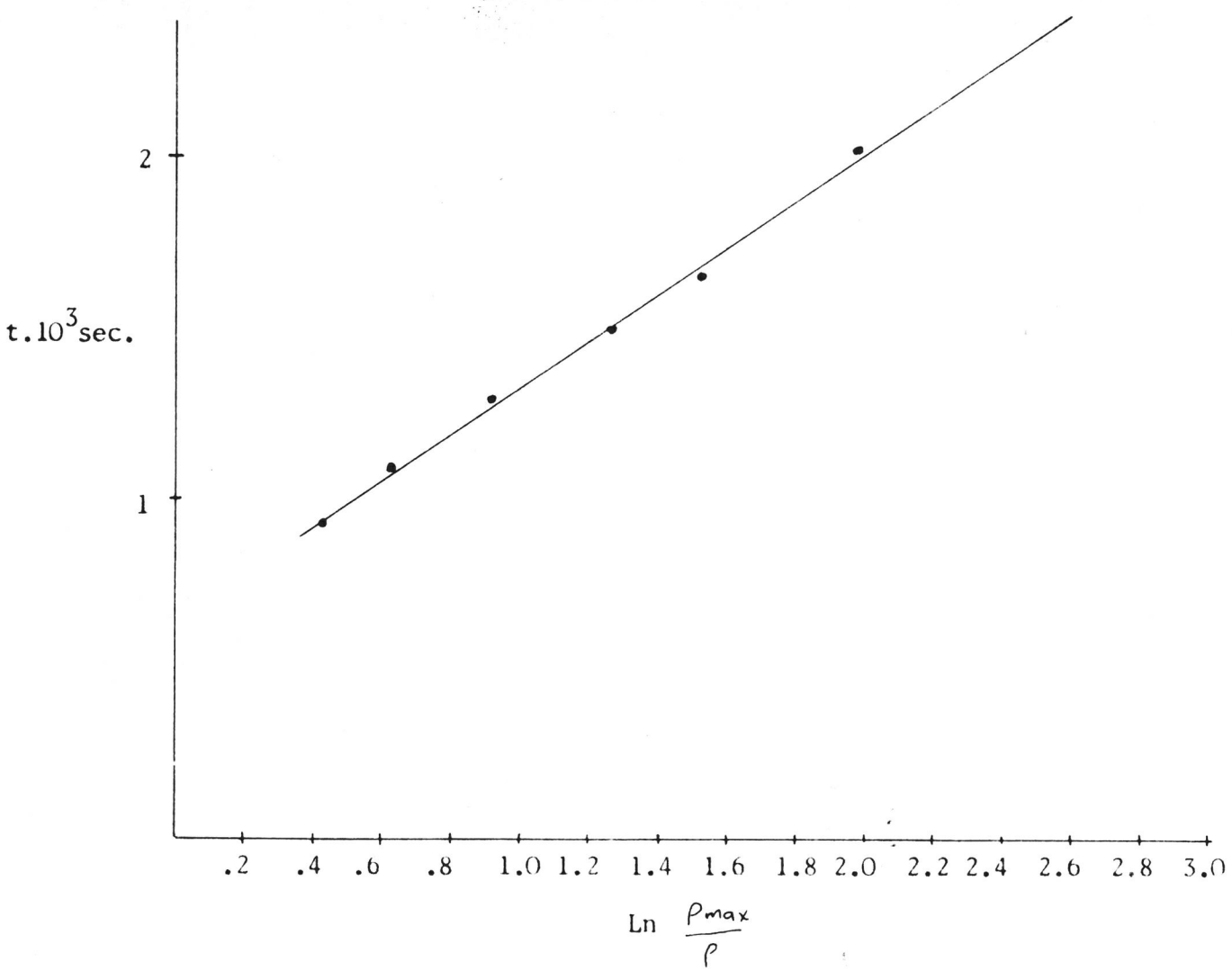

Graph 3.

Zn 43,18°C.

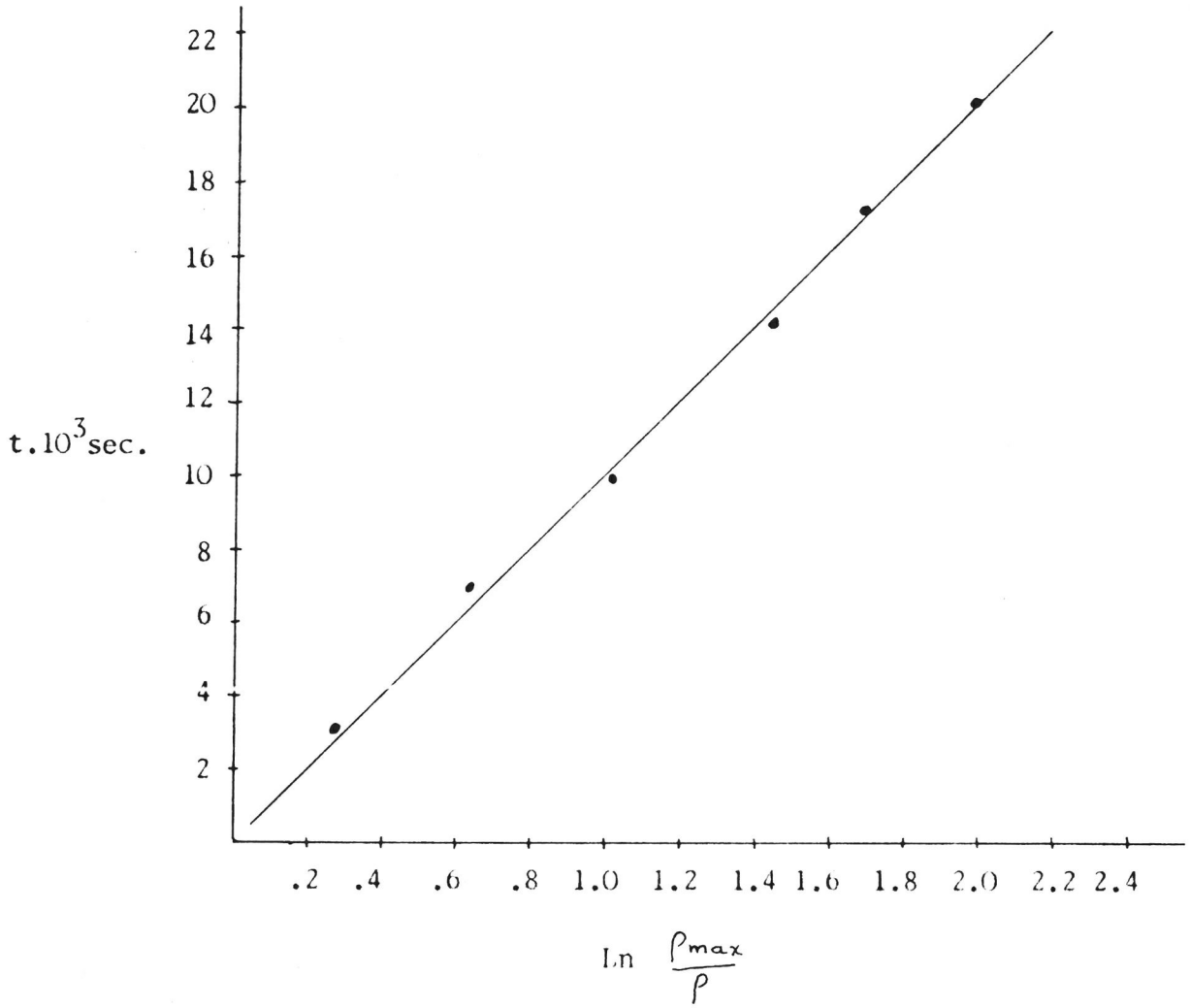

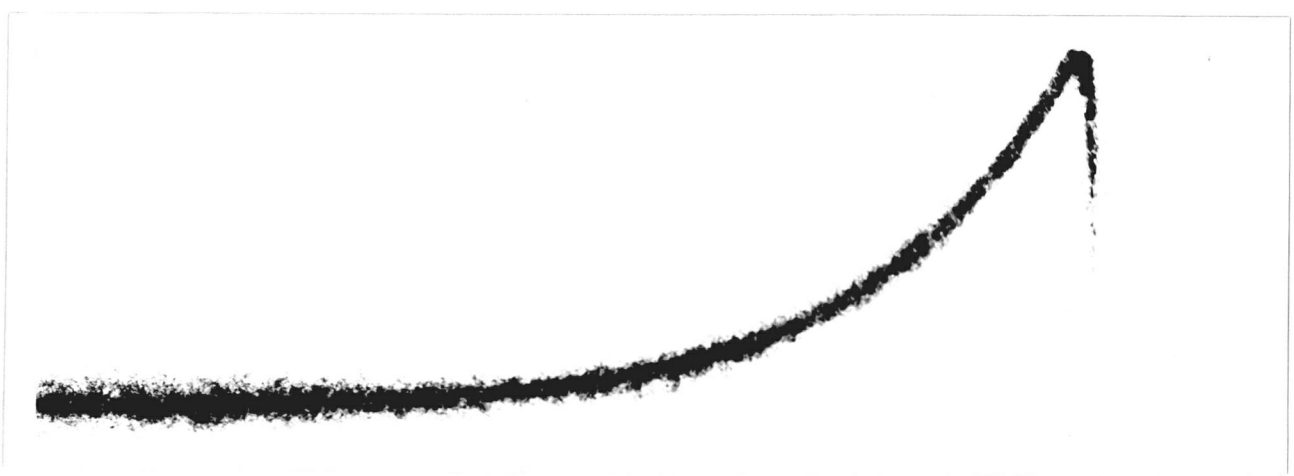

Graph 4.

Zn 43,40°C.

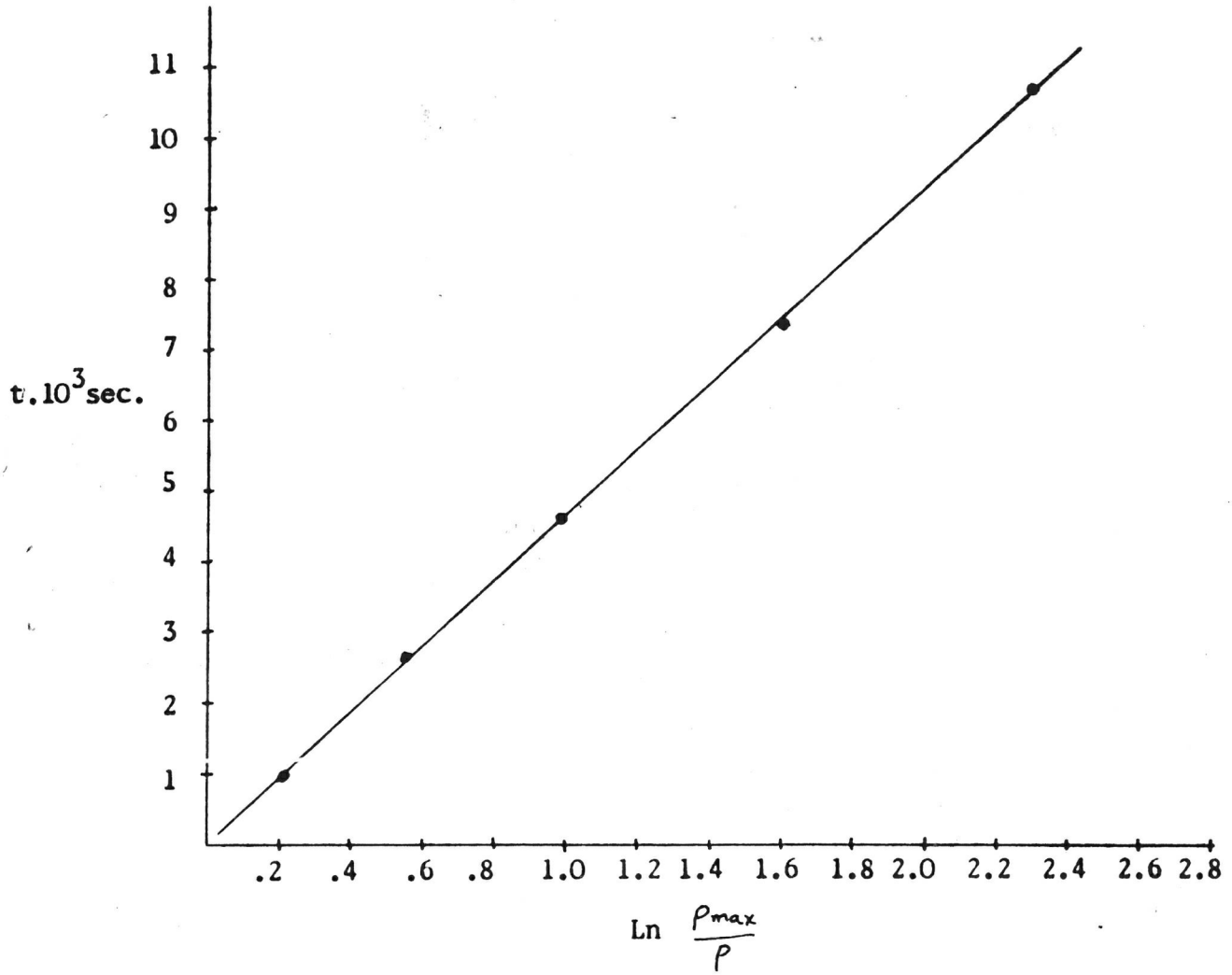

Graph 5.

Zn 43,100°C.

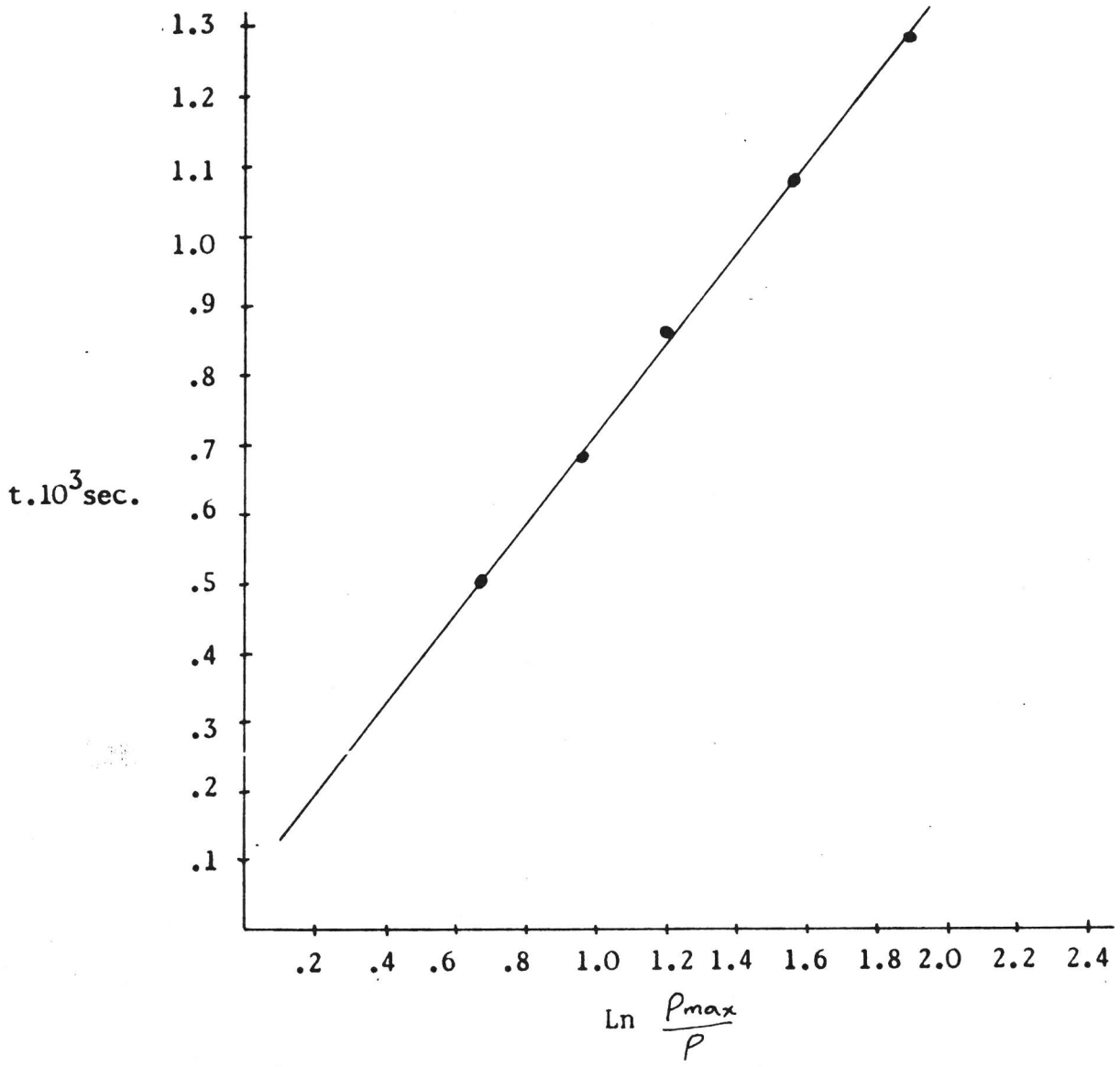

Graph 6.

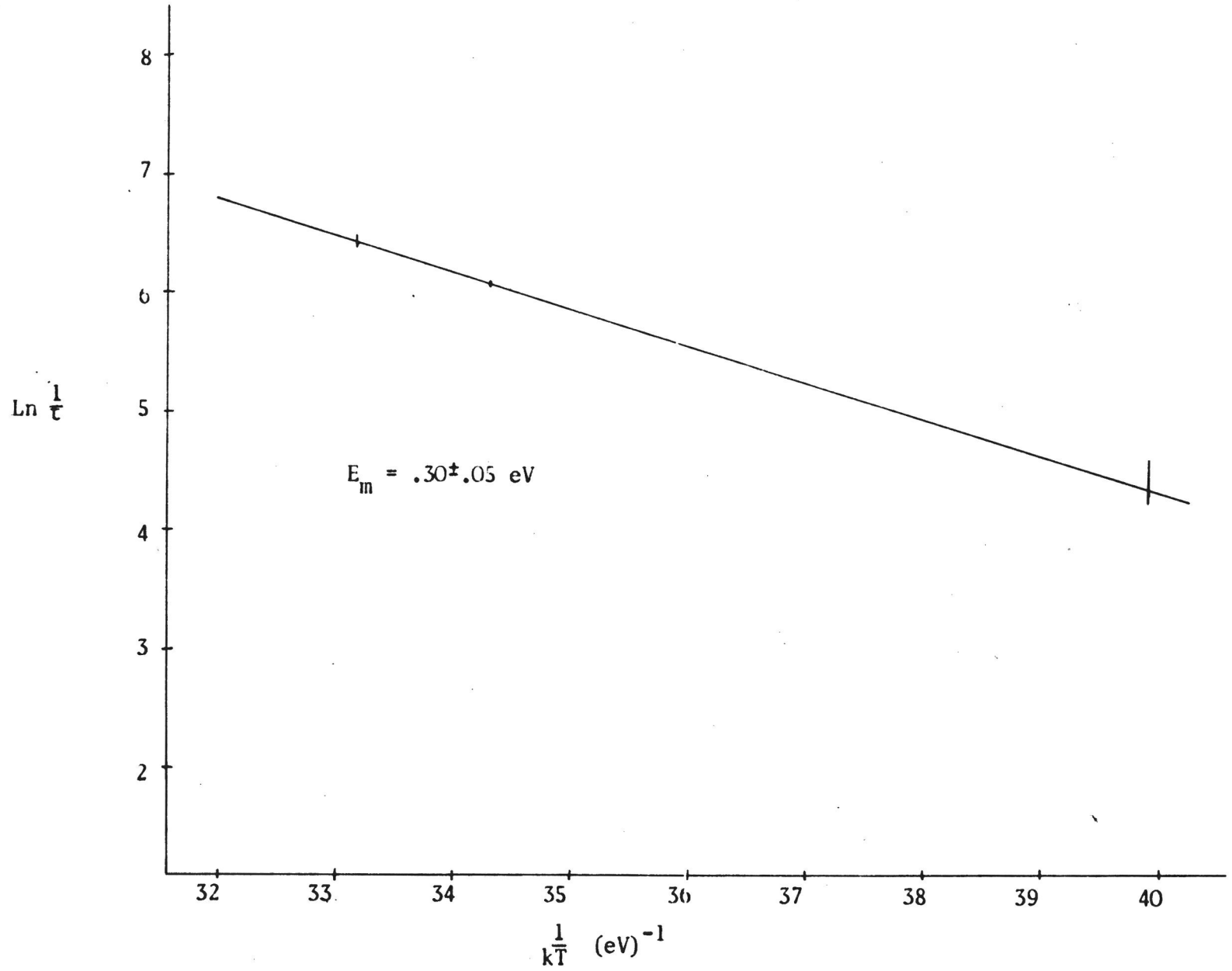
8
7
6
5
4
3
2
Ln $\frac{1}{\tau}$
E_m = .30±.05 eV
32
33
34
35
36
37
38
39
40
$\frac{1}{kT}$ (eV)$^{-1}$

Graph 7.

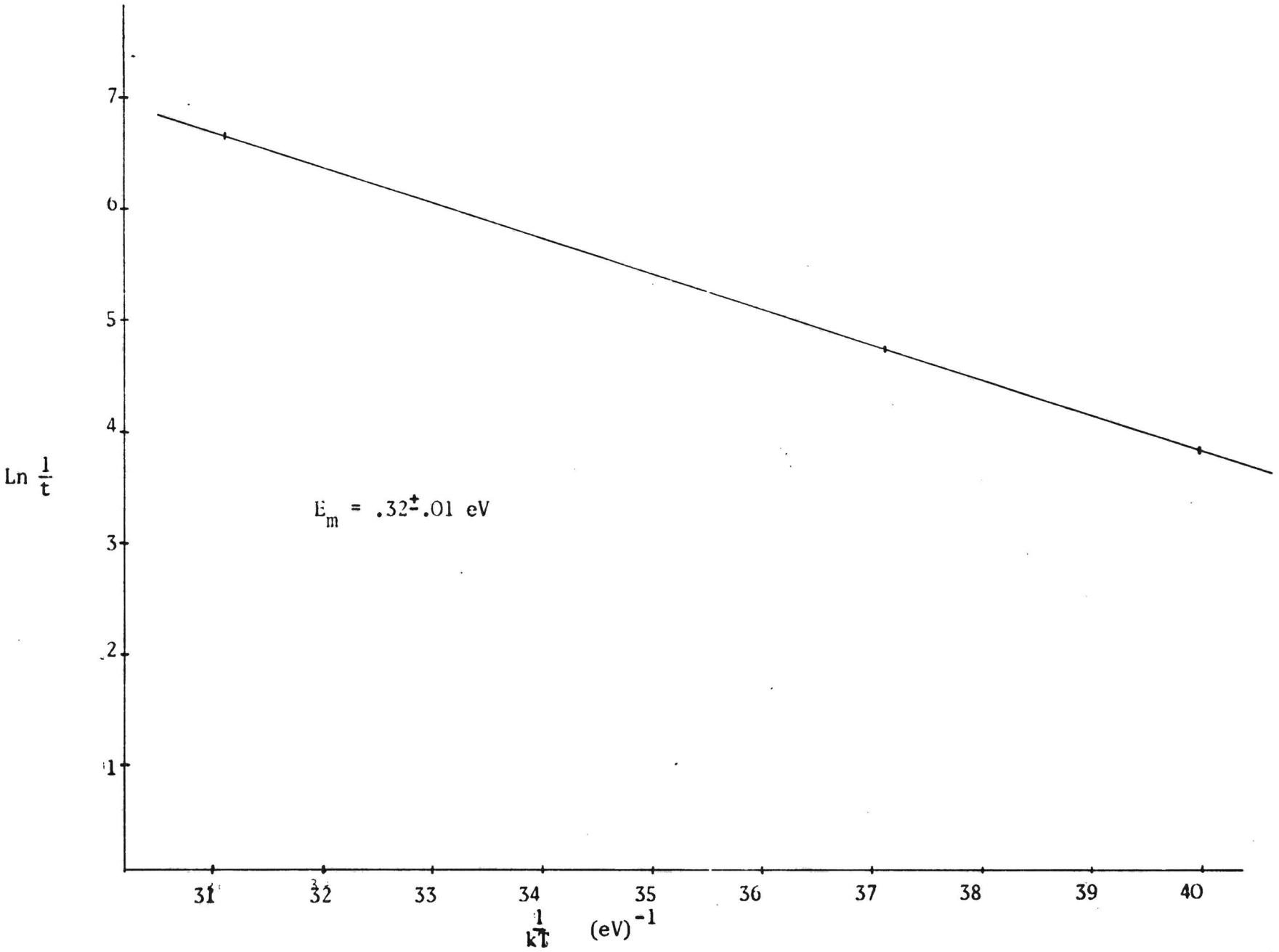

Graph 8.

ACKNOWLEDGEMENTS

I am indebted to Professor N. Feather, F.R.S. for affording me the facilities of his laboratory and to Dr. A.F. Brown for his advice and encouragement during this work and extend my thanks to both.

A maintenance grant received from the Department of Scientific & Industrial Research during part of the work I gratefully acknowledge.